Influence of Moisture in Polyurethane Shape Memory Polymers and Their Electrically Conductive Composites

Yang Bin

School of Mechanical & Aerospace Engineering

A thesis submitted to the Nanyang Technological University
in fulfillment of the requirement for the degree of
Doctor of Philosophy

2007

Abstract

This dissertation presents a systematic study on the influence of moisture in polyurethane shape memory polymers (SMPs) and their electrically conductive composites.

It was found that T_g of the SMP decreases by about 40 °C after immersion in water. This phenomenon is caused by the weakening of the hydrogen bonding between N-H and C=O groups due to the absorbed water. Furthermore, the water absorbed into the SMP can be separated into two parts, free water and bound water. Each part was quantified in the course of this study. The bound water in the SMP significantly reduces T_g in an almost linear manner, while the effect of free water is negligible. Based on these findings three new features of the polyurethane SMPs were proposed: SMPs with functionally gradient T_g, water actuated shape recovery, and porous SMPs using water as a non-toxic foaming agent.

Electrically conductive polyurethane SMPs were fabricated by filling the SMP with conductive carbon powders. Their microstructure, electrical conductivity, response upon uniaxial tensile, dynamic mechanical properties and shape memory properties were characterized experimentally both at dry and wet states. Good electrical conductivity and the shape memory effect were observed. It was demonstrated that shape recovery can be activated by directly passing an electrical current.

Keywords: shape memory polymer; polyurethane; glass transition temperature; moisture; thermomechanical; electrical conductivity.

Acknowledgments

First and foremost I would like to express my warmest and sincere thanks to my supervisors, Dr. Huang Weimin and Dr. Li Chuan, for their guidance, keen insights, encouragements and friendships. Special gratitude goes to Dr. Li Lin for his help and advice on my research.

I am also grateful to the director of the Photonics and Microsciences Lab, Dr. Xiao Zhongmin, for supplying the lab facilities.

The technicians in the Photonics and Microsciences Lab, the Materials Lab and the Strength of Materials Lab are appreciated for their assistance and kindness in various aspects. Special thanks are given to Mr. Koh Hai Tong, Mrs. Tan-Ho Ser Luan and Mr. Sa'Don Bin Ahmad.

Lastly I thank Nanyang Technological University for giving me a chance to study here with a research scholarship.

Table of Contents

List of Figures

List of Tables

List of Symbols

A	Critical coefficient relating to the electrical resistivity of polymer matrix
B	Critical coefficient relating to the electrical resistivity of conductive filler
b	Critical coefficient
E	Modulus of elasticity
k	Materials coefficient
L	Gauge length
M_m	Mass of SMP
M_f	Mass of carbon powder
m	Critical exponent
n	Critical exponent
R	Real ratio of water to SMP in weight
R_e	Measured weight ratio of water
R_f	Ratio of fixable strain
R_r	Ratio of recoverable strain
R_t	Ratio of moisture to SMP composite in weight at the intersection point (positive valve)
r	Critical exponent
R'	Electrical resistance
S	Ratio of ε_s to $\varepsilon_c + \varepsilon_p$

s	Critical exponent
S'	Cross sectional area
T	Temperature
T_g	Glass transition temperature
T_h	Temperature above T_g
T_l	Temperature below T_g
T_m	Melting temperature
T_c	Crystallization temperature
T_r	Room temperature
t	Time
w	Weight loss of SMP at 240°C
X	Materials parameter
X_g	Materials parameter at T_g
α	Coefficient of thermal expansion
ε	Strain
ε_e	Elastic strain
ε_h	Free recoverable strain
ε_m	Maximum strain
ε_t	Instant recovery strain
ε_f	Fixed strain
ε_i	Residual strain
ε_c	Creep strain

ε_p	Plastic strain
ε_r	Recoverable strain
σ	Stress
σ_y	Yield stress
σ_c	Creep limit stress
μ	Viscosity
λ	Retardation time
δ	Phase angle
τ	Relaxation time
φ_f	Volume fraction of carbon powder
φ_c	Percolation threshold
ρ	Electrical resistivity
ρ_m	Bulk density of SMP
ρ_f	Bulk density of carbon powder

Chapter 1 Introduction

1.1 Background of shape memory polymers (SMPs)

Shape memory materials have been a subject under intensive investigation in recent years. At present, a variety of engineering and biomedical applications are based on shape memory alloys (SMAs) and ceramics (Otsuka and Wayman 1998, Huang 1998, Wever et al 1998, Duerig et al 1999). Shape memory polymers are lagging well behind despite their many novel properties, e.g. maximum recoverable strain up to 400% (Hayashi et al 1995 and Liang et al 1997), and great potential, e.g. shape recovery activated by other methods besides external heating.

Similar to other shape memory materials, shape memory polymers (SMPs) have the typical shape memory effect (SME), but unlike SMAs, their recovery can be triggered by various external stimuli, other than heat, such as light and PH change. Consequently, SMPs are categorized by the different stimuli into three types, namely, thermal-responsive SMP, photo-responsive SMP and chemo-responsive SMP (Otsuka and Wayman 1998, Seki et al 1997). Among them, the thermo-responsive SMPs have been the major focus of investigation in the past years and some products utilizing their properties are commercially available at present. SMPs have many apparent advantages over SMAs, such as very high shape recoverability, low density, low cost, easy shaping procedure, easy control of recovery temperature and color variation.

The first generation of SMP was made of polyethylene crosslinked by reaction with ionizing radiation during processing (Ota 1981). After that, various kinds of SMPs have been developed in order to meet the requirements of different applications. To name a few, poly (isoprene-butadiene-styrene), polyurethane, polyacrylamide and polystyrene series (Hu et al 1995, Takahashi et al 1996, Lee et al 2001, Yang et al 2003, Cao et al 2003) are typical ones.

Recently, a biodegradable thermoplastic SMP was developed (Lendlein and Langer 2002). This novel material is a biodegradable multiblock copolymer, in which block-building segments are linked together in linear chains. Specifically, this polymer contains a hard segment and a "switching" segment. These two segments have significantly different thermal properties. Upon heating, the "switching" segment either melts or goes through a transition. A suture made of this degradable SMP, pre-stretched and formed into the temporary shape (loose knot) can tighten itself in 20 s upon heating to 40°C. A more fascinating point is that the polymer will degrade within a predetermined time period, so that a follow-up surgery for suture removal becomes unnecessary. As reported in *Science*, this is a suitable material for replacing large and bulky ones currently in use in minimally invasive surgery.

1.2 Innovative applications of SMPs

With these unique properties, SMPs are gradually gaining attention recently. The applications in active devices, self-deployable structures and micro-system assembly have been proposed and are in developing (Hayashi 1993, Hayashi et al 1994, Tobushi et al 1996, Chiodo et al 1999, Monkman 2000). Utilizing the extremely large recovery strain in SMPs up to 400% (Hayashi et al 1995 and Liang et al 1997), many novel

medical devices and biological micro electro-mechanical systems may be realized. The SMP-based biological micro-electro mechanical systems can perform in-vivo functions, for instance, gripping and releasing of therapeutic medical devices within blood vessels (Lee and Fitch 2000, Lee et al 2000, Gall et al 2004). More recently, it has been demonstrated that SMPs can fully recover from nano-scale deformation upon heating. It sheds light on numerous potential applications in nano-actuation, nano-manipulation, active surface texturing, data storage, and nano-fluidics (Nelson et al 2005).

Polyurethane SMPs used in the current research are thermo-responsive SMPs developed by Mitsubishi Heavy Industries (MHI), Japan. The reported applications of polyurethane SMPs are largely in daily consumable, industrial, and biomedical devices. Polyurethane SMPs with good shape memory, high resistance to corrosion, good chemical stability and, more importantly, excellent biocompatibilities are potential candidates for biomedical applications. Wache et al (2003) fabricated expandable SMP stents by injection molding, extrusion and dip coating for drug delivery. One of the major advantages of this stent is that during processing, the drug is introduced into the polyurethane SMP, so that the risk of complications is reduced. Figure 1.1 illustrates the principle of this stent. First, the stent is pre-deformed (stretched) at a temperature above its glass transition temperature (T_g). The deformed shape is then fixed, and subsequently, cooled to below T_g. After the constraint is removed, the deformation is retained as long as the temperature is below T_g. Recovery can be activated by heating after the stent has been placed at the required location. The stent can be applied as a drug delivery system in the cardial area with minimally invasive effects. It also reduces

chances of restenosis and thrombosis. Applications in other organs, such as the trachea, oesophagus and urethra, have also been proposed.

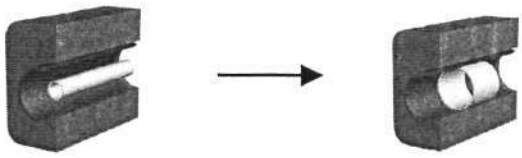

Figure 1.1 Schematic of principle of a stent made of the polyurethane SMP. Left: prior to shape recovery; right: after shape recovery (Wache et al 2003).

Active disassembly using SMP is one of the applications of polyurethane SMP in industry. Chiodo et al (1999) conducted an initial investigation on active disassembly of mobile phones. In his study, the liquid cystal display (LCD) bracket of a mobile phone with a original shape as shown in Figure 1.2 (a) was molded from polyurethane SMP. At a high temperature, the SMP bracket is deformed and assembled with the LCD. The position of LCD in Figure 1.2 (b) is the intended configuration after assembly. Figure 1.2 (c) shows that the SMP bracket is fixed with LCD and other components upon cooling by cold bathing. If disassembly of the SMP bracket and LCD is needed, reheating the SMP bracket is an efficient way that triggers shape recovery of the SMP bracket, so that LCD is rejected in a nondestructive way. As we can see in Figure 1.2 (d), the SMP bracket recovers its original shape [refer to Figure 1.2 (a)], and separates from LCD. This investigation concluded that the active disassembly using SMP is an effecient and low cost way to ensure reliable active disassembly not only with minor change in the product design but also without any destruction to the product components.

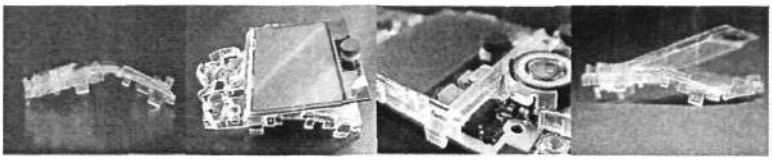

(a) (b) (c) (d)

Figure 1.2 Active disassembly using polyurethane SMP (Chiodo et al © [1999] IEEE).

SMPs have also been proposed for applications in Micro-ElectroMecahnical Systems (MEMS) or Bio-MEMS. Figure 1.3 illustrates the fabrication and operation of a SMP-based micro-fluidic reservoir, which can be used to store liquid chemicals (Gall et al 2004). Figure 1.3 (a) shows a circular section made of SMP with a smooth surface. Micro-channels are machined into the surface of SMP by laser cutting or multilayer soft-lithography method [Figure 1.3 (b)]. A reservoir for the chemicals is built at the end of the micro-channel by indenting SMP at temperature above T_g [Figure1.4 (c) and (d)]. Then, the surface is covered with a glass slide to seal the reservoir [Figure 1.3 (e)]. By heating the reservoir to induce shape recovery, the fluid in the reservoir flows down from the micro-channel [Figure 1.3 (f)].

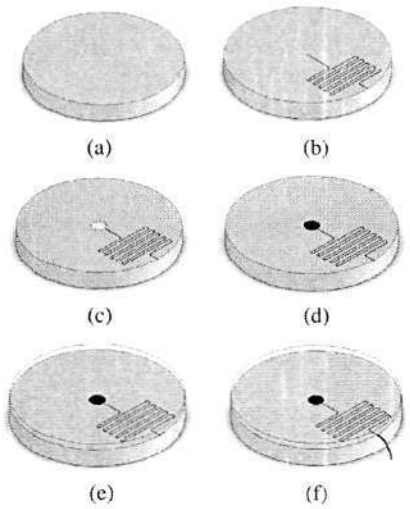

Figure 1.3 Illustration of fabrication and operation of a SMP-based micro-fluidic reservoir (Gall et al 2004).

1.3 Objectives of the dissertation

Although there are some applications of SMPs, they have not fully reached their technological potential. This is largely due to the lack of available data of SMPs for engineering applications. On the other hand, the effects of environmental factors, e.g., moisture, on the properties of SMP have yet been investigated. Moreover, a significant drawback in SMPs is the low stiffness, which results in a low recovery force as compared with metals and ceramics (Wei et al 1998, Gall et al 2002). Therefore, the SMPs are normally used for free recovery or low recovery force. Apart from these, the actuation of shape recovery in thermal-responsive SMPs requires external heat. So far, thermal induction and optical radiation are the only methods for heating, which are not efficient.

The aim of this research is twofold. One is to systematically investigate the effects of moisture on the thermomechanical properties of a polyurethane SMP, and utilizing the effects of moisture for making SMPs with gradient T_g and demonstrating water-driven shape recovery. Thermal tests (including, differential scanning calorimetry [DSC] and thermogravimetric analysis [TGA]) and thermomechanical tests (including, dynamic mechanical analysis [DMA] and uniaxial tension/compression test at different temperatures) are used for the characterization. In addition, fourier transform infrared (FTIR) spectroscopy is used to investigate the interaction between water and SMP.

The second is to fabricate electrically conductive SMPs (by filling with conductive fillers, namely nano carbon black). Because nano carbon black is much lighter and cheaper, and more importantly is easier for processing than other materials (e.g. Jäger et al 2001, Thommerel et al 2002, Carmona F and Ravier J 2002, Zheng and Wong 2003), in particular metallic powders (which can easily become rusty upon being exposed in air [Thommerel et al 2002]), it is used in this study. The SMP composites are characterized at both dry and wet states. The carbon filled conductive SMP composites can improve not only the electrical conductivity, but also the stiffness, and in the mean time, still have good shape memory properties. As such, electrically conductive SMPs can have more potential applications.

1.4 Outline of the dissertation

The outline of the dissertation is as follows,

Chapter 1 briefly introduces backgrounds and applications of SMPs and presents the objectives of this research.

Chapter 2 reviews the research results and conclusions on polyurethane SMPs reported in the literature.

Chapter 3 investigates the thermomechanical properties of polyurethane SMPs experimentally.

Chapter 4 studies the effects of moisture on T_g of polyurethane SMP and applications.

In Chapter 5 the electrically conductive SMPs are prepared and characterized.

Chapter 6 investigates the effects of moisture on the electrically conductive SMPs.

The dissertation is concluded by some conclusions and future works in Chapter 7.

Chapter 2 Literature Review

2.1 Polymerization of polyurethane SMPs and hydrogen bonding

Polyurethane SMPs are thermo-responsive SMPs, in that the shape memory effect (SME) can be activated by heat. Several forms of polyurethane SMPs are commercially available from Mitsubishi Heavy Industry, Japan (MHI) for different materials processing methods, namely, molding, potting, casting and coating as listed in Table 2.1. Polyurethane SMPs in pellet form are used in this study. Their technical data of them are listed in Appendix A.

Type	Description
MM	Pellets or flakes for injection and extrusion molding. MM materials are also available as filaments and alloys.
MB	Micro beads of modified MM material; spheres approximately 10μm in diameter for possible use in paints and cosmetics.
MS	Solution of polymer in dimethylformamide (DMF), suitable for coatings.
MP	Two liquids, the primary agent and the curing agent, used for casting and potting. This is mainly for experimental use or small-quantity production and is applicable to RIM moldings and adhesives.
MF	Foamed material; foaming ratios of 5 through 40.

Table 2.1 Polyurethane SMPs in different forms (from MHI).

As compared with other shape memory materials, polyurethane SMPs have many advantages, such as low density, low cost for fabrication, a remarkable recovery strain of up to 400%, easy of processing, wide shape recovery temperature range, excellent chemical properties, and biocompatibility (Liang et al 1997, Wei et al 1998, Zdrahala et al 1999, Metcalfe et al 2003).

Polyurethane SMPs are multiblock copolymers usually polymerized from bifunctional diisocyanates, polyols and chain extenders. No solvent is involved in the polymerization. The molecule chain of polyurethane SMPs consists of alternating sequences of soft segments with low molecular weight, and hard segments built from diisocyanates and extenders to form the points for physical linking as follows (Kim 1996),

$$\text{H-[O-(CH}_2\text{)}_5\text{-CO-]}_n\text{-O-R}\text{———}\text{OOCHN-R'-NHCOO-R''-OOCHN-R'}$$

(Soft segment, polyol) (Hard segment, diisocyanate + extender)

Five diisocyanates, ten polyols and six chain extenders have been used to polymerize polyurethane SMPs with different T_g. Shirai and Hayashi (1988) concluded that to achieve T_g in the vicinity of room temperature, the molar ratios of the starting materials for SMPs must follow the following criterion,

$$\frac{\text{Mole of NCO group}}{\text{Total mole of OH group}} \leq 1$$

Polyurethane SMPs can be formulated with a T_g ranging from –20°C to +120°C, which depends on the molecular design of compounds (Hayashi 1993).

Control of hard segment structure and soft segment chain length are both very important for obtaining good characteristics of polyurethane SMP. It has been found that T_g increases with the content of hard segment. The formation of hard segment domains becomes very difficult in polyurethane SMPs that have low hard-segment content and a short hard-segment length. There is a lower limit of hard-segment content and segment length in preparing polyurethane SMPs. Only above this limit polyurethane SMP can have enough hard-segment domains acting as physical crosslinks (Li et al 1996, Yang et al 2003).

The formation of hydrogen bonding in polyurethane is generally known to have a major effect on its morphology and overall properties (Yen et al 1999, Luo et al 1997, Yoon et al 2000, Heintz et al 2002, Teo et al 1997). It has been found that the primary bands in polyurethane, the N-H stretching as a proton donor and the carbonyl stretching as a proton acceptor, are sensitive to hydrogen bonding. Therefore, the formation of hydrogen bonds is characterized by the shift of Fourier transform infrared (FTIR) absorbance peak to a lower frequency. The strength of hydrogen bonding can be quantified by the magnitude of the shift (Yen et al 1999, Luo et al 1997, Yoon et al 2000, Chen et al 2000, Brunette et al 1982).

2.2 Shape memory effect and mechanism

Raw materials are processed into a pre-determined shape (the original shape) by molding, casting or coating. Shape memory effect (SME) of polyurethane SMPs in a thermomechanical cycle is illustrated as shown in Figure 2.1.

a. SMPs are easily deformed at a temperature above T_g. Only a small force is required to maintain the deformed shape.
b. After cooling to below T_g, the removal of the constraint results in a very small elastic shape recovery, but the deformed shape is largely maintained.
c. This deformed shape can be held until shape recovery is activated by reheating SMPs to or above T_g. SMPs show the typical SME by fully regaining the original shape upon heating.

The SME cycle is repeatable.

The mechanism of the SME in polyurethane SMPs can be explained by examining their microstructures. Polyurethane SMPs consisting of soft and hard segments can be described by a microstructure model as shown in Figure 2.2 (Yang 1997). Hard and soft segments are usually thermodynamically immiscible, so that micro-phase separation of the segments occurs. In the relaxed state upon processing, partially separated soft and hard segments exist in the material as shown in Figure 2.2. Hard segments can form physical cross-links between themselves through hydrogen bonding and crystallization, making the material solid at below the melting temperature. These hard segments act as pivot points for shape recovery. Soft segments formed from polyesters or polyethers responsible for SME can absorb most of the external stress applied on the polymers.

At a temperature below T_g, micro-Brownian motion is almost negligible and the soft segment cannot gain enough kinetic energy to achieve the mobility. Thus, polyurethane SMPs are more difficult to deform in the glass state. Upon heating over T_g, however,

micro-Brownian motion in soft segments is activated, and enough kinetic energy can be obtained to overcome the restriction for large-scale motion in the segments. Hence, above T_g polyurethane SMPs transit from the glass state to the rubber state and becomes easy to deform. Now if a tensile load is applied, the soft and hard segments reorient themselves in the direction of external force, and the curled soft segments are stretched. By cooling SMPs below T_g while maintaining the deformed shape maintained and then removing the constraint, micro-Brownian motion in soft segments is frozen due to the halt of the long-range motion of soft segments so that the deformation is maintained even after removal of the constraints, as shown in Figure 2.2. However, upon re-heating above T_g micro-Brownian motion is triggered for action again. Soft segments achieve the mobility to return to its original curled-shape. It results in the recovery of the original shape of polyurethane SMPs.

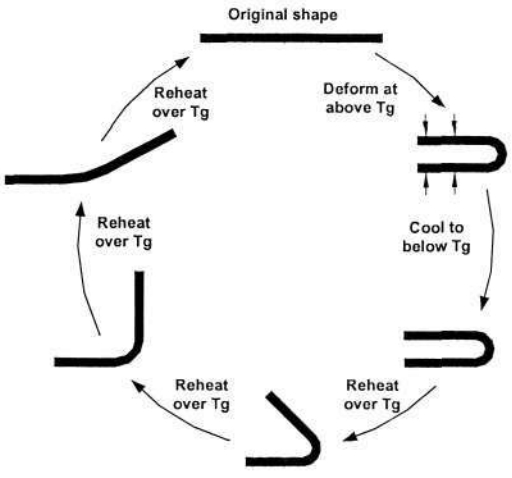

Figure 2.1 Illustration of SME.

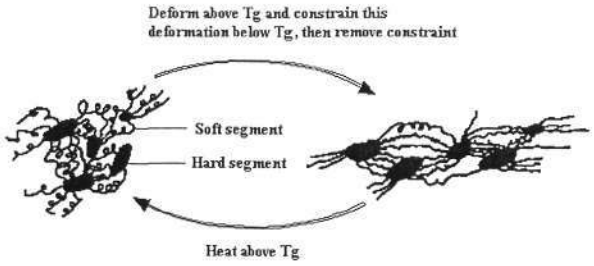

Figure 2.2 Schematic representation of microstructure of polyurethane SMPs (Yang 1997).

2.3 Thermomechanical properties and modeling

Thermomechanical properties are very important in evaluating SMPs. Cyclic thermomechanical test is a standard approach for characterization of the shape memory properties of SMPs. A typical stress-strain-temperature relationship of polyurethane SMPs is plotted in Figure 2.3 (Tobushi et al 1992, Tobushi et al 2001). The thermomechanical test is performed via the following steps.

a. At a temperature T_h ($> T_g$), the SMP specimen is loaded to a pre-determined maximum strain (ε_m) at a constant strain rate ($\dot{\varepsilon}$).

b. The SMP sample is held with ε_m fixed and cooled to a new temperature T_l ($< T_g$).

c. The stress is reduced to zero at T_l. Upon unloading, only a very small elastic strain is recovered. ε_f is the remaining strain after the applied stress is fully removed.

d. The sample is reheated from T_l to T_h at a constant heating rate ($\dot{T}$) without applying any external stress. The pre-strain is almost fully recovered with only a very small strain ε_i left at T_h.

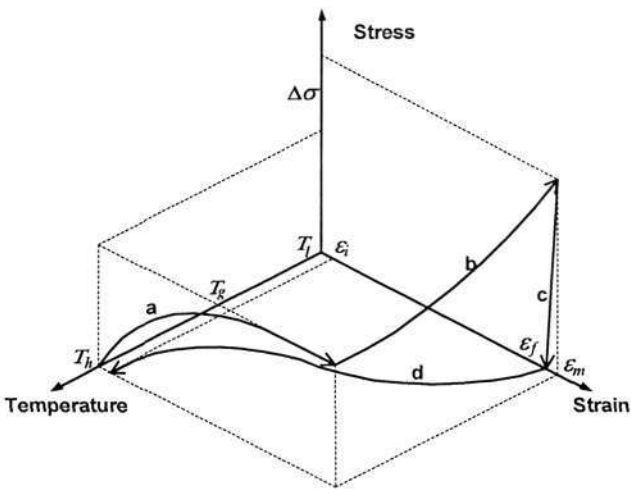

Figure 2.3 Scheme of a thermomechanical test (Tobushi et al 2001).

In the literature, a few constitutive models have been proposed to describe the thermomechanical properties of SMPs. Among them, Tobushi et al (1997a) presented a linear constitutive model by including a slip mechanism and thermal expansion into a standard linear viscoelastic model. Note that, although the reversible strain of polyurethane SMPs is up to several hundred percent, in most engineering practices, the polyurethane SMP elements are only loaded to 20% strain or less (Hayashi 1993, Tobushi et al 1998). However, at around 10% strain or more, one has to consider the influence of nonlinearity. So that, the linear constitutive model is presented in a differential format in order to incorporate such influence (Tobushi et al 2001) as

$$\dot{\varepsilon} = \frac{\dot{\sigma}}{E} + m\left(\frac{\sigma - \sigma_y}{k}\right)^{m-1}\frac{\dot{\sigma}}{k} + \frac{\sigma}{\mu} + \frac{1}{b}\left(\frac{\sigma}{\sigma_c} - 1\right)^{n} - \frac{\varepsilon - \varepsilon_s}{\lambda} + \alpha\dot{T} \qquad (2.1)$$

where σ_y and σ_c correspond to the yield stress and the creep limit, and m, n and b are critical coefficients. σ, ε and T are stress, strain and temperature, respectively. E, μ, λ and α represent the modulus of elasticity, viscosity, retardation time and coefficient of thermal expansion. A dot denotes the time derivative of a variable.

A nonlinear term presented as a power function in terms of stress is included in this model for the nonlinear time-independent strain with respect to a linear elastic term $\dot{\sigma}/E$. On the other hand, because the rate of increase in creep strain is nonlinear against the increase of stress (Tobushi et al 1996), another nonlinear term presented as a power function of stress is added to the linear viscous term σ/μ. When high strain is reached, the time dependent plastic strain ε_p and the irrecoverable strain ε_s emerge. ε_s can be expressed as

$$\varepsilon_s = S\left(\varepsilon_c + \varepsilon_p\right) \qquad (2.2)$$

where S is a material constant.

All material parameters, namely, $E, k, \sigma_y, \mu, \sigma_c, \lambda$ and S, within the glass transition range (e.g. from T_g -15°C to T_g +15°C) are expressed as a single exponential function in terms of temperature in the following format,

$$X = X_g Exp\left[a\left(\frac{T_g}{T}\right) - 1\right] \qquad (2.3)$$

Here, X denotes a material parameter while X_g is the characteristic value of a material parameter at T_g. The exponent coefficient a is assumed to be a constant for all material parameters. Outside the transition range, they are constants.

This nonlinear model has been verified by some thermomechanical tests on polyurethane SMPs up to 20% strain. In addition, based on the linear rheological model proposed by Tobushi et al (1997), Bhattacharyya and Tobushi (2000) have derived an analytical solution for the isothermal mechanical response of polyurethane SMPs in the following five cases: (a) constant stress, (b) constant strain, (c) constant stress rate, (d) constant strain rate, and (e) periodic strain.

2.4 SMP blends and composites

SMP blends have been investigated in the literature in recent years. Li et al (1998) prepared a series of polyethylene/nylon 6 blends, which show good shape memory properties. Two conditions are necessary for the shape memory effect in these SMP blends. One is the high crystallization of polyethylene segments at room temperature. The other is the formation of stable network structure by nylon domains acting as the physical crosslinks.

Although there are some niche applications of SMPs, in particular as smart materials, they have yet reached their full technological potential. A significant drawback of un-reinforced SMP materials is their low stiffness as compared with metals and ceramics. It results in a relatively small recovery force. In order to improve their strength and stiffness, one may reinforce SMPs with fillers.

Preliminary work has been reported by Liang et al (1997) on reinforcing a polyurethane SMP with glass fiber and Kevlar. The SMP composites were prepared by blending the polyurethane SMP melt or 30% DMF SMP solution with fillers. It was found that the reinforcements increased the ultimate strength and the Young's modulus, but reduced the elongation limit at room temperature dramatically even when loaded with a very small volume fraction of fillers. Moreover, the continuous fiber reinforced polyurethane SMPs were founded to be anisotropic, and no SME in the fiber direction. In addition, recovery in bending was found to be limited. On the other hand, SME persists in all discontinuous fiber reinforced SMP composites in all directions.

Thermosetting SMP-based composites have been investigated for deployable space structures (Gall et al 2000, Cadogan et al 2002, Abrahamson et al 2002). Reinforced by fibers, these composites exhibit not only excellent shape memory and environmental durability, but also good stiffness and strength. The mechanisms in interaction between SMP and reinforcement fibers have been studied. These fiber-reinforced SMP composites have some apparent advantages over shape memory alloys and shape memory ceramics. Lower density, higher elastic strain capability and lower processing cost are some among others. Both stiffness and recovery stress of thermosetting SMP-based composites were found to be dramatically improved by filling with different fibers.

One of the interesting progresses made in recent years is SMP nanocomposites. Gall et al (2002) fabricated some SMP nano-composites by adding SiC nano-particulates (average diameter: 300 nm) into a thermosetting epoxy-based SMP matrix. These SMP composites with different weight fractions of SiC nano-particles have been

characterized at macro and micro-scales. The results show that the presence of SiC nano-particles can remarkably reduce T_g and the temperature range of transition process in SMPs. The micro-hardness and the elastic modulus of the nanocomposites increase with the concentration of SiC particles. The reinforcement is considered as a direct consequence of the high hardness/modulus of SiC particles as compared with the SMP matrix. Furthermore, the bending force in constrained recovery of a SMP composite filled with 20% weight fraction of SiC increases by 50%. Unconstrained strain recoverability of the SMP nanocomposites characterized by bending tests depends on the weight fraction of SiC. SiC particulates reduce the limit of recoverable strain in unconstrained recovery. With below 40% weight fraction of SiC, the SMP nanocomposites can fully recover a pre- strain of up to 10%.

In the SiC nano particles filled SMP composites, the nano-particles store a finite compressive stress, which can be determined by measuring the changes in the lattice parameters of the SiC particles using X-ray diffraction (XRD) methods. A quantitative Rietveld analysis of diffraction peaks of XRD measurements was used to analyze changes in the lattice parameter of the SiC particles after deformation and strain recovery. It shows that the stored compressive stress under 50% compression strain is almost completely released upon strain recovery induced by heating (Gall et al 2004).

2.5 Electrically conductive SMP

Conductive polymers can be realized in two ways. One is to produce a polymer that is intrinsically conductive. Heeger et al received the Nobel Prize in Chemistry in 2000 for developing these intrinsically conductive polymers (ICPs). However, commonly used

ICPs such as polyacetylene, polyaniline and polypyrrole, have a typical value of conductivity around $10^{-10} \sim 10^{5}$ S/m. They are not stable in mechanical properties, expensive and difficult in preparation, in particular in polymerization (Cotts and Reyes 1986, Nalwa 1997, Morgan and Foot 2001). The other approach is to dope or load with conductive fillers into an insulator. Graphite, carbon powders and metallic particles are widely used. Due to very low cost and convenient in fabrication (requires only conventional processes in preparing polymers), the later approach is more popular in engineering practice (e.g. Jäger et al 2001, Thommerel et al 2002, Zheng and Wong 2003).

The percolation theory (Stauffer and Aharony 1994, Wu and Mclachlan 1997, Jäger et al 2001) can be used to describe the dependence of the electrical resistivity on the volume fraction of conductive fillers in the conductive composites. The electrical resistivity (ρ) for randomly distributed conductors in an insulator matrix of insulator-conductor binary composites is expressed as follows,

$$\rho = A\left(\varphi_c - \varphi_f\right)^{s} \qquad \text{for } \varphi_f < \varphi_c \tag{2.4}$$

$$\rho = B\left(\varphi_f - \varphi_c\right)^{-r} \qquad \text{for } \varphi_f > \varphi_c \tag{2.5}$$

where φ_f is the volume fraction of the conductive filler, φ_c is the percolation threshold, s and r are the critical exponents close to 0.7 and 2.0, respectively, which is affected by the distribution, geometry of conductive fillers and other factors (Sahimi 1994, Das et al 2002). A and B are critical coefficients relating to the resistivity of the polymer matrix and the conductive filler.

Although filler-type conductive polymers have been targets of investigation for a few decades, so far only Li et al (2000) have reported some preliminary results on SMPs. These SMP composites are polyurethane SMP/carbon black composites, and are prepared by a solution-precipitation process, followed by compressive molding. Their investigation focused on the structure, electrical conductivity, strain recovery and their relationships of these composites. The percolation threshold was obtained at 20% weight fraction of carbon black. However, a highly loaded composite has a very low strain recovery speed and recoverable strain ratio, although the stiffness and strength are improved, e.g. SMP filled with 25% weight fraction of carbon has an electrical conductivity of 10^{-1} $\Omega \times m$ but only can recover less than 70% of preloaded strain. To the best knowledge of this author, at the time of writing, no detailed report on their thermomechanical properties is available.

Chapter 3 Thermomechanical Behavior of Polyurethane SMP

The ester-based thermoplastic polyurethane SMP in pellet form from MHI (refer to Appendix A) was used in the course of this study. It was prepared from diphenylmethane-4, 4'-diisocyanate, adipic acid, ethylene glycol, ethylene oxide, polypropylene oxide, 1, 4-butanediol and bisphenol A. T_g can be tailored in order to meet the requirement of a particular application. The raw material used in the study in this chapter is SMP MM3520 in pellets form. Its T_g provided by MHI is 35°C. The dimensions of samples for testing is shown in Figure 3.1. After drying in a vacuum oven at 80°C for 12 hours, the samples were prepared with a laboratory injection-molding machine (Manumold 77/30) following the procedure suggested by MHI (refer to Appendix B). The testing is repeated with different samples. But only the representative results are plotted in the dissertation. The results for each kind of test repeated with different samples are plotted in the Appendix D.

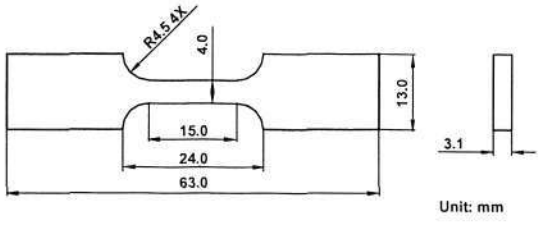

Figure 3.1 Samples' dimensions.

3.1 Glass transition temperature and thermal stability

T_g is not only the glass transition temperature, but also shape recovery temperature in thermally responsive SMPs, at which the shape memory effect (SME) is activated. At a temperature below T_g, polyurethane SMP is in the glass state and rigid with a high modulus. In this state, both the soft and hard segments of SMP are frozen in place. They may be able to vibrate slightly, but do not have any segmental motion. Hence, the bulk material is difficult to deform in this state.

If polyurethane SMP is heated gradually, the glass transition will occur. It does not occur suddenly but takes place gradually over a temperature range. Within this range, soft segments wiggle around and the heat capacity of SMP increases by an order of magnitude. In this study, differential scanning calorimetry (DSC) was used to detect the step-increase in heat capacity for determination of T_g, which is defined as the median point of the glass transition range in the heating ramp. A constant heating/cooling rate of 20°C/min was applied. The specimens used for the DSC test (PerkinElmer DSC 7) were cut out from samples as shown in Figure 3.1 and with a weight of around 10 mg. One test was carried out on one specimen.

Figure 3.2 plots the DSC curve of SMP MM3520 in one heating and cooling cycle. From it, T_g is determined as 36.7°C, which is very close to the value provided by MHI, 35°C. The glass transition occurs within a temperature range from 30°C to 40°C. Furthermore, the result reveals that this polyurethane SMP is a semi-crystalline polymer, which experiences both the glass transition and melting in the heating ramp. SMP melts at a temperature between 110°C and 180°C in the heating ramp while it

crystallizes at about 100.2°C in the cooling ramp. The melting temperature (T_m) and the crystallization temperature (T_c) are defined as the peak points in the melting range and the crystallization range, respectively.

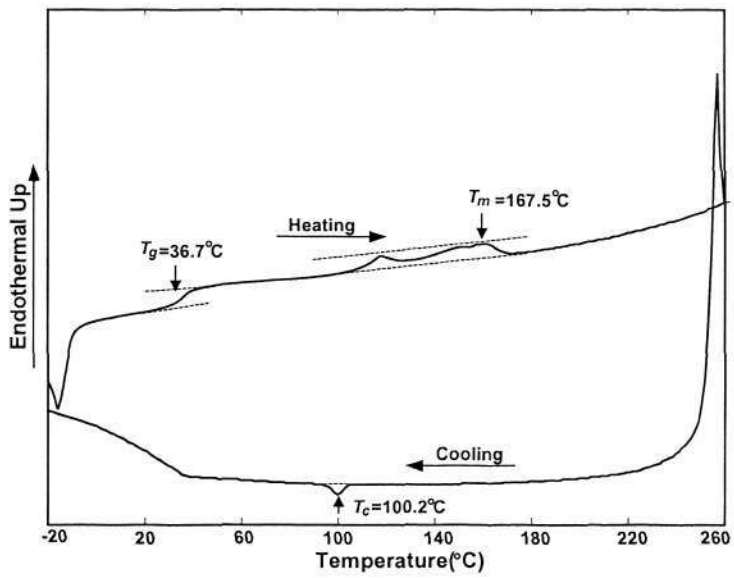

Figure 3.2 DSC result of SMP MM3520.

Thermogravimetric analysis (TGA) test was applied to investigate the thermal stability of polyurethane SMP experimentally. TGA test was carried out with a specimen weighed around 20 mg at a constant heating rate of 10°C/min purging with nitrogen gas on a PerkinElmer TGA 7. Figure 3.3 reveals that there is only a slight weight loss before heating to 260°C in SMP MM3520, which is largely attributed to the evaporation of moisture in the material. 260°C is defined as the decomposition temperature of this polyurethane SMP.

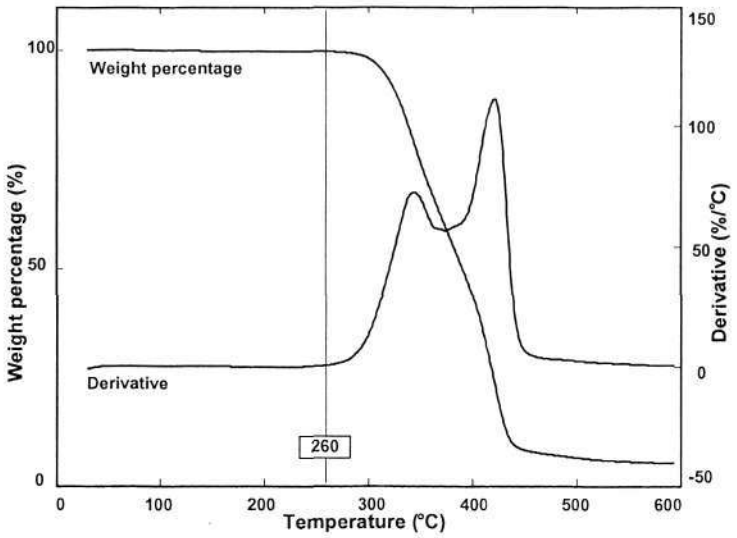

Figure 3.3 TGA result of SMP MM3520.

3.2 Dynamic mechanical properties

Dynamic mechanical analysis (DMA) was used to investigate the dynamic mechanical properties of the polyurethane SMP (MM3520). In the DMA test, a low stress is applied on a sample in a sinusoidal fashion so that the sample is always deformed elastically. For a perfectly elastic material the stress and strain are perfectly in phase. Instead of deforming reversibly under load, a perfectly viscous material flows. Under dynamic loading, its stress-strain curves are out of phase by 90° since the strain is proportional to the changing rate of the stress. The polyurethane SMP behaves in a way combining both, i.e. it simultaneously reacts elastically and flows to some extent. Therefore, its stress and strain curves are out of phase by a phase angle (δ) less than 90°. DMA is used to measure the amplitudes of stress and strain as well as δ. The storage modulus, the loss modulus and tangent delta can be recorded against the temperature. The storage modulus is the modulus of the elastic portion of material

while the loss modulus is the modulus of the viscous portion. Tangent delta is defined as the ratio of the loss modulus over the storage modulus indicating the damping capability of a material.

DMA test (PerkinElmer DMA 7) was carried out in the three-point bending mode with a 10 mm span. The specimens were heated in a hot chamber at a constant rate of 5°C/min. The viscoelastic behavior of polymers means that there is a time dependence of their properties. Thus, the mechanical vibration frequency used for DMA tests has a remarkable effect on the results (Merzlyakov M et al 1999, Zheng W et al 2003, Jiansong Zhou et al 2005). Here, a constant frequency of 1 Hz recommended in the manual of the instrument was used. The rectangular specimens with dimensions of 15×4.0×3.1mm were cut from samples as shown in Figure 3.1. The DMA result for SMP MM3520 plotted in Figure 3.4 reveals that the storage modulus, which corresponds to the stiffness of the material, decreases sharply in the glass transition region. The ratio of storage modulus in the glass state to that in the rubber state is up to 200~300 in this SMP. Furthermore, tangent delta reaches its maximum of about 1.45 during the glass transition, while the tangent delta of a typical rubber is 0.2~0.4. Thus, in the glass transition region the polyurethane SMP can be used as a good damping material for dissipating strain energy. The temperature corresponding to the peak of tangent delta is an alternative definition of T_g. T_g defined in this way is determined to be 35°C, which is slightly lower than that obtained from DSC. The small difference can be ascribed to the higher heating rate applied in the DSC test, which results in a slight lag in the transition. Note that the sample used for the DMA test was much bigger than

that used for the DSC test. In order to get the reliable testing results, a lower heating rate was applied in the DMA test in order to heat the sample more evenly.

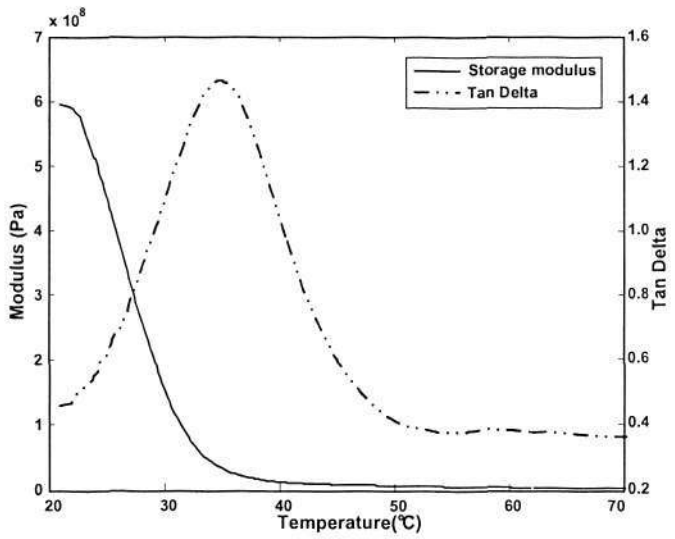

Figure 3.4 DMA result of SMP MM3520.

3.3 Uniaxial tension in the glass state

Uniaxial tensile tests were carried out to investigate the behavior of the polyurethane SMP under uniaxial tension. In these tests, the SMP samples were stretched unaxially at a constant strain rate at room temperature (about 22°C) on an Instron 5569 as shown in Figure 3.5. Note that at room temperature the polyurethane SMP is in the glass state.

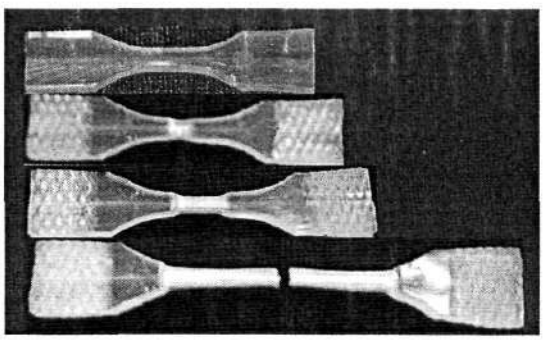

Figure 3.6 Illustration of uniaxial tension at room temperature.

Figure 3.7 presents the strain-stress relationships of SMP MM3520 in some loading/unloading tests. In these tests, the SMP samples were loaded to different maximum strains, namely, 20%, 50% and 100%, and then unloaded to zero stress. The constant loading/unloading strain rate was 10^{-3} /sec. It reveals that upon unloading, the recovery is largely attributed to the elastic recovery, in particular at the early unloading stages in the small maximum strain case.

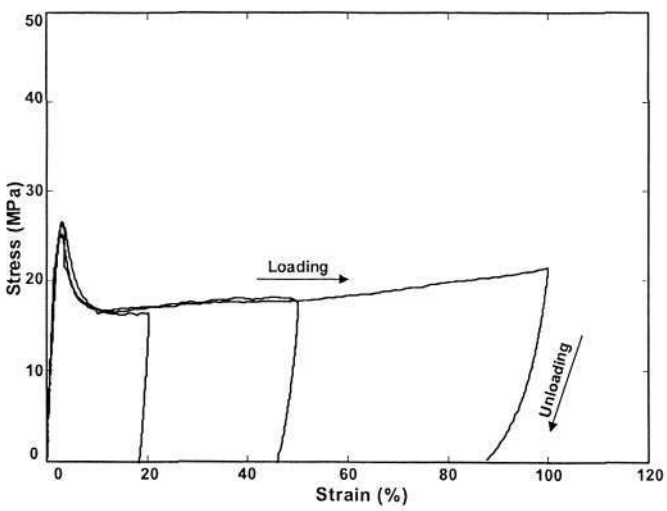

Figure 3.7 Strain vs. stress relationships of SMP MM3520 in loading/unloading test.

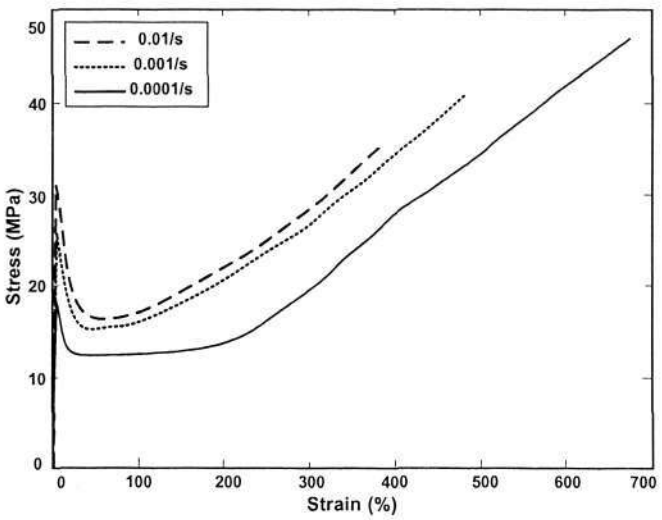

Figure 3.5 Strain vs. stress relationships of SMP MM3520 at room temperature.

Figure 3.5 plots the strain vs. stress relationship of SMP MM3520 at room temperature under different strain rates. Note that unless otherwise specified, all strain and stress are engineering strain and engineering stress. It shows that similar to that in mild steels, after a small linear elastic deformation, this material experiences a distinct upper yield point, followed by an apparent plateau and then hardening in all tested strain rates. The yielding-plateau phenomenon is similar to the well-known Luder band phenomenon, in which necking and propagation can be observed upon stretching. This is evidenced by Figure 3.6. The hardening is a result of the reorientation of polyurethane SMP molecular chains, which induces crystallization. The elongation limit of this material is over 300% in terms of the engineering strain, and increases with the decrease of the strain rate. Furthermore, the yield strength increases with the increase of the strain rate, while the ultimate strength is opposite.

In order to check whether the remaining strain after unloading is recoverable, the SMP samples were heated up gradually atop a digital hot plate. Figure 3.8 shows that a SMP sample can virtually fully recover its original shape upon heating over its T_g after a pre-stretching to 100% strain. It demonstrates that there is no apparent permanent deformation in this polyurethane SMP even when pre-stretched up to 100% strain in its glass state. Unlike that upon stretching, the recovery is rather uniform everywhere. No propagation phenomenon can be found.

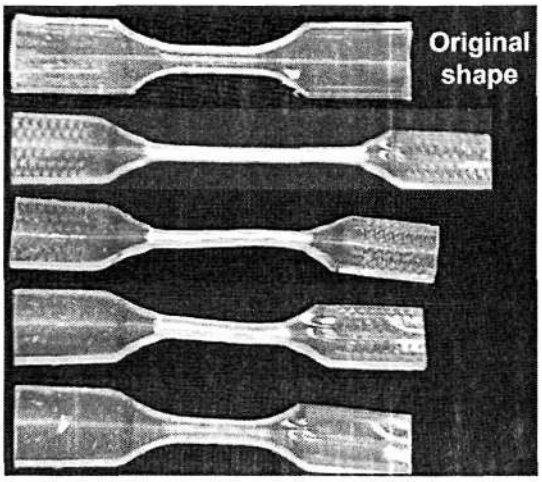

Figure 3.8 Illustration of Recovery of SMP MM3520 after stretching at room temperature.

3.4 Uniaxial tension in the rubber state

Uniaxial tensile tests were carried out at different constant strain rates and at T_g + 15°C, where the polyurethane SMP is in the rubber state. Here, T_g is taken to be 36.7°C, which was obtained from the previous DSC test. The obtained stress-strain responses are plotted in Figure 3.9, which reveals the typical viscoelastic properties of the

polyurethane SMP MM3520. At all strain rates, the elongation limit is above 600% strain, but the exact stress-strain response is highly strain rate dependent. At a high strain rate of 0.1/sec, the curve closely resembles that in the glass state, while at low strain rates the curve is dominated by creep, where the extension increases continuously with very little variation in the applied force.

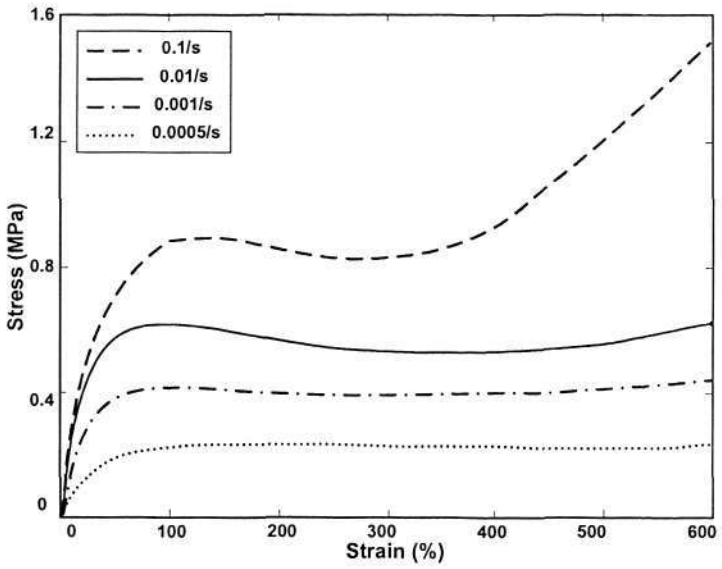

Figure 3.9 Strain vs. stress relationships of SMP MM3520 at T_g +15°C.

To investigate the strain recovery properties of the polyurethane SMP (MM3520), loading/unloading uniaxial tensile tests were conducted following the procedure described below (refer to Figure 3.10),

a. Stretch the sample uniaxially to a prescribed maximum strain (ε_m), e.g., 50%, at a constant strain rate ($\dot{\varepsilon}$) and a temperature above T_g;

b. Unload to zero stress at the same constant strain rate ($\dot{\varepsilon}$) and temperature;

c. Hold the sample at this temperature for a given period of time, e.g., 40 minutes, without any external load applied.

As illustrated in Figure 3.10, ε_e, ε_t, ε_h and ε_i denote the elastic strain, total instant recovery strain upon unloading, free recovery strain during holding (without any external load), and final residual strain, respectively. In the deformation of viscoelastic polymer materials, ε_m can be defined as (Clegg and Collyer 1986)

$$\varepsilon_m = \varepsilon_e + \varepsilon_r + \varepsilon_i \tag{3.1}$$

where ε_r is the rubber elastic strain. Practically, the elastic strain (ε_e) is part of the total instant recovery strain (ε_t). Hence,

$$\varepsilon_m = \varepsilon_t + \varepsilon_h + \varepsilon_i \tag{3.2}$$

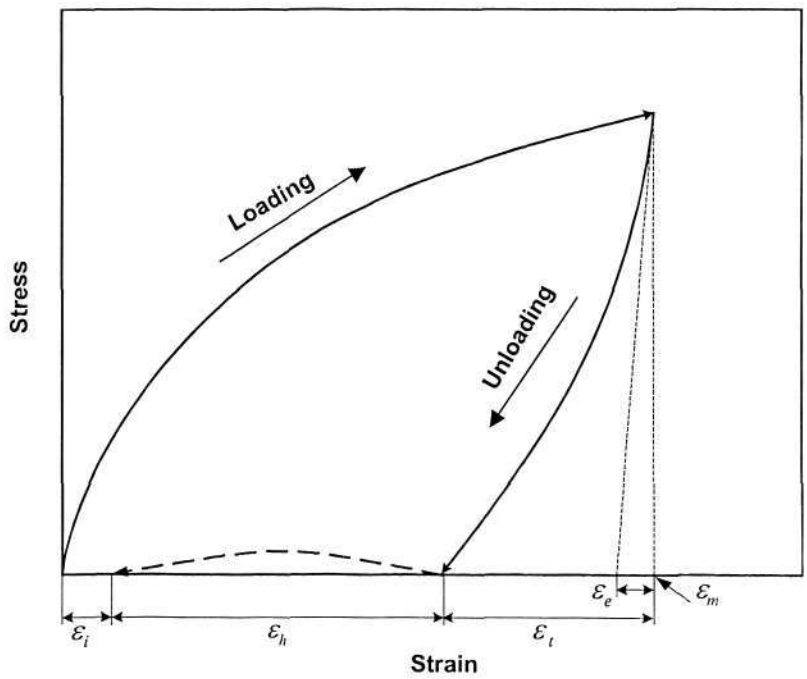

Figure 3.10 Procedure of loading/unloading uniaxial tensile test.

Results of loading/unloading tensile tests carried out at four different strain rates at T_g+15°C following the above procedure are plotted in Figure 3.11. It shows that, in general, the recovery is almost complete. The residual strain (ε_i) is a very small portion of ε_m and decreases continuously upon further holding. Thus, ε_i can be attributed largely to the viscous flow, and the contribution of reorientation in polymer chains should be limited. The result also reveals that a higher strain rate results in more instant recovery strain. It is known that, if $t << \tau$, the strain energy can be stored in a polymer by quick mechanical deformation at a temperature above T_g (Wineman and Rajagopal 2000). Here, t is the deformation time and τ is a characteristic relaxation time for a polymer at this temperature. Recovery happens upon unloading, which indicates the return of the stretched polymer chains to more equilibrium and coiled conformations. Thus, quick deformation is preferred for more recoverable strain.

Furthermore, Figure 3.11 shows that a large portion of ε_m (up to 20%) is ε_h, i.e. the polyurethane SMP only can partially recover upon mechanical unloading, and a significant amount of strain can be recovered only gradually with the elapse of time. The strain recovery, especially, ε_t, is highly dependent on the strain rate. With the increase of strain rate, ε_t becomes smaller while ε_h increases. Since ε_i mainly is ascribed to the viscous flow of a material that is highly dependent on the strain rate, ε_i increases with the strain rate. Therefore, in the applications of polyurethane SMP, an instant load is preferred, so that the pre-strain in a polyurethane SMP can be fully recovered upon heating to above T_g.

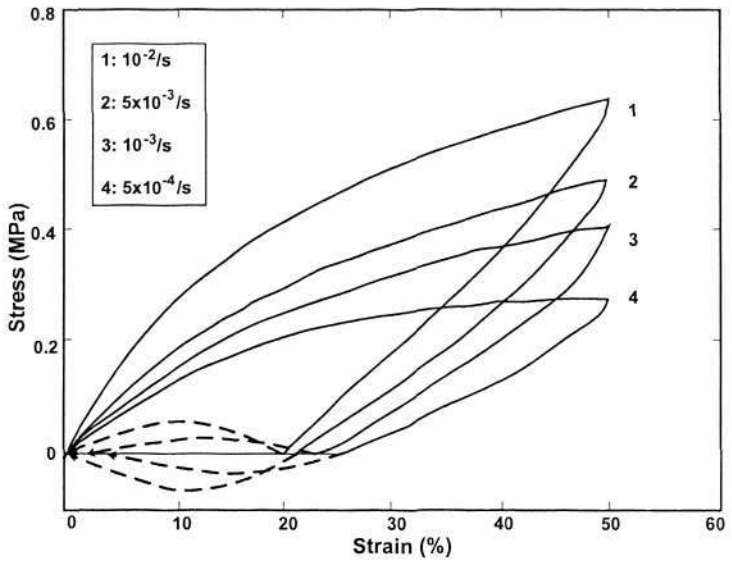

Figure 3.11 Results of loading/unloading tensile tests at four different strain rates and at T_g+15°C.

In order to investigate the dependence of strain recovery on temperature and deformation, the SMP samples were loaded to a maximum strain (50%) and then unloaded to zero stress at a constant strain rate of 10^{-2}/s at four different temperatures all above T_g. The resultant stress-strain curves are plotted in Figure 3.12. It reveals that ε_t deceases while ε_i increases with the increase of temperature. At a low temperature, the polyurethane SMP can instantly recover more upon unloading than that at a high temperature. As the polyurethane SMP is easier to deform at a high temperature, a smaller stress is required for reaching the same strain. At above T_g the polyurethane SMP, as a viscoelastic material, shows more viscous properties at a high temperature, while the strain induced by viscous flow cannot be fully recovered immediately. Hence, ε_i increases with the temperature as shown in Figure 3.12. Thus, the working

temperature range of this SMP is suggested to be from T_g+5°C to T_g+10°C for better instant recovery.

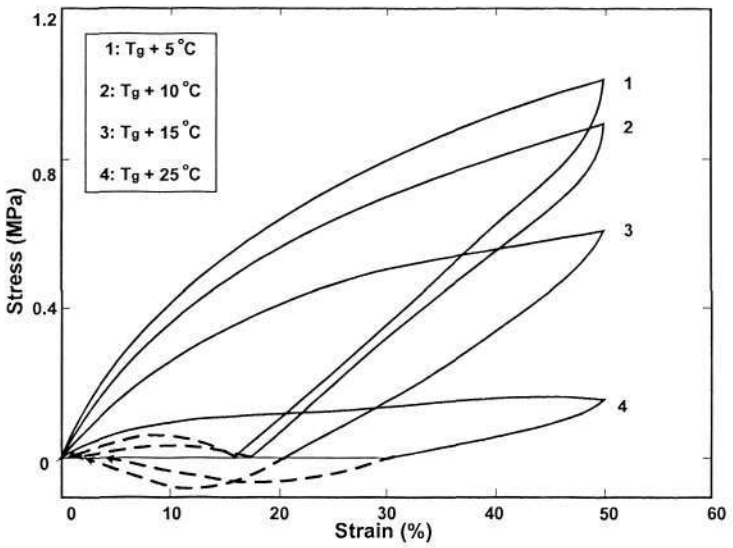

Figure 3.12 Results of loading/unloading tensile tests at a constant strain rate of 0.01/s at different temperatures.

The dependence of strain recovery upon the maximum pre-strain was investigated by a series of cyclical tensile tests. In these tests, the samples were loaded to different maximum strains and then unloaded to zero stress at a strain rate of 10^{-2} /s and at T_g+5°C. The maximum pre-strains were from 50% to 600% in a 50% interval.

The relationships of stress vs. strain in these tests are plotted in Figure 3.13. As we can see, the envelop formed by these cycles coincides with the stress-strain curve of the single extension test quite well. The SMP samples experience obvious "creeping" in the strain range from 100% to 300% and then hardening due to the reorientation and

crystallization of the material. Loading/unloading cycling shares the same effect on the stress-strain behavior as the single stretching test.

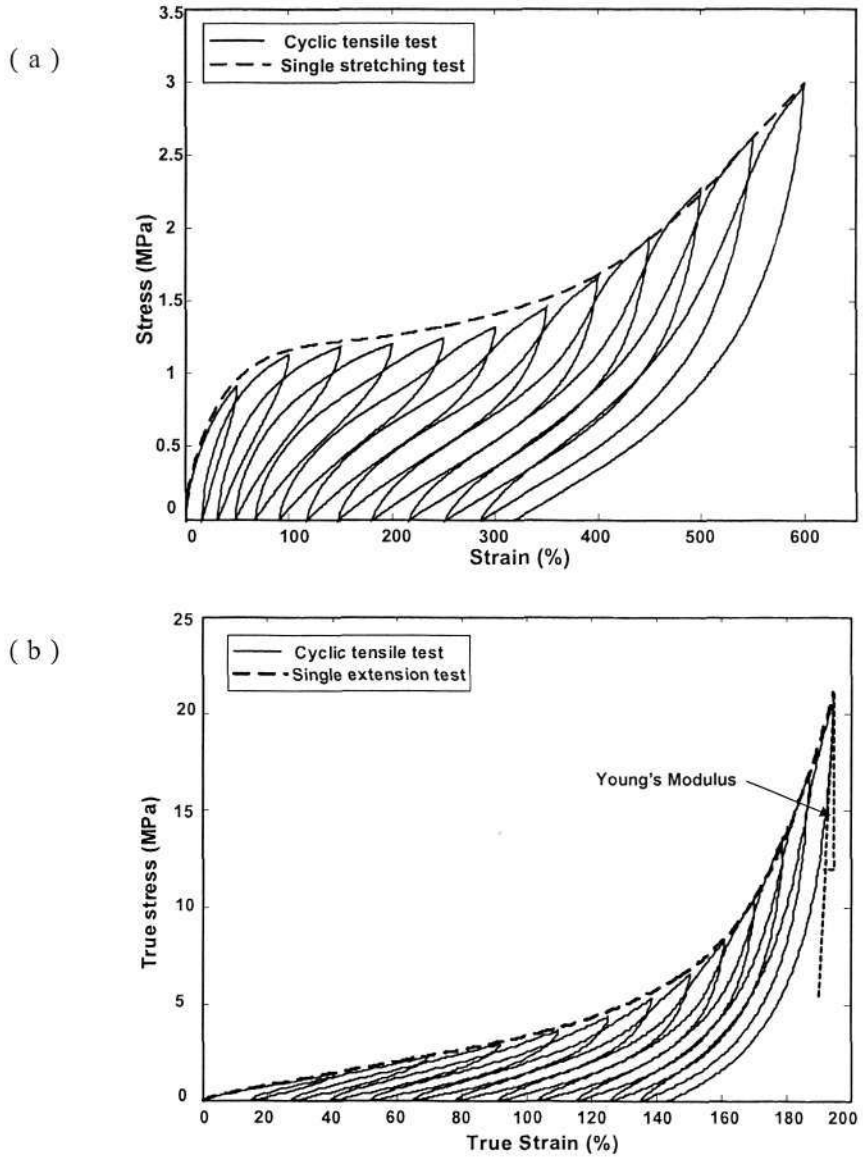

Figure 3.13 Results of cyclic tensile test and the single stretching test at a constant stain rate of 0.01/s at T_g +5°C. (a) Engineering stress vs. engineering strain; (b) true stress vs. true strain.

In Figure 3.14, the ratio of total instant recovery is plotted against the maximum strain. The ratio of total instant recovery is calculated as the total instant recovery strain over the maximum strain in a cycle. It reveals that, generally, the ratio decreases with the increase of the maximum strain. The decrease is more obvious at a maximum strain above 200%. It is negligible in a maximum strain range from 100% to 200%. As we can see from the results, the material is hardened at above 200% due to the reorientation and crystallization of the polymer chains. Thus, the decrease in the total instant recovery ratio can also be attributed to reorientation and crystallization.

Furthermore, there is a one-step sudden decrease in the ratio of total instant recovery, which may be a result of the decoupling in the imperfect crystalline part of polymer in the first two cycles (Tobushi et al 1996).

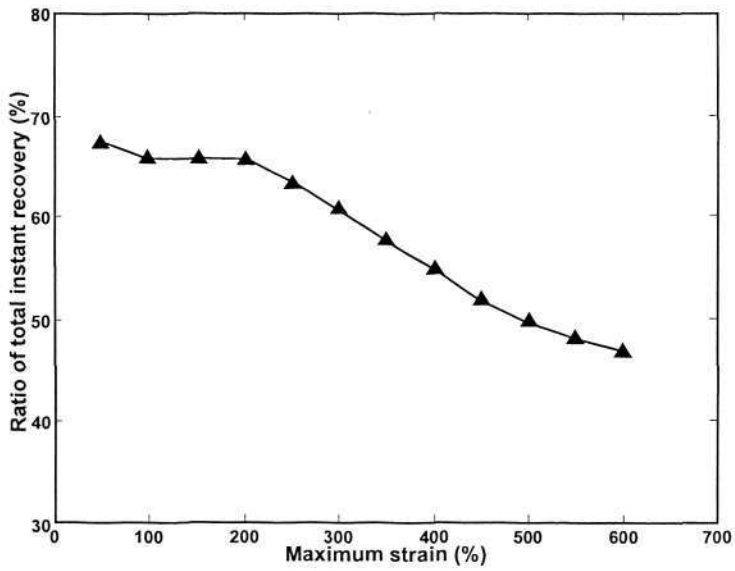

Figure 3.14 Ratio of total instant recovery at different maximum strains.

The evolution of the Young's modulus with changes in the maximum strain is plotted in Figure 3.15. The Young's modulus was calculated from the linear portion of the true stress- true strain curve at the beginning of unloading in each cycle. It shows that the Young's modulus decreases in the first two cycles. This is due to the fact that the polymer chains with imperfect crystalline part are decoupled in these two cycles at the beginning of the test (Tobushi et al 1996). After that the Young's modulus increases gradually until 250% strain. Beyond that, it increases almost linearly due to the hardening resulted by the reorientation and crystallization of the polymer chains.

At this point we may conclude that the polyurethane SMP is better for applications with a maximum strain below 200% for a high ratio of total instant recovery of over 60% at T_g+5°C. Above that maximum strain, hardening of the SMP results in the increase of the Young's modulus and the decrease of the ratio of total instant recovery.

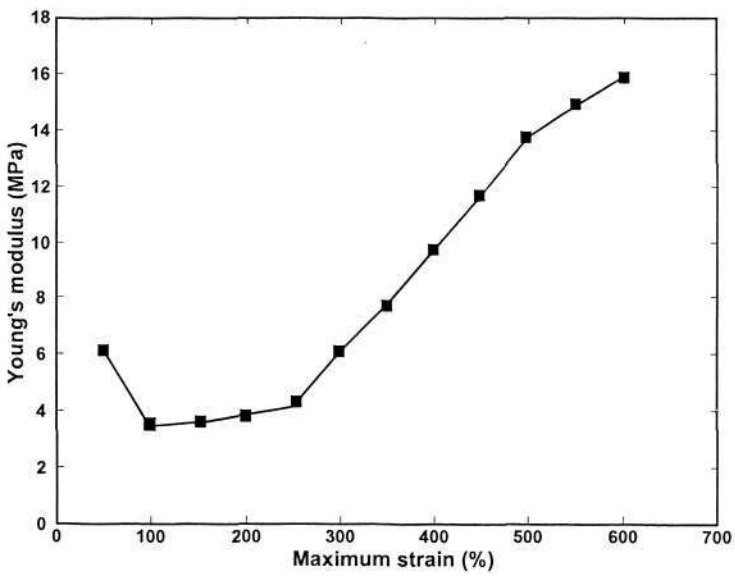

Figure 3.15 Evolution of Young's modulus with the maximum strain.

The stability of shape recovery properties of the polyurethane SMP was investigated experimentally by cyclic tensile tests at a constant maximum strain of 100%, a constant strain rate of 0.01/ s and T_g +5°C. One hundred cycles were carried out on polyurethane SMP MM3520. Figure 3.16 plots some of the results. It shows stress desreases with the increase of the cycle number. But the decrease is sharp at the beginning and then becomes gradual. This can be explained as follows: the loading distorts the polymer chains to trigger viscous flow. This distortion causes the reorientation of polymer chains and thus results in the decrease of stress. But the reorientation is rather limited by the physical links among the polymer chains. Thus, after a sufficient number of cycles and over a long period of time, the reorientation and viscous flow become stable gradually (Wineman and Rajagopal 2000).

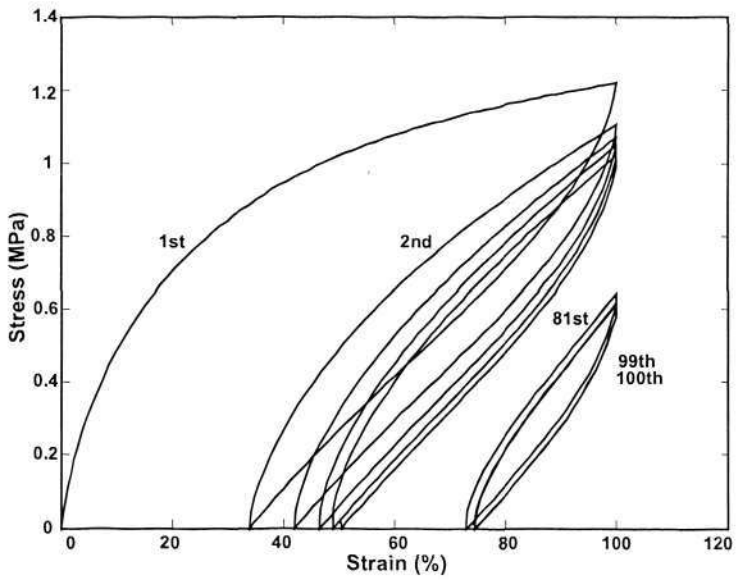

Figure 3.16 Stress-strain relationship of SMP MM3520 in cyclic tensile test at a constant maximum strain of 100% and T_g +5°C.

For a better view, the time/cycle number vs. strain relationship is plotted in Figure 3.17, where the strain at the bottom point of each cycle corresponds to the residual strain after unloading. It reveals that the residual strain, corresponding to zero stress, increases substantially in the first twenty cycles and then becomes gradual. After about forty cycles, a stabilized instant recoverable strain of about 30% can be obtained. This can be ascribed to the slow-down or cease of the viscous flow of polymer after many cycles in a long period of time.

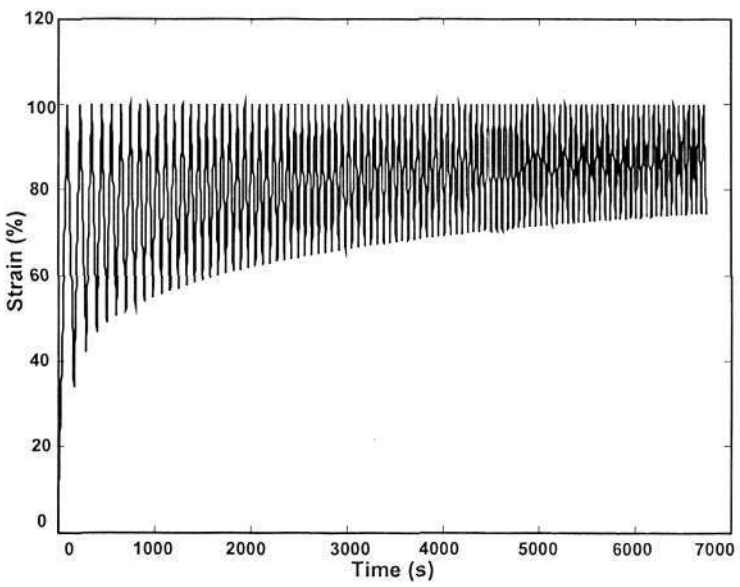

Figure 3.17 Time/cycle number vs. strain relationship of SMP MM3520 in cyclic tensile test with a constant maximum strain of 100% at T_g +5°C.

3.5 Summary

During the glass transition, the dynamic mechanical properties of the polyurethane SMP change abruptly. Its storage modulus slumps by 200~300 times while its damping ratio increases to 1.45. It appears to be a good damping material for efficient energy

dissipation. The polyurethane SMP is thermally stable as it only loses a little weight due to the evaporation of moisture before the decomposition starts at 260°C in a nitrogen environment.

The polyurethane SMP has an elongation limit of over 300%, and experiences the yielding and hardening in uniaxial extension in the glass state. On the other hand, it has an elongation limit of over 600% and behaves just like a typical visoelastic material upon loading in the rubber state.

The thermomechanical behavior and shape recovery ability of the polyurethane SMP are highly dependent on the strain rate, temperature and the maximum strain. Polyurethane SMP can almost fully recover a pre-strain loaded below and above its T_g. For more strain recovery, higher strain rate is preferred during loading. Furthermore, it is preferable for the polyurethane SMP to deform in a temperature range from T_g+5°C to T_g+10°C for more recoverable strain, especially for more instant recoverable strain. Since severe hardening at over 200% strain results in some irreversible strain, the polyurethane SMP is advised to be used under a strain less than 200%.

The stability of shape recovery properties of the polyurethane SMP shows strong dependence on the cycle number. Upon cycling, the total instant recoverable strain deteriorates and the stress corresponding to the maximum strain decreases. However, the total instant strain recovery almost stabilizes after enough number of loading/unloading cycles.

Chapter 4 Effects of Moisture on Glass Transition Temperature and Applications

Moisture is one of the most important environmental factors which may have significant effects on the properties of polyurethane SMPs. It is necessary to know the reliability of SMPs under different environments, for instance, a humid environment. This chapter will address the effects of moisture on T_g of SMP, which is also shape recovery temperature, a key parameter for SMP applications. Furthermore, the mechanism behind the effects of moisture on T_g was investigated. Upon understanding the effects of moisture on T_g , two new features were proposed for potential applications of SMP.

4.1 Moisture absorption in room temperature water

In order to study the moisture absorption of the polyurethane SMP, the hot pressed SMP sheets (MM3520, refer to Appendix A) with a thickness of about 1.0 mm were immersed into room temperature water. After different hours of immersion, these sheets were taken out of water and blow with an air gun to remove water from the surface. Then they were cut into small pieces for TGA test to determine the moisture fraction in them. In the test, thin samples around 20 mg sliced from the SMP sheet were heated in a TGA 2950 (TA Instruments) from 30°C to 330°C at a heating rate of 20°C/min. Note that because the TGA results were used together with the DSC results

for analysis later on, the heating rate for TGA tests must be the same as that for DSC tests.

Figure 4.1 presents two sets of TGA results after different hours of immersion. Note that all samples start to decompose at about 260°C, which can be seen from the rapid decrease in weight fraction. As expected, weight loss becomes more significant with the increase of immersion time. In the samples that were immersed in water for more than 12 hours significant weight loss gradually emerges at between 100°C and 180°C before decomposition. This loss could be attributed to the evaporation of absorbed water in the polymer. For convenience, the weight fraction at 240°C was chosen as the reference for comparisons of results in the subsequent study. This means that the total loss of weight at 240°C is roughly taken as the total amount of water absorbed in the samples, though some water may still evaporate at above 240°C before decomposition occurs.

Figure 4.2 further summarizes the weight ratio of water (R_e) to SMP vs. immersion time. Note that R_e is obtained by the following equation,

$$R_e = w/(1-w)\times 100\% \tag{4.1}$$

where w is the loss of weight of SMP at 240°C in the TGA test. Figure 4.2 shows that the moisture content in the material increases at the beginning and gradually becomes almost constant after 240 immersion hours. Thus, the sample after 240 immersion hours can be taken as saturated. At the saturated state in room temperature water, there is about 4.8% water in weight.

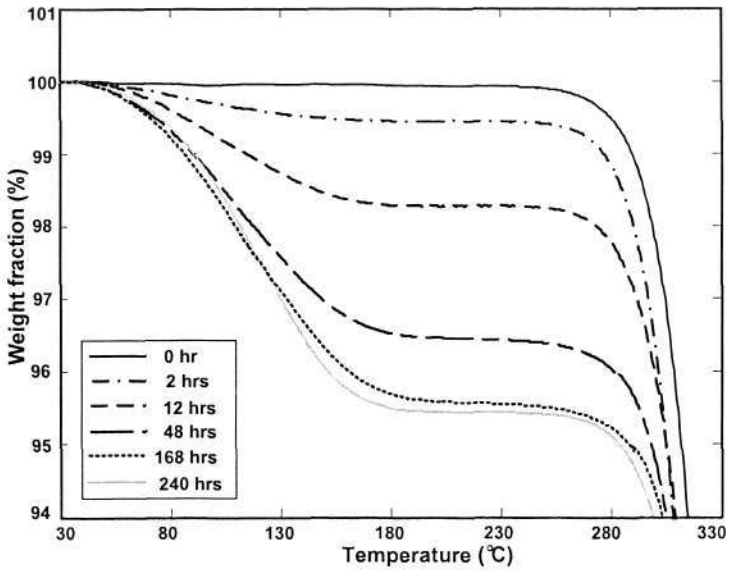

Figure 4.1 TGA results of SMP after immersed in water for different hours.

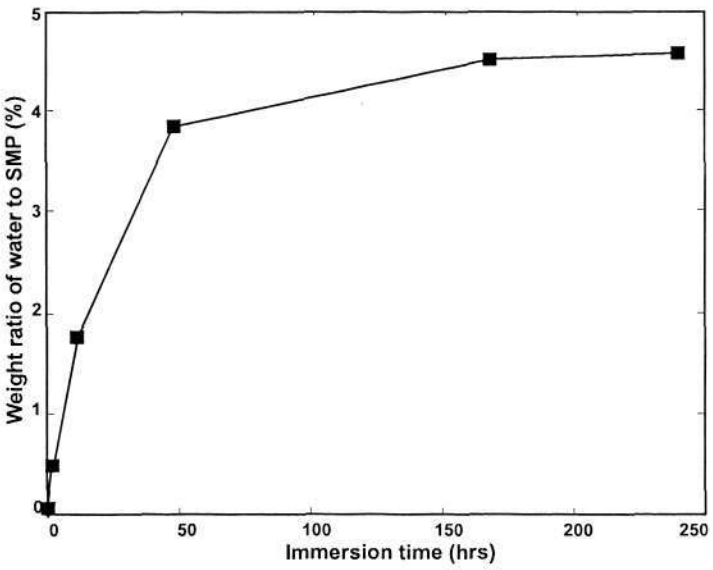

Figure 4.2 Ratio of water to SMP in weight vs. immersion time.

4.2 Glass transition temperature after immersion

In addition, DSC tests were carried out on these specimens using DSC 2920 (TA Instruments) to examine the change of T_g after immersion in water for different hours. The specimens for testing weighed around 10 mg and the constant heating/cooling rate was 20°C/min. T_g was taken at the median point in the range of glass transition during heating process.

Figure 4.3 plots the DSC results of these specimens. It reveals that T_g decreases remarkably with the increase of immersion time. For a better illustration, T_g, together with the onset and end of T_g, against the immersion time was summarized in Figure 4.4. Note that the onset and end of T_g were obtained by drawing a tangent to the inclining portions of DSC curve in the glass transition region at the start and finish parts, respectively. It shows that with the increase of immersion time T_g decreases significantly; it dropped by about 35°C after 240 immersion hours. The decrease is rapid at the beginning and becomes more moderate as the immersion time is prolonged. For immersion time more than 168 hours, the samples are close to a saturated state and the change in T_g with immersion time is minor. Moreover, it also reveals that the temperature range of glass transition is widened from about 10°C to 40°C with the increase of immersion time.

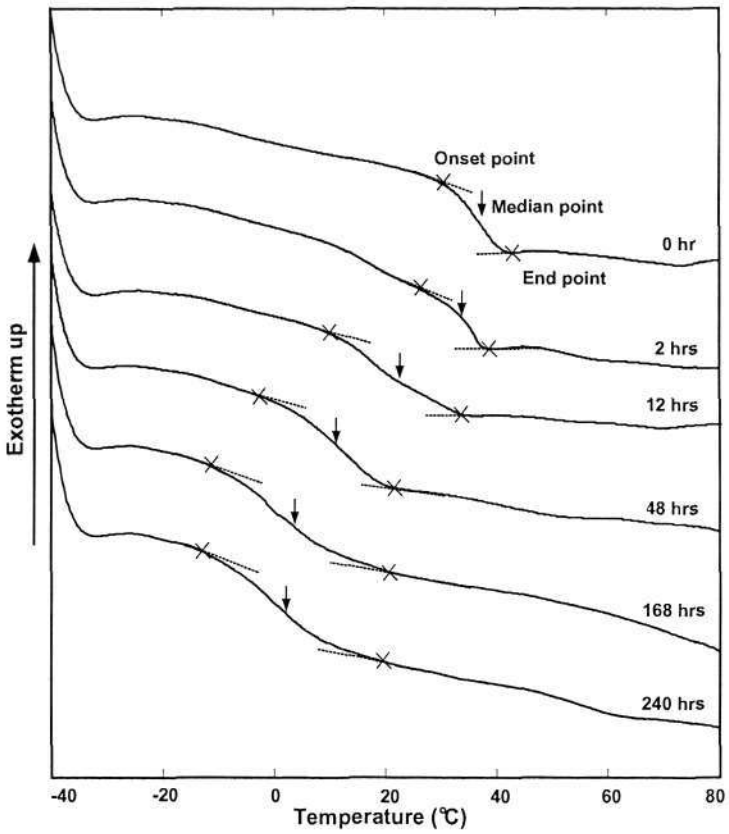

Figure 4.3 DSC results after immersion in water for different hours.

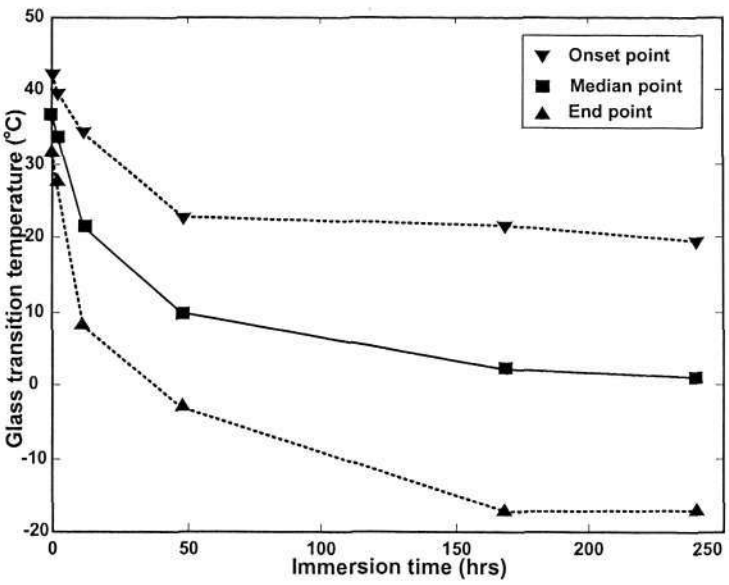

Figure 4.4 Changes of T_g with the immersion time.

4.3 Evolution of glass transition temperature upon thermal cycling

The results from the previous sections show that the absorbed moisture can significantly decrease T_g of SMPs. A very important issue in materials processing and applications is whether T_g can be restored to its original value via dehydration since in most of the engineering applications it is important to have a reliable and stable material. In order to answer this question, cyclic DSC tests were carried out on the SMP samples after different immersion hours. In each cycle, the sample was first heated from -20°C to a selected temperature and then cooled back to -20°C at a constant heating/cooling rate of 20°C/min. In each test carried out on the same sample, six temperatures, 80°C, 100°C, 140°C, 160°C, 180°C and 240°C, were selected for heating in increasing order.

Figures 4.5 (a) and (b) plot one typical cyclic DSC result and the zoom-in view of the saturated SMP after 240 hrs immersion. It is found that T_g changes distinctly upon both heating and cooling in the temperature range from 140°C to 180°C. The evolution of T_g with heating temperature is plotted in Figure 4.6. It shows that with the increase in heating temperature, T_g gradually approaches its original value of 35°C. When heating to below 100°C, the increase in T_g is minor. The increase is more significant upon heating to over 100°C up to 180°C, which almost coincides with the temperature range where the evaporation of water takes place as shown in Figure 4.1. Further heating to 240°C can bring T_g almost back to its original value.

A significant part of the moisture is removed from the sample at a temperature above 100°C (Figure 4.1). Thus, the restoration of T_g can be directly attributed to the evaporation of moisture. Since the moisture is removed only through evaporation, the whole process is reversible, thus, T_g can be reduced if samples are immersed into water again, but after that T_g also can be restored by heating the samples to 180°C or above. From an engineering application point of view, 180°C appears to be the critical temperature for refreshing the SMPs.

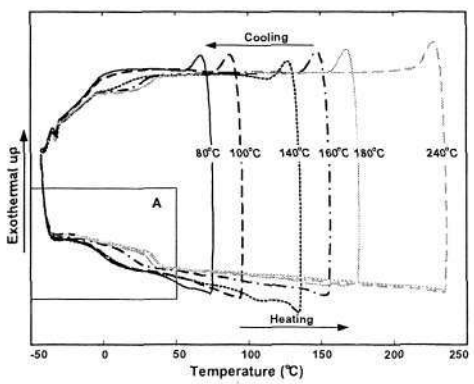

(a)

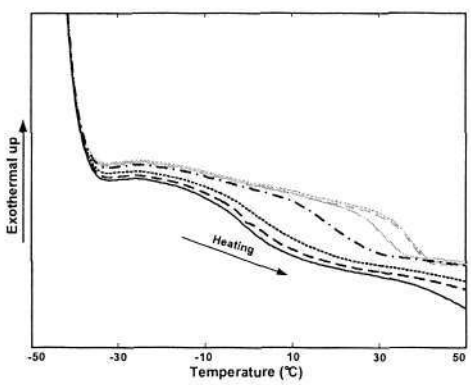

(b)

Figure 4.5 Cyclic DSC curves of saturated SMP. (a) Overall view; (b) zoom-in of A.

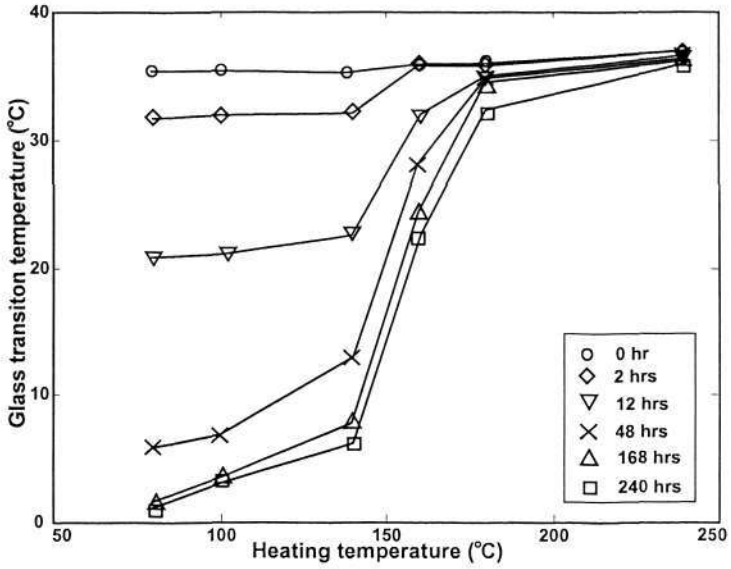

Figure 4.6 Evolution of T_g upon thermal cycling.

4.4 Interaction between water and the polyurethane SMP

At this point, we have demonstrated that moisture has a strong influence on the glass transition of the polyurethane SMP. However, the mechanism behind this phenomenon remains unknown. The following sections aim to identify the exact mechanism behind the effects of moisture on T_g of SMP, in particular, the interaction between water and polyurethane SMP.

In this study, FTIR spectroscopy was used to identify the interactions of water with the SMP. The specimens for FTIR tests were thin polyurethane SMP sheets with a thickness of 1.0 mm. FTIR spectra were collected by averaging 70 scans at a resolution of 4 cm^{-1} in a reflection mode from a FTIR spectrometer (Nicolet Magna IR-560).

The full FTIR spectrum of the polyurethane SMP at room temperature without immersion in water is presented in Figure 4.7. Some peaks of our interest in this study are marked according to some references (Yen et al 1999, Luo et al 1997, Yoon et al 2000). It shows that the strong hydrogen bonding is evidenced in the polyurethane SMP where the infrared band of the bonded N-H stretching occurs at 3289 cm^{-1} while that of free N-H stretching occurs at 3498 cm^{-1}, on the other hand, the infrared band of free C=O stretching at 1724 cm^{-1} shifts to that of the bonded one at 1701 cm^{-1}.

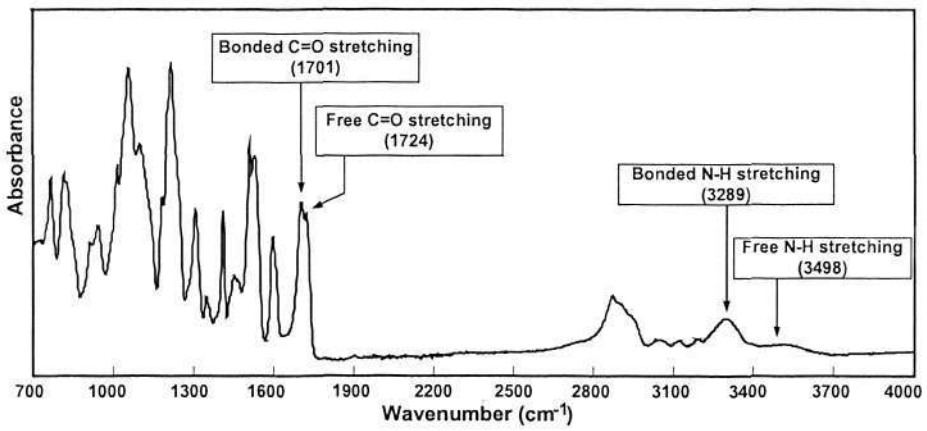

Figure 4.7 FTIR spectra of polyurethane SMP without immersion.

Figures 4.8 (a) and (b) give the FTIR spectra for samples after different immersion hours in the N-H and C=O stretching regions, respectively. Figure 4.8 (a) shows that the infrared band intensity of hydrogen bonded N-H stretching has no significant change as compared with that of the free N-H stretching. However, with the increase of immersion time the infrared band of hydrogen bonded N-H stretching shifts to a higher frequency. The shift is more significant in samples with short immersion times and becomes stable in samples with immersion times longer than 48 hours. On the other

hand, Figure 4.8 (b) shows that after immersion the infrared band of hydrogen bonded C=O stretching shifts to a lower frequency slightly. Furthermore, with the increase of immersion time the infrared band intensity of bonded C=O stretching becomes more striking as compared with that of free C=O stretching, which indicates that a longer immersion time results in more C=O groups being involved in hydrogen bonding.

The heating process mentioned above has a direct influence on the absorbed water in the polymer. The FTIR spectra of the saturated polyurethane SMP sample after 240 hours of immersion under different heating temperatures in the heating process are plotted in Figure 4.9. As revealed in Figure 4.9 (a), with the increase of heating temperature both the infrared band position and the intensity of the hydrogen bonded N-H stretching shift back to their original values of a dry sample as shown in Figure 4.8 (a). Meanwhile, as shown in Figure 4.9 (b), the infrared band of the bonded C=O stretching not only shifts to a higher frequency almost identical to that of dry samples but also regains its dominance among the intensities (Figure 4.8 (b)).

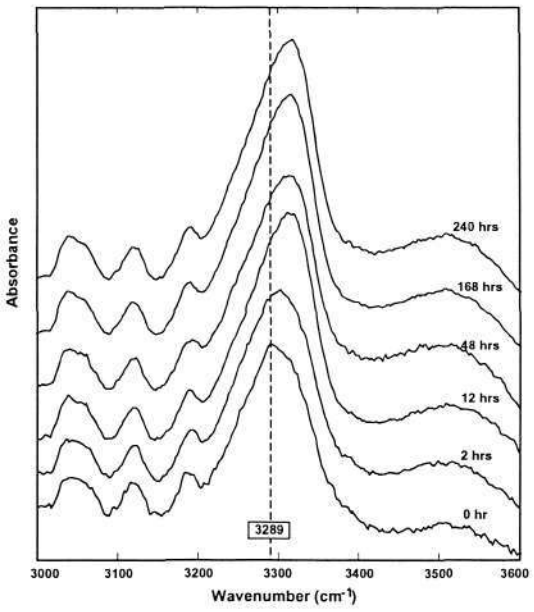

(a)

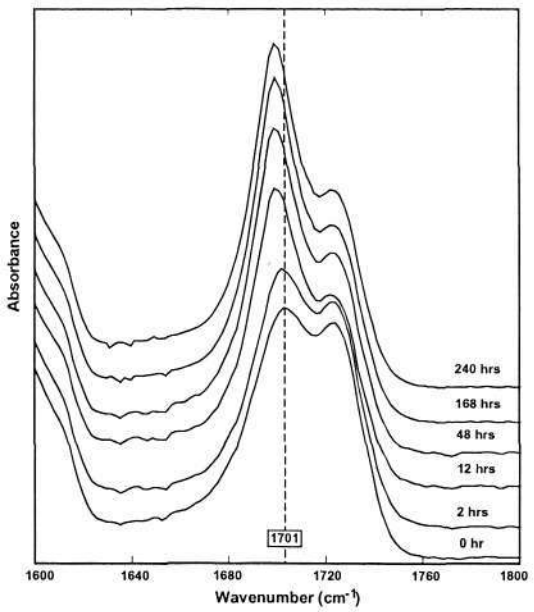

(b)

Figure 4.8 FTIR spectra of polyurethane SMPs after different immersion hours. (a) N-H stretching region, (b) C=O stretching region.

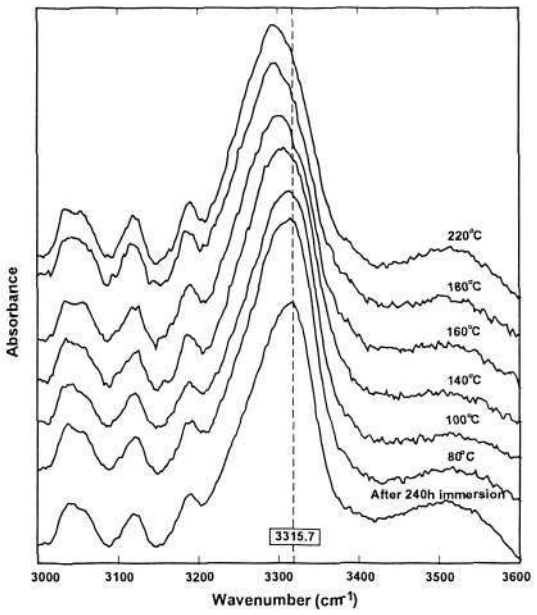

(a)

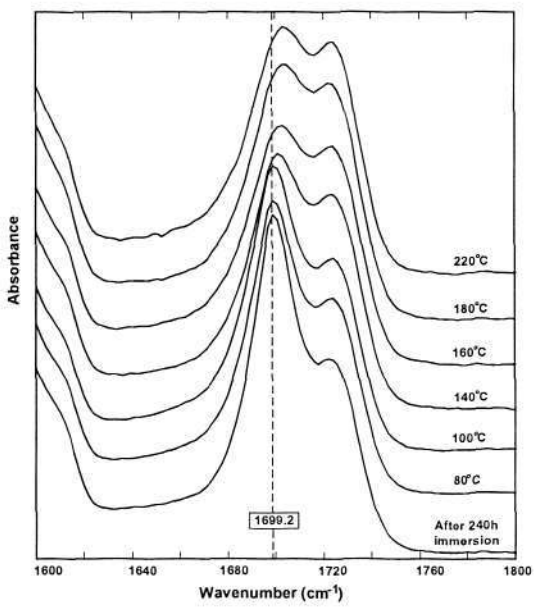

(b)

Figure 4.9 FTIR spectra of saturated samples (240 hours of immersion) after heating to different temperatures. (a) N-H stretching region, (b) C=O stretching region.

4.5 Correlation among moisture, glass transition temperature and hydrogen bonding

Utilizing the data obtained from previous tests, namely the TGA and DSC tests, the relation between T_g and ratio of moisture to SMP in weight % for all SMP samples in immersion and heating processes can be found. In Figure 4.10, samples upon different immersion time and then heated to different temperatures were found to have similar slanted L-shaped curves relating T_g and water content. The change in T_g is clearly divided into two stages. At a lower heating temperature, the transition temperature is kept almost constant despite the continuous reduction of water content. However, beyond a critical temperature, T_g starts to increase linearly with further decrease in water content. Note that there is a turning point in the L-shaped curve during the heating process in Figure 4.10. Referring to the water ratio in weight % at this turning point in the TGA heating curve in Figure 4.1, the critical temperature can be identified as being 120°C.

The heating temperature of 120°C discovered from Figure 4.10 and 4.1 has a physical significance, as the total absorbed water in the polyurethane SMP can be divided into two parts, namely, free water and bound water (Herrera-Gómez et al 2001). Bound water can be removed from the polymer only at a higher heating temperature. In this case, the critical heating temperature is around 120°C and bound water moves out of the polymer in an approximate linear fashion with the increase of heating temperature. Regarding free water, all horizontal segments in Figure 4.10 indicate that free water has negligible effect on T_g.

As shown in Figure 4.10, the lines for the immersion and heating processes have an intersection in the minus zone of moisture content. This point corresponds to the real dry state of polyurethane SMP. That is to say, at 240°C where we take as reference in the above-calculation, there is still some moisture trapped in the material. The real ratio of moisture to SMP in weight, R, can be obtained by

$$R = \left(R_t + R_e\right) \Big/ \left(1 - R_t\right) \tag{4.2}$$

where R_t is the positive valued ratio of moisture to SMP composite in weight at the intersection point (Figure 4.10), and R_e is the measured ratio of moisture to SMP in weight based on the weight of sample at 240°C.

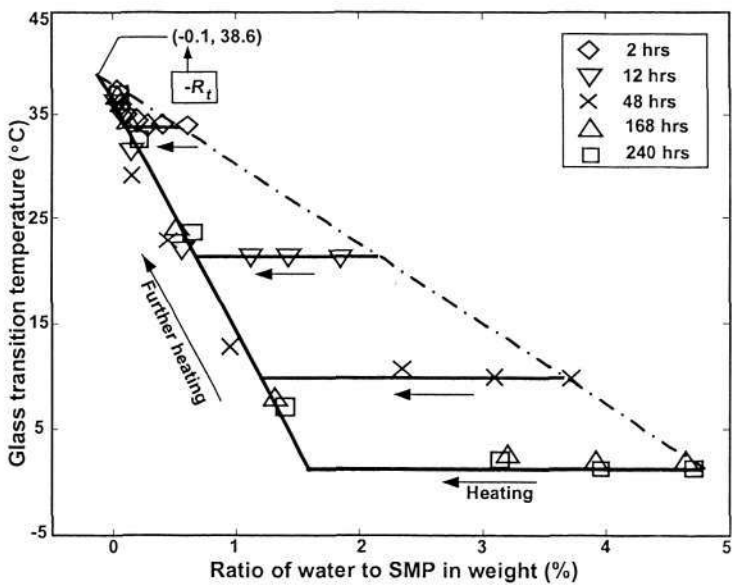

Figure 4.10 T_g vs. ratio of water to SMP in weight %.

The amounts of free and bound water during immersion process now can be further identified by applying Equation 4.1. Using the two segments in those slanted L-shaped

curves, the ratios of free, bound and total absorbed water in the polymer can be determined as functions of immersion time, as shown in Figure 4.11. It reveals that moisture absorption increases dramatically in the first 48 hours of immersion and is predominant in free water form than in bound water form at any instant.

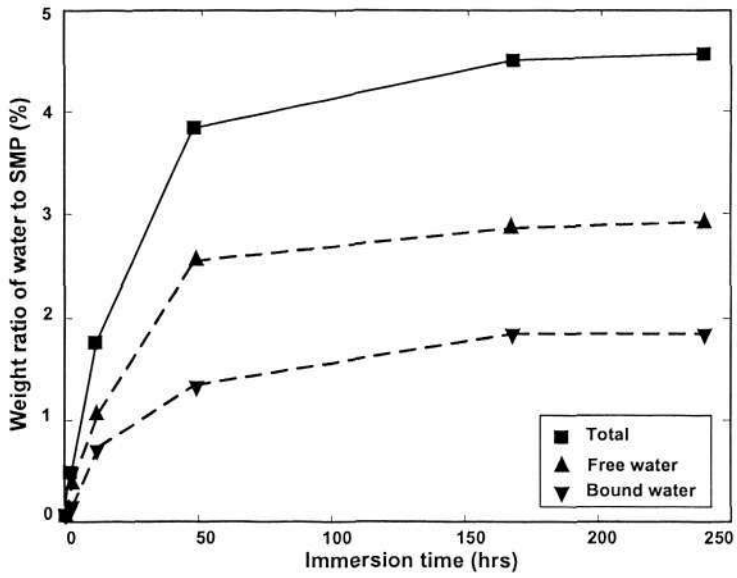

Figure 4.11 Ratio of water to SMP in weight vs. immersion time.

FTIR results provide a clearer picture of the hydrogen bonding mechanism behind the change of T_g in polyurethane SMPs (Figures 4.8 and 4.9). The mechanism is largely dominated by specifically the hydrogen bonding between N-H and C=O groups. As a better illustration, Figure 4.12 plots the infrared bands of the hydrogen bonded N-H and C=O stretchings as a function of immersion time in water based on Figure 4.8. The shifts of infrared bands in hydrogen bonded N-H and C=O groups is significant in the first 48 hours of immersion and then flatten out. The water content in the polyurethane SMP also increases with the increase of immersion time in a similar manner (Figure

4.11). This reveals that water has direct effects on the hydrogen bonding in the polyurethane SMP, which can be explained by the model in Figure 4.13 (Lim et al 1999). Some water molecules absorbed in the polyurethane SMP upon immersion act as bridges between the hydrogen bonded N-H and C=O groups (site 'a' in Figure 4.13). In this model, there is only one possible interaction between water and bonded N=O (site 'a') that directly relates to the hydrogen bonding in SMP. Thus, the change of bonded N-H infrared band induced by water can be interpreted as the effect of water on this hydrogen bonding. The loosely bound water directly weakens the hydrogen bonding, which is evidenced by the shift of the infrared band of the hydrogen-bonded N-H to a higher frequency. Together with the function of water as a plasticizer, T_g is reduced. On the other hand, some absorbed water molecules can form double hydrogen bonds with two already hydrogen-bonded C=O groups (site 'b' in Figure 4.13). Due to the hydrogen bonding in site 'a', the infrared band of bonded C=O stretching shifts up to a higher frequency while the hydrogen bond in site 'b' brings it down to a lower frequency. These two hydrogen bonds may work together and counteract. According to the study of Puffr and Sebenda, water in site 'b' is more firmly bounded than that in site 'a' (Lim et al 1999, Puffr and Sebenda 1967). Consequently, the infrared band of hydrogen-bonded C=O decreases (Figure 4.12).

In the heating process, the infrared bands of hydrogen bonded N-H and C=O stretchings against heating temperature is presented in Figure 4.14. Both N-H and C=O infrared bands change remarkably in the range of 100°C to 180°C, coinciding with the temperature range of significant water loss in Figure 4.1. With the evaporation of water, especially bound water (Figure 4.11), in the heating process, the interaction between

water and polymer is removed. Therefore, the hydrogen bonding between N-H and C=O gradually reverts to its original state. Also, water as a plasticizer is removed upon heating. Therefore, SMP finally recovers its original T_g.

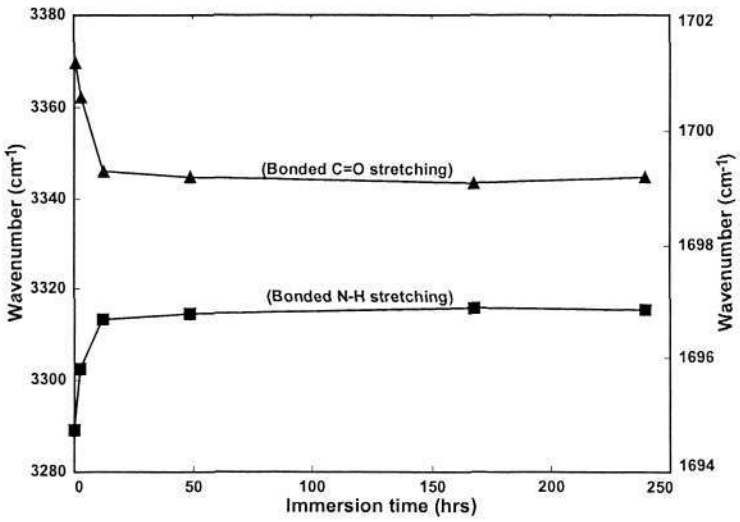

Figure 4.12 infrared band of bonded C=O and N-H stretchings vs. immersion time in water.

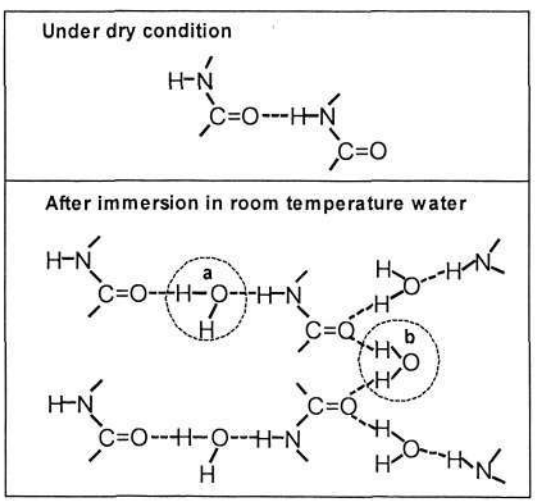

Figure 4.13 Effects of water on the hydrogen bonding in the polyurethane SMP (modified from Lim et al 1999).

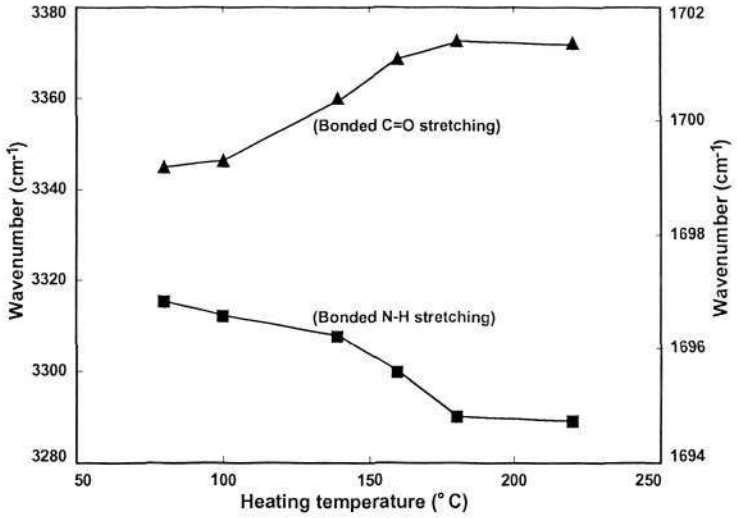

Figure 4.14 infrared band of bonded C=O and N-H stretchings vs. heating temperature.

4.6 Applications based on the effects of moisture

4.6.1 Water driven functionally gradient SMP

Since T_g of polyurethane SMPs can be reduced by immersion in water, it is therefore possible to utilize this to design water driven functionally gradient SMP. The basic idea is to lower T_g of SMP by immersing it into water. In order to verify the suggested new features, which can dramatically widen the applications of SMPs, three tests were carried out on polyurethane SMP MM3520 wires with a diameter of 1.5 mm, which were prepared by extrusion at 200°C.

The first test was water-driven recovery. The straight SMP wire was bent into a circular shape at 40°C and retained this shape during cooling back to room temperature (about 22°C). No apparent shape recovery was found after the deformed wire was kept in a dry cabinet under 30 Relative Humidity (RH) at room temperature for one week. However,

after immersing in room temperature water for about 30 minutes it started to recover gradually (Figure 4.15).

Another piece of SMP wire was used for the gradient T_g test. The wire was divided into three segments of identical length from the top to the bottom. These segments were immersed in room temperature water for 0 minute, 30 minutes and 5 hours, respectively. This resulted in three different T_g s, 36°C, 28°C, and 15°C, respectively, from the top segment to the bottom one as measured by a DSC 2920 (TA Instrument) at a heating rate of 20°C/min,. Subsequently, it was deformed at 40°C into an "m" shape and cooled to 10°C with the shape fixed. Upon exposed to air, the bottom segment recovered in about 30 seconds (Figure 4.16). Heating to about 30°C by a hot plate, the middle segment became straight in about one minute. Upon further heating to 40°C and holding for about one minute, the top segment regained its original shape. This experiment successfully demonstrates the recovery in sequence, a feature that can be utilized for programmable recovery.

Combining both features, the recovery of SMPs can be actuated by water in a programmable manner. Another SMP wire was used for this test. In this test, the top half of the SMP wire was immersed in room temperature water for about 20 minutes, while the bottom half was kept dry. Subsequently, the wire was deformed into a "Z" shape at a high temperature and then cooled to room temperature with the deformed shape retained. Figure 4.17 shows its recovery in water in sequence, i.e., the top half with a lower T_g recovered firstly followed by the recovery of the bottom half. After about 75 minutes, it almost fully regained its original shape.

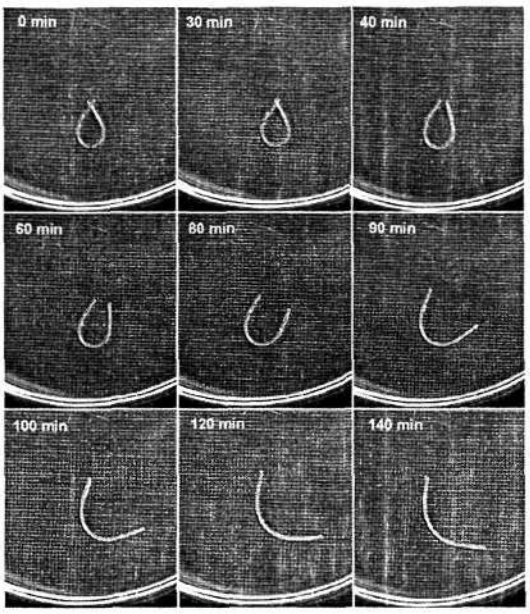

Figure 4.15 Water-driven recovery.

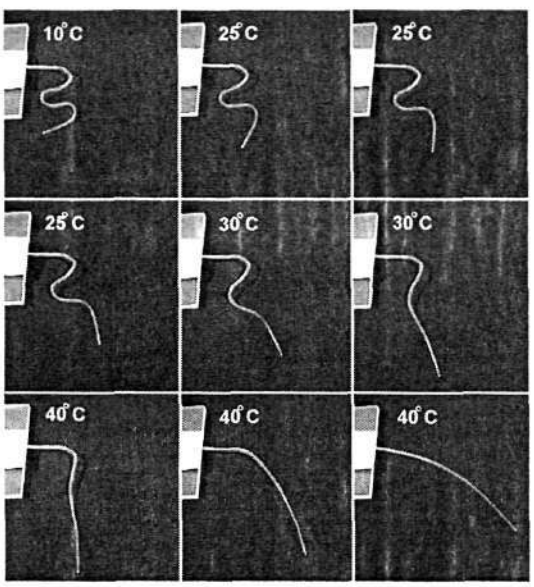

Figure 4.16 Recovery in a programmable manner of a SMP wire upon heating.

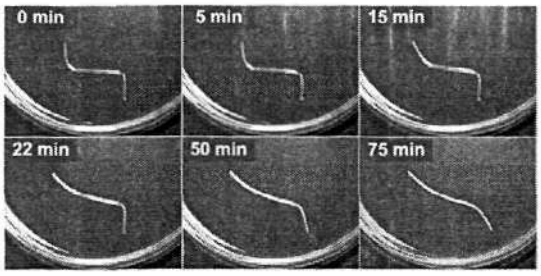

Figure 4.17 Recovery of functionally gradient SMP actuated by water in a sequence.

4.6.2 Porous SMP

Porous polymers are very important in many applications, such as, in tissue engineering where they are applied as scaffold for cellular attachment and tissue development (Thompson et al 2000). The common agents used for polyurethane to develop porous or foaming structures are organic solvents. The residues of these agents remaining in the material may be harmful to cell and tissue (Mooney et al 1996). Based on the findings in this chapter, the possibility of using water as a non-toxic agent to develop porous SMPs is investigated below.

SMP sheet samples were immersed in room temperature water for different hours to absorb various amount of water. After that, two types of testing were carried out on these samples. In one test, SMP sheet samples after 2 hours of immersion were heated to various temperatures, 110°C, 120°C, 130°C and 150°C, in 3 minutes and, subsequently, quenched in air to room temperature. Then, an optical microscope was used to observe these samples. Figure 4.18 presents the optical images of the samples. It shows the formation of closed pores in SMPs after 2 hours of immersion in water. In general, the diameter of pores formed at 110°C is around 20 microns. With the increase

of heating temperature, the size of pores increases remarkably. The dependence of the pore size on heating temperature is due to the further softening of SMP and the higher pressure in steam at higher temperature.

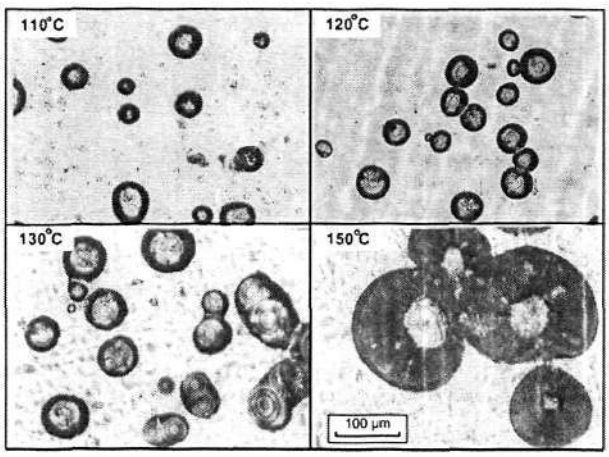

Figure 4.18 Polyurethane SMP (soaked for 2 hours) heated to various temperatures.

In another test, the SMP samples were heat at a same temperature of 120°C in 3 minutes and then quenched in air to room temperature after 1, 2, 6 and 48 hours of immersion, respectively. Figure 4.19 presents their images as obtained by an optical microscope. It reveals that there are some pores developed in the sample after 1-hour immersion in water. With the increase of immersion time more moisture is absorbed in SMP and more pores can be built upon heating to over 100°C. In general, at a lower ratio of moisture the individual closed pores are formed whereas if more moisture is absorbed, the pores expand and coalesce. This results in larger pores with open cells.

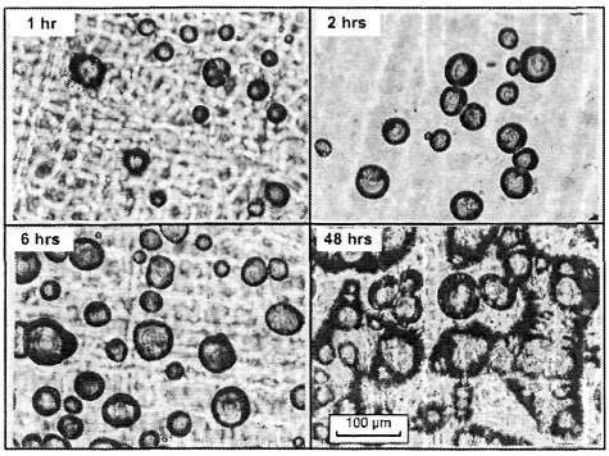

Figure 4.19 Polyurethane soaked for different periods of time heated to 120 °C.

4.7 Summary

In this chapter the effects of moisture on T_g of polyurethane SMP have been investigated systematically. Experimental results show that T_g can be reduced substantially by immersion in room temperature water, and the reduction in T_g continues until the SMP is saturated. Moreover, it was found that the change in T_g is reversed by heating or dehydrating.

Water absorbed in the polyurethane SMP interacts with the polymer chains and weakens the hydrogen bonding between N-H and C=O groups. Together with the function of water as a plasticizer, T_g of SMP is reduced significantly. Heating or dehydrating can cancel these effects so that the SMP reverts to its original T_g.

Water absorbed in the polyurethane SMP can be split into two parts, namely, free water and bond water. They are quantified during immersion and heating processes. The free

water can be fully removed at around 120°C by evaporation. Free water absorbed in the polyurethane SMP has a negligible effect on T_g, while bound water significantly reduces T_g in an almost linear manner.

Based on the above findings two features of the polyurethane SMP were demonstrated. One is the actuation triggered by water and recovery in a programmable manner due to the gradient T_g formed by immersing different parts of the SMP in water for different periods of time. Another is the formation of porous SMP by using moisture as a nontoxic agent for pore generation. It was found that the size and number of pores formed in SMPs are dependent on the heating temperature and ratio of moisture in the materials.

Chapter 5 Fabrication and Characterization of Electrically conductive Polyurethane SMP

5.1 Preparation of electrically conductive polyurethane SMP

The polymer matrix used in the study is MM5520 (refer to Appendix A). This polyurethane SMP with a T_g of 55°C and a melting temperature around 200°C has a bulk density of 1.25 g/cm^3. In Chapter 4, it was found that T_g of polyurethane SMP can drop to below room temperature due to the influence of moisture. However, special instruments for sub-ambient temperature tests were not available during the course of this study. Therefore, SMP MM5520, which has a higher T_g than SMP MM3520, was chosen in this chapter in order to avoid sub-ambient temperature tests.

Carbon nano-powders bought from Degussa were used as conductive fillers. The technical data of carbon nano-powders are listed in Table 5.1 (from the Degussa). It shows that these carbon powders are highly structured with the Brunauer, Emmett and Teller (BET) surface area up to 1000 m^2/g, which is a measure of the total area of carbon powder including the external and internal surface area[1]. Furthermore, it shows that these carbon powders with a dibutylphthalate (DBP) absorption of 420 ml/100 g is more highly aggregated than the ordinary carbon powders that have a DBP absorption

[1] Technical bulletin pigments 2002, Degussa.

lower than 90 ml/100 g. Note that DBP absorption is an indirect measure to determine the carbon powder structure by measuring the void volume between the individual carbon aggregates and carbon agglomerates.

Material	Average powder size	Specific gravity	Purity	DBP absorption	BET surface area
Carbon powders	~30 nm	~1.85	98.4%	420 ml/100 g	1000 m^2/g

Table 5.1 Technical data of conductive carbon powders (from the Degussa).

Before processing, the polyurethane SMP and carbon powders were dried in a vacuum oven at 80°C for 12 hours to remove moisture. After the pellets of polyurethane SMP were melted at 200°C in the mixing head of a Haake Rheocord 90 for one minute, carbon powders were added in slowly and blended with the melted SMP at 200°C. The rotation speed of the mixer was 60 rpm. The whole process lasted about 20 minutes. SMP composites with five different volume fractions of carbon powder, namely, 4%, 7%, 10%, 13% and 15%, were fabricated. The volume fraction of carbon powders (φ_f) was calculated by,

$$\varphi_f = \frac{1}{1+(M_m/\rho_m)\times(\rho_f/M_f)}\times 100\% \tag{5.1}$$

where M_m, ρ_m, M_f and ρ_f denote the mass of SMP, the bulk density of SMP as given by MHI, the mass of carbon powders and the bulk density of carbon powders as given by Degussa, respectively.

In this study, CBX denotes the polyurethane SMP composites with X% of volume fraction of carbon powders. Hence, CB0 is the pure SMP without any carbon powder.

After blending the mixture was processed into desired shapes at 200°C for testing. Three kinds of samples were prepared in the study, i.e., thin sheets with thickness of 1.0 mm and 0.5 mm were pressed on a laboratory hot press, wires with a diameter of 2.0 were prepared by extrusion, and cylindrical samples (with a diameter of 15.0 mm and a length of 20.0 mm) were molded. Before testing, all samples were kept in a dry cabinet with a Relative Humidity (RH) below 30%.

5.2 Shape recovery by passing an electrical current

The SMP composite CB13 was hot-pressed into a plate shape with a thickness of 2.0 mm and then cut into a 'n' shape for demonstrating the shape memory effect upon heating by passing an electrical current through it. The sample in a 'n' shape was connected to a 15-voltage DC power supply through two electrodes. An infrared camera (thermo-vision 900, AGEMA) was used to observe the temperature distribution in the sample. Figure 5.1 (a) shows the sample heated by an electrical current for 45 seconds. The sample can be easily bent at 60°C, which is above T_g. After switching off the electrical power and cooling back to 22°C room temperature with the deformed shape held still, the bent shape was formed. When reheated above T_g by passing an electrical current, the sample recovered its original shape as shown in Figure 5.1 (b).

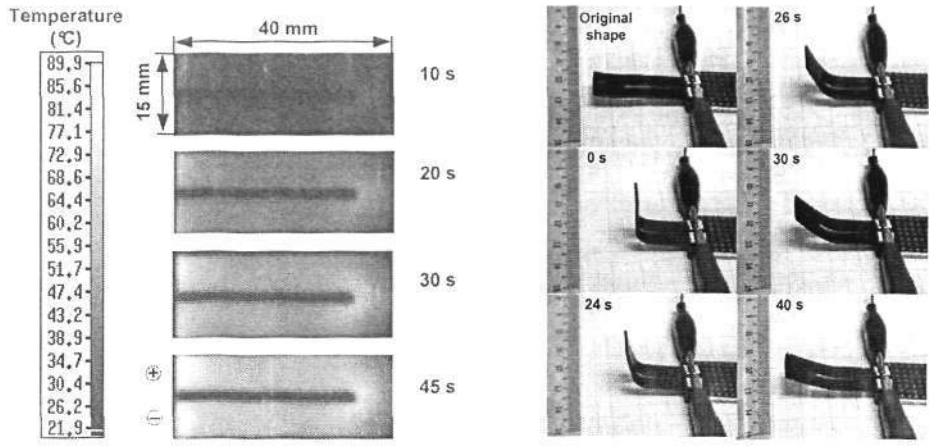

(a) (b)

Figure 5.1 Shape memory effect in conductive SMP CB13. (a) Temperature distribution taken by an infrared camera, (b) shape recovery upon passing an electrical current.

5.3 Distribution of carbon powder in polyurethane SMP

The dispersion of carbon powders in the conductive SMP was studied by investigating the cryofracture surface of samples without coating using a scanning electronic microscope (SEM, Leica Cambridge S360). Figure 5.2 illustrates the formation of carbon networks in the SMP composites filled with different volume fractions of carbon powders. Note that the white areas are carbon powders. It shows that carbon powders distribute in the polyurethane SMP matrix randomly, aggregating as clusters instead of separating from each other. The average size of these clusters is around 100~200 nm in diameter. The aggregation of carbon powders has been investigated in some other carbon fine powder-filled polymers (Flanin et al 2001, Knite et al 2002, Carmona and Ravier 2002). Carbon powders distribute randomly in CB4 as isolated agglomerates (Figure 5.2 (a)). With the increase of carbon powder content, carbon

agglomerates connect with each other and continuous carbon networks are formed (Figure 5.2 (b)). With the continuous increase of carbon loading up to 13%, the number of carbon networks increases dramatically (Figure 5.2 (c)).

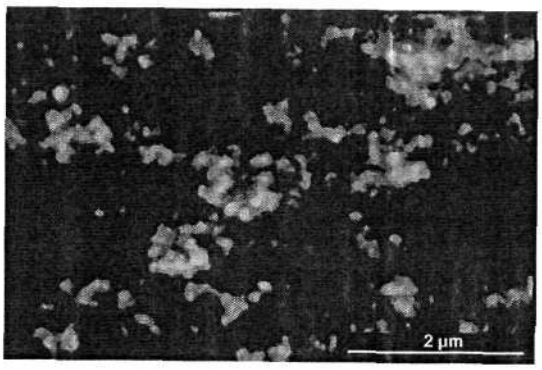

(a)

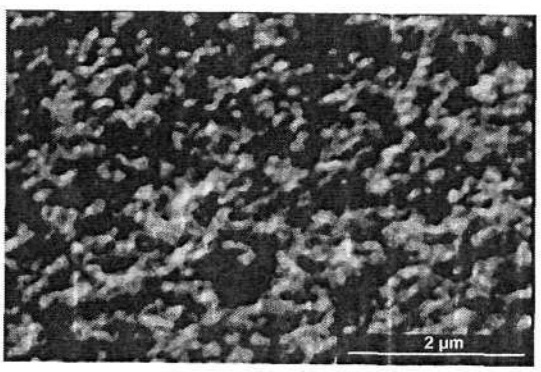

(b)

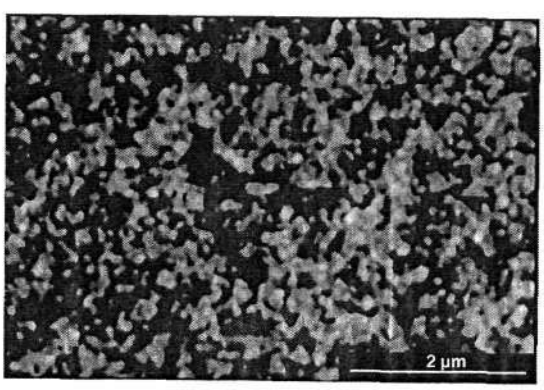

(c)

Figure 5.2 SEM images of cryofracture surfaces. (a) CB4; (b) CB7; (c) CB13.

5.4 Electrical resistivity

5.4.1 Dependence on loading of carbon powder

Electrical resistivity of the conductive SMPs was measured by a four-point resistivity probe system (SINGNTONE) with an upper limit of 10^{10} Ωm. The resistivity of the SMP composites with a smaller volume fraction of carbon powder is over this limit. Therefore, a digital high resistivity determiner (RP2680) was used instead.

Figure 5.3 presents the electrical resistivity of SMP composites filled with different volume fractions of carbon powders. It shows that the electrical resistivity of the composite with less than 4% volume fraction of carbon powders is almost constant. A sharp transition occurs between 4% to 7% volume fraction, known as the percolation threshold range (Ishigure et al 1999, Zheng and Wong 2003). The percolation threshold is a critical value, and it indicates the transition of the material from insulating to conductive (Ishigure et al 1999, El-Tantawy et al 2002). For the SMP composites with a low volume fraction of carbon powders (e.g., <4%), the carbon aggregates in the SMP matrix are relatively more separated [refer to Figure 5.2 (a)]. Large gaps between the conductive carbon aggregates present significant physical barriers to electron flow, so that almost no conductive channel can be formed in the material. Hence, the electrical resistivity is very high. As the volume fraction of conductive filler reaches the percolation threshold, the gaps between conductive carbon aggregates are reduced, as shown in Figure 5.2 (b). Some carbon aggregates even directly contact each other. Thus, electrons can jump more easily. The three-dimensional conducting network is constructed and the composite becomes much more conductive (Sheng P et al 1978, Azulay D et al 2003). It results in a sharp decrease in the electrical resistivity with the increase of carbon powder content. A further increase of volume fraction of carbon

powders reduces the gap slightly, and only a few more conductive channels are formed (Figure 5.2 (c)). Hence, reduction in resistivity is in a much gradual manner.

By data fitting with the experimental results, two equations are obtained as follows,

$$\rho = 1.0 \times 10^{13} \left(6\% - \varphi_f\right)^{0.7} \quad \text{for } \varphi_f < 6\% \tag{5.2}$$

$$\rho = 1.6 \times 10^{-4} \left(\varphi_f - 6\%\right)^{-1.9} \quad \text{for } \varphi_f > 6\% \tag{5.3}$$

Hence, the percolation threshold for this carbon powder filled polyurethane SMP is 6% (volume fraction), a shown in Figure 5.3.

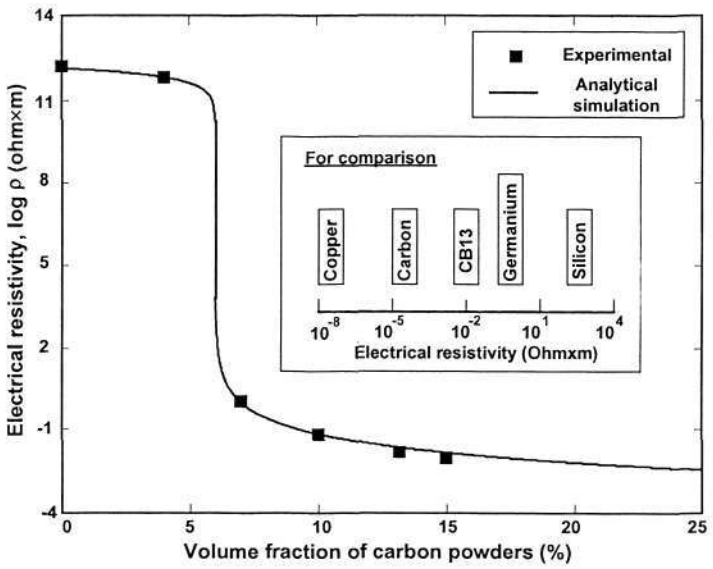

Figure 5.3 Electrical resistivity vs. volume fraction of carbon powders.

5.4.2 Effects of temperature and uniaxial mechanical strain

Normally, the temperature range in a real engineering application of the polyurethane SMP and its conductive composites is from room temperature to about 100°C as reported in the literatures and technical articles (Chiodo JD et al 1999, Cadogan DP

2002 et al, Wache HM et al 2003, Gall K et al 2004). Here, each conductive SMP was heated from room temperature to around 100°C and the electrical resistivity of each composite was recorded against temperature using the four-point resistivity probe system. The result is plotted in Figure 5.4. It reveals that there is no apparent change in electrical resistivity in all conductive SMP composites within this temperature range.

In real applications, the conductive SMPs are deformed and then heated for recovery. Therefore, to understand the effects of strain on the electrical resistivity of conductive SMPs is very important. A testing setup as illustrated in Figure 5.5 was designed and fabricated for this purpose. An Instron 5569 with a hot chamber was used to stretch/compress the conductive SMP samples at 60°C and at a constant crosshead speed, which gives a fixed strain rate of 10^{-3}/s. Conductive SMP wires with a diameter of 2.0 mm and a gauge length of 30.0 mm were used for tensile tests while cylindrical samples with a diameter of 15.0 mm and gauge length of 20.0 mm were used for compressive tests. Two copper electrodes were attached to the ends of the samples. A multimeter was coupled with the Instron machine to measure the resistance of the sample (R'). The electrical volume resistivity (ρ) was calculated by,

$$\rho = R' \times S' / L \tag{5.4}$$

where S' is the cross-sectional area of the sample and L is the gauge length.

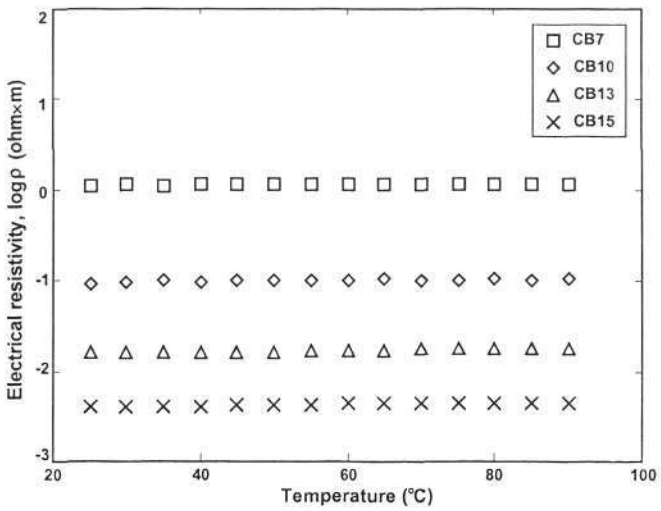

Figure 5.4 Electrical resistivity as a function of temperature.

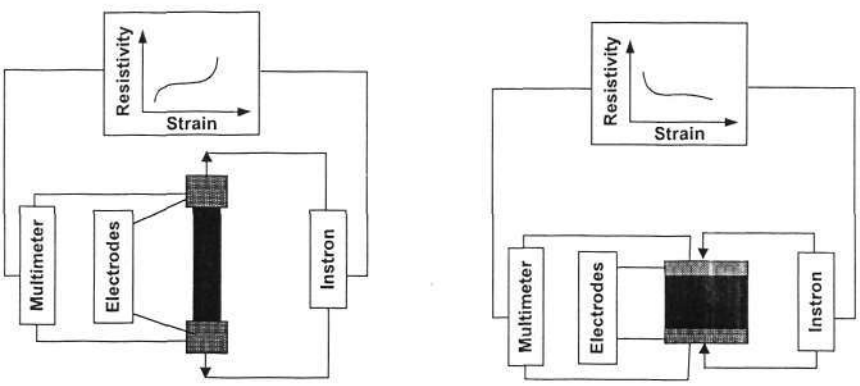

Figure 5.5 Experimental setup. Left: tensile test; right: compressive test.

Figure 5.6 (a) plots the tensile strain against the electrical resistivity. It shows that, generally, with the increase of strain the electrical resistivity increases but not in a linear fashion. The increase of electrical resistivity is much remarkable in the lower strain range, i.e., below 10%. With the increase of loading of carbon powders the increase of electrical resistivity in the lower strain range becomes more significant.

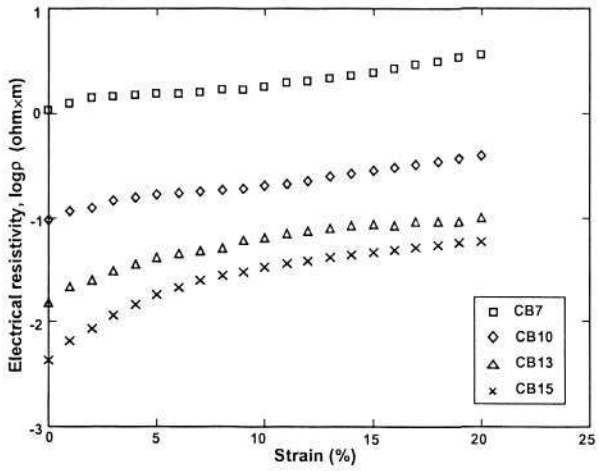

(a)

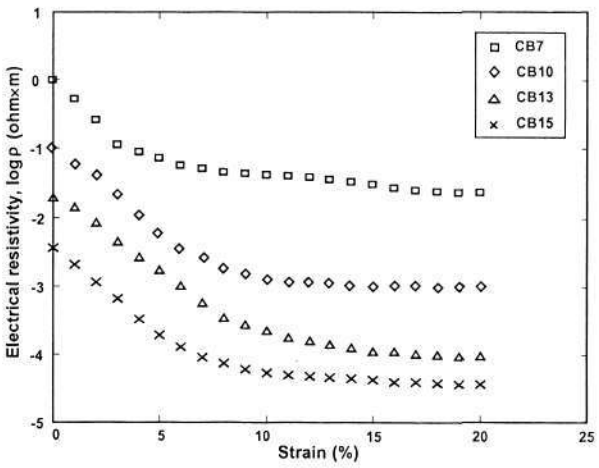

(b)

Figure 5.6 Electrical resistivity vs. strain relationship. (a) In tension, and (b) in compression.

When a conductive composite is subjected to a tensile strain, it is expected that two simultaneous processes will be operative in the material: breakdown of existing conductive networks due to an increase in the gap between the carbon powder aggregates, and reformation of new conductive networks due to reorientation of carbon

aggregates (Aneli et al 1999, Flandin et al 2000). At a lower tensile strain, the breakdown process is more prominent than the formation process. Thus, the net result is a reduction in the number of conductive networks, which indicates the increase of resistivity. However, at higher tensile stain, rather than formation of holes and destruction of the conductive networks in the material, the extension produces new conductive pathways and/or improves the existing pathways by reorientation of carbon powders. For high structured carbon powders, rotation, translation, and possible shape changes of the asymmetric aggregates can preserve the number of contacts and conductive pathways. These processes somewhat counterbalance the effect of breakdown of conductive networks, resulting in a slower rate of change in resistivity against the extension at a higher strain (Kost et al 1984, Pramanik et al 1993, Das et al 2002).

However, a compressive strain has a different effect on the electrical resistivity. The testing results are plotted in Figure 5.6 (b). It reveals that with the increase of compressive strain the electrical resistivity decreases instead. The most significant decrease happens at a lower strain range, i.e., below 10%, same as that in tension. Under a lower compressive strain, the gap between carbon aggregates in SMP is reduced so that the tunneling conduction is possible between some aggregates. Some aggregates may even contact each other physically. Thus, more conducive pathways are constructed resulting in a decrease in resistivity. These effects are less significant at a higher strain range because all the possible conductive pathways are formed upon compression at lower strain range.

5.5 Thermal stability

The thermal stability of carbon powder filled polyurethane SMP composites was tested using a TGA 2950 (TA Instruments). The samples weighing 20~25 mg were heated at a constant heating rate of 20°C/min in nitrogen atmosphere. The results are plotted in Figure 5.7. It shows that the decomposition of pure polyurethane SMP (CB0) starts at about 260°C. In general, with the addition of carbon powders the onset of decomposition temperature increases slightly and the full decomposition occurs at a higher temperature.

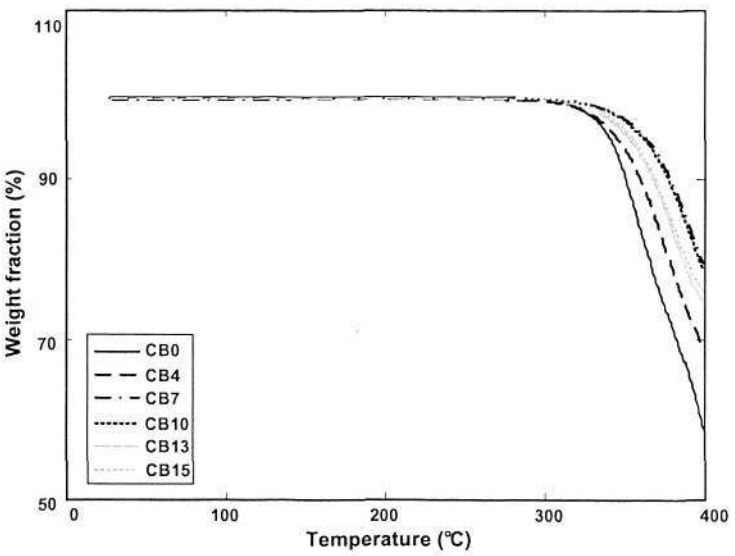

Figure 5.7 TGA results of dry SMP composites.

It has been reported that the incorporation of nano-fillers could improve the thermal stability of some polymer composites (Gilman et al 2000, Zeng et al 2004). The increase in the degradation temperature can be explained by two possible reasons. One is the restriction on the mobility of the macromolecules imposed by, in our case, the

carbon nano-powders, which causes a reduction upon tension induced by thermal excitation in the carbon–carbon bond (Bryk 1991, Ahmad et al 1995). The other probable explanation may be offered in terms of the capacity of heat absorption in carbon powders. According to the black body principle, black carbon nano-powders are excellent absorber of heat. Thermal degradation in a polymer matrix occurs only after a certain amount of heat energy has been absorbed by the material. Heat initiates the degradation process and breaks down of the matrix structure by causing rupture or scission in molecular chain. With the increase of the carbon nano-powder content in a SMP composite, more heat is absorbed by carbon powders. Thus, higher temperature is required to overcome the required threshold energy for commencement of the degradation process.

5.6 Properties in uniaxial tensile at room temperature

Uniaxial tensile tests were carried out using an Instron 5569 with a 1 kN load cell to investigate the properties of SMP composites in uniaxial tensile at room temperature. Figure 5.8 illustrates the dimensions of the sample for testing. The gauge length (the distance between two clamps) was set as 20 mm. During testing a constant strain rate of 5×10^{-3}/s was applied. Here, engineering strain and engineering stress were used, and the strain was calculated from the displacement of the crosshead over the original gauge length, while the original sectional dimension of sample, namely 4.0×1.0 mm^2, was used to calculate the stress.

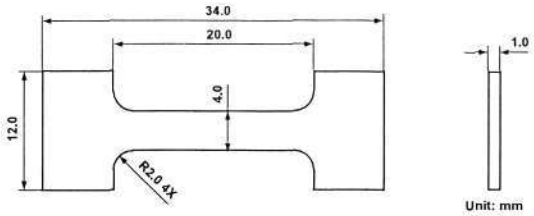

Figure 5.8 Dimensions of sample.

Figure 5.9 plots the stress-strain curves of the uniaxial tensile tests at room temperature. In general, upon loading the SMP composites behave in a more or less similar way. They experience yielding, cold drawing and then failure. With the increase of carbon powders, the yielding strength of SMP is significantly increased.

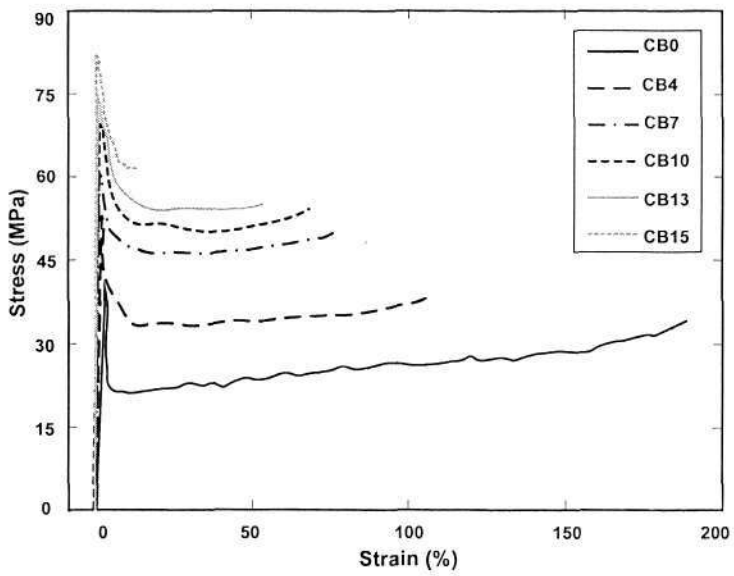

Figure 5.9 Stress-strain curves at the room temperature.

The relationship of Young's modulus and the elongation limit vs. volume fraction of carbon powder (φ_f) are plotted in Figure 5.10. Note that the Young's modulus is calculated from the early loading part of the stress-strain curve. It shows that carbon

powders reinforce the conductive SMP so that the Young's modulus of CB15 is about 2 times of that of pure SMP. However, the presence of carbon powders reduces the elongation limit significantly. Even a mere 4% volume fraction of carbon powders results in a serious decrease in the elongation limit from 185% in CB0 to 110 % in CB4.

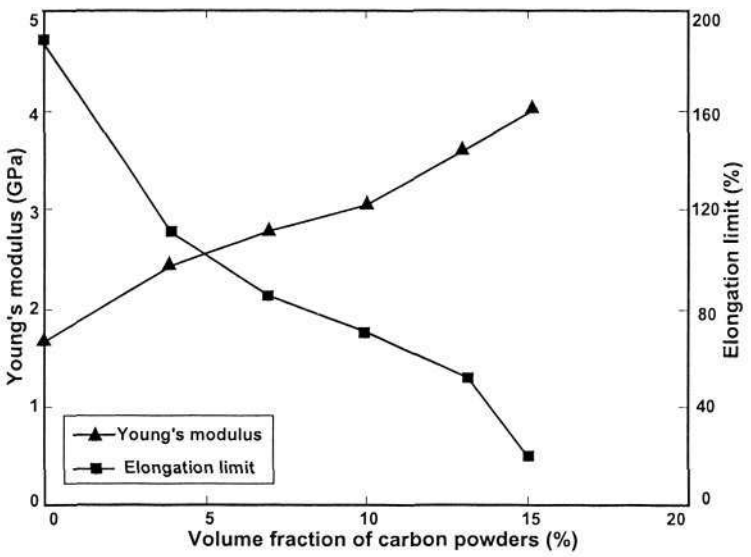

Figure 5.10 Relationship of Young's modulus and elongation limit vs. φ_f.

5.7 Shape memory properties upon heating

Thermomechanical tests were carried out to investigate the shape memory properties of SMP composites. Smples with dimensions as shown in Figure 5.8 were used. The testing procedure is illustrated in Figure 5.11. In step *a*, the sample is stretched uniaxially to a maximum strain (ε_m) of 20% at a constant strain rate of 5×10^{-3}/s by an Instron Micro-force Materials Test System with a 100 N load cell. The sample is tested at a constant temperature (T_h) of 65°C inside a hot chamber. Then, the sample is held at ε_m and cooled to room temperature (T_r) in 4 minutes (step *b*). In this step, the stress

relaxes at the very beginning during holding due to viscous flow as the material is in the rubber state. In step *c*, the sample is unloaded to zero stress, which results in a small amount of strain recovery. The fixed strain (ε_f) corresponds to the strain at the end of unloading.

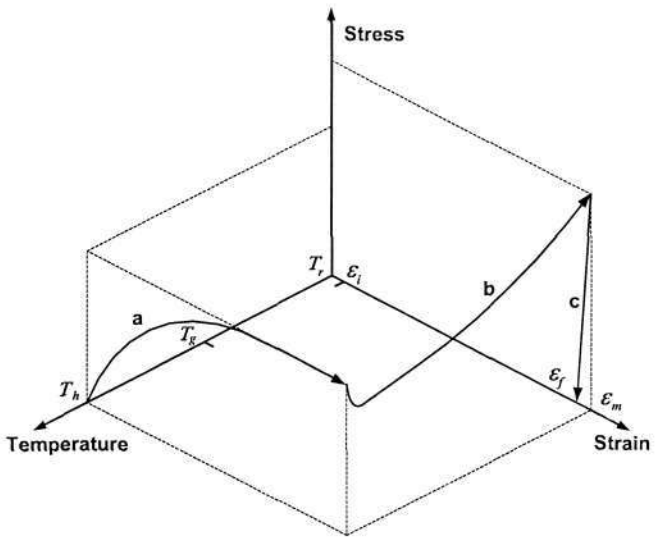

Figure 5.11 Procedure of the thermomechanical test (modified from Tobushi et al 2001).

From a thermomechanical point of view, the recovery stress and recoverable strain are essential concerns in applications of SMPs. Thus, two types of tests were performed, namely, the constrained and free recovery tests after step *c* to measure the maximum recoverable strain and recovery stress during recovery. The samples were separated into two groups for different recovery tests. The samples from one group were heated on a digital hot plate at a constant rate of 2°C/min and their lengths were allowed to vary. The length of sample was measured using a microscope and then the recovered strain was calculated and recorded together with the temperature. This is the so-called free recovery test. The second group of samples was tested under the same conditions

as that of the first group except that the lengths of these samples were fixed. The recovery stress was recorded by the Instron machine against temperature. This is so-called constrained recovery test.

In order to evaluate the shape memory properties of the SMP composites, the ratio of fixable strain (R_f) and the ratio of recoverable strain (R_r) are calculated by the following equations,

$$R_f = \varepsilon_f / \varepsilon_m \times 100\% \tag{5.5}$$

$$R_r = \left(\varepsilon_m - \varepsilon_f + \varepsilon_r\right) / \varepsilon_m \times 100\% \tag{5.6}$$

where ε_r is the total recovered strain at the end of the free recovery test.

5.7.1 Fixable strain

The stress-strain relationships in the thermomechanical tests are plotted in Figure 5.12. It shows that with the increase in volume fraction of carbon powders the SMP composite gains more resistance to deformation. The change is more remarkable from CB4 to CB7. At the beginning of holding and cooling the stress relaxes, which is attributed to the viscous flow of SMPs in the rubber state. And then, it increases due to the increase of Young's modulus of materials in transition from the rubber state to the glass state, and thermal contraction upon cooling. Only a small linear elastic strain recovery results from unloading. The linear elastic recovery strain at the end of unloading in all SMP composites is below 3%.

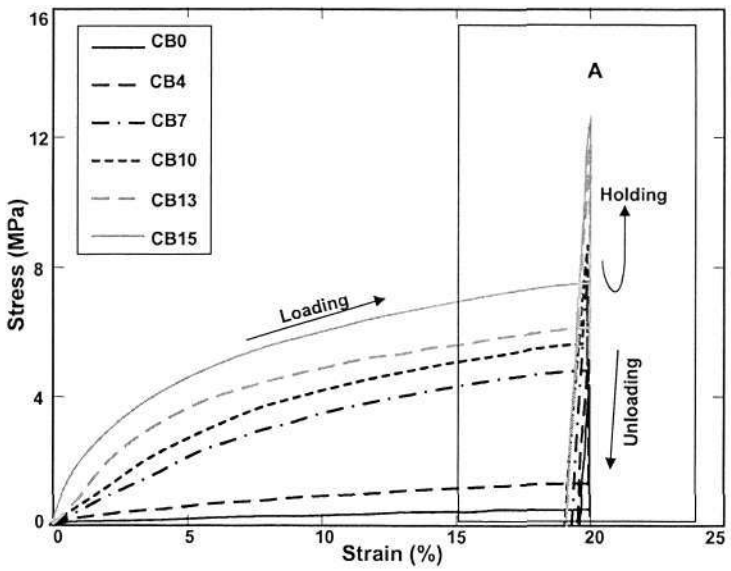

(a)

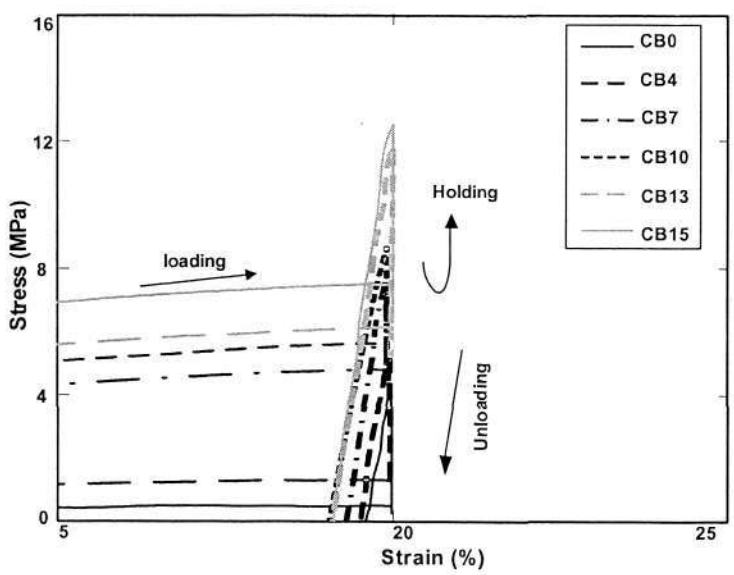

(b)

Figure 5.12 Stress-strain curves at T_g +10°C. (a) Overall view; (b) zoom-in view of A.

Figure 5.13 plots the ratio of fixable strain against the volume fraction of carbon powder. It reveals that the presence of carbon powders in the SMP matrix deteriorates the shape fixity. But at a lower loading of carbon powders, below 4% volume fraction, this effect is almost negligible while the ratio of fixable strain gains significant reduction when the content of carbon powder reaches 7%. Further increase of carbon powders only reduces the ratio of fixable strain gradually. In general, although carbon powders decrease the shape fixity, all SMP composites still have reasonable shape fixity so that over 95% of preload strain is fixable after cooling and subsequent removal of the external constraint.

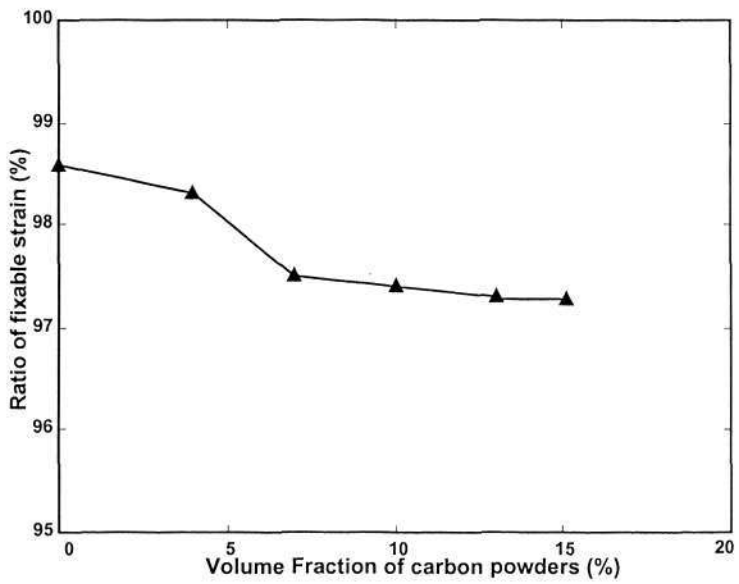

Figure 5.13 Ratio of fixable strain vs. volume fraction of carbon powders.

5.7.2 Recoverable strain

The free recovery strain as a function of temperature in the free recovery test is plotted in Figure 5.14. It reveals that all samples recover the preloaded strain abruptly between

50°C to 60°C. With the increase of carbon powders the start temperature for recovery becomes lower, while the finish temperature is higher, so that the temperature range for strain recovery is widened. Such effects may be attributed to the change of glass transition kinetics due to the loading of carbon powders.

For a better illustration, Figure 5.15 plots the ratio of recoverable strain against the volume fraction of carbon powder. It reveals that carbon powders have limited effect on shape recovery ability of SMP at a lower φ_f. Even when the volume fraction reaches 10%, the SMP composite is still capable of recovering over 90% of the pre-strain. However, with the increase of carbon powders to over 13% in φ_f, the trend in decrease of the ratio of recoverable strain becomes significant.

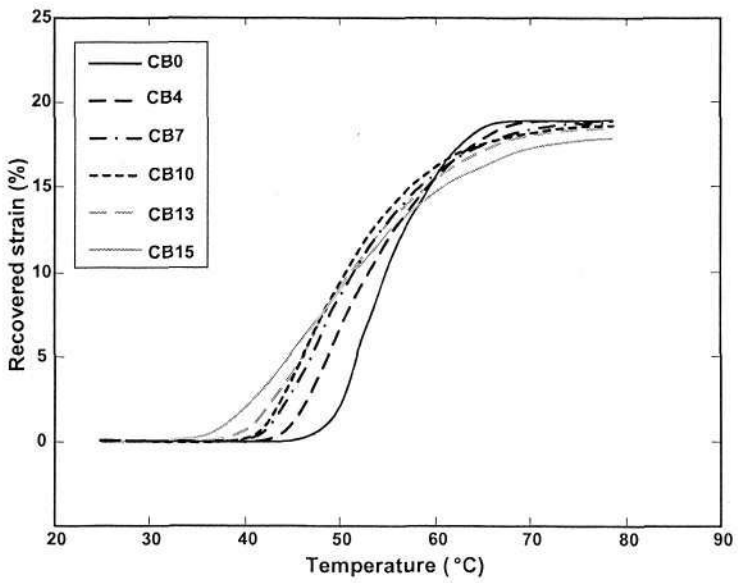

Figure 5.14 Recovered strain as a function of temperature.

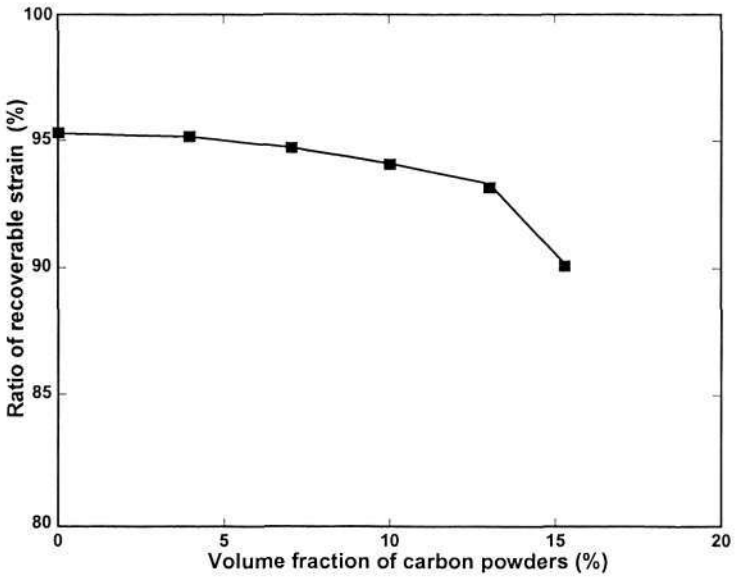

Figure 5.15 Ratio of recoverable strain against volume fraction of carbon powders.

5.7.3 Recovery stress

Figure 5.16 plots the recovery stress against temperature in the constrained recovery test. Generally, there is very little change in the recovery stress below 35°C. The change is largely negative, which can be attributed to the thermal expansion of SMP composites. With further increase in temperature, the recovery stress increases quickly because of the shape memory effect and then reaches a peak. After that, it decreases gradually and even approaches zero. The decrease of recovery stress is a result of the relaxation in SMPs, which is attributed to the viscous flow of polymer chains at higher temperature.

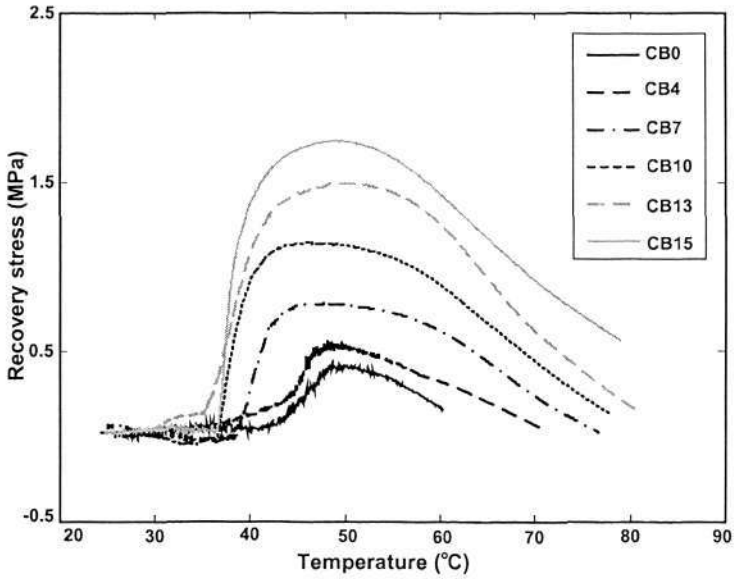

Figure 5.16 Recovery stress as a function temperature.

Furthermore, the results reveal that the loading of carbon powders significantly increases the maximum recovery stress of SMP composites. With the increasein volume fraction of carbon powders, the decrease of recovery stress upon further heating becomes slow after the maximum stress is reached. As carbon powders restrict the viscous flow in SMPs, a slower relaxation in heavily carbon-loaded SMP composites is expected.

Maximum recovery stress upon heating is plotted against volume fraction of carbon powders in Figure 5.17. It shows that the loading of carbon powders almost leads to an exponential increase in the maximum recovery stress. It demonstrates that the loading of carbon powders is an efficient way to increase the recovery stress.

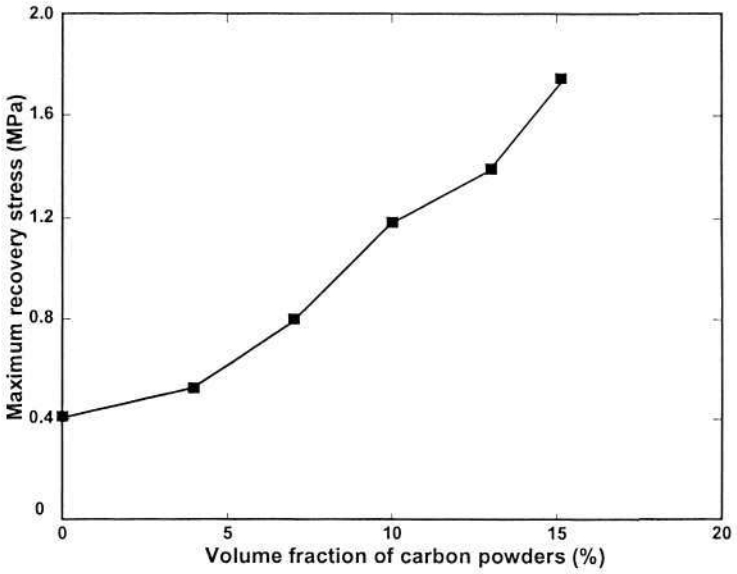

Figure 5.17 Maximum recovery stress against volume fraction of carbon powders.

5.8 Summary

Nano-carbon powders distribute in the SMP matrix randomly with an agglomerate size of 100~200 nm in diameter. 6% volume fraction of carbon powders is the percolation threshold. Over this threshold, the conductive network is virtually formed in the SMP composites resulting in a sharp transition from insulating to electrically conductive.

The electrical resistivity of SMP composite with 13% volume fraction of carbon powders is about 10^{-2} $\Omega \times$ m. Furthermore, carbon powders reinforce the SMP composites resulting in an increase of its Young's modulus. The elongation limit, however, is reduced.

These conductive SMPs show good shape memory properties. The ratio of fixable strain is above 90% when the maximum strain is 20%. The presence of carbon powders has a significant effect on shape recovery ability. Given a maximum strain 20%, over 90% strain is recoverable in low φ_f (<15%) SMP composites, but the freely recoverable strain decreases to below 90% due to a high φ_f (≥15%).

The carbon powders-filled SMP composite (CB13) shows excellent electrical conductivity as well as good shape memory properties. It can be heated directly and efficiently by passing an electrical current for recovery.

Chapter 6 Effects of Moisture on Electrically conductive SMP Composites

As presented in Chapter 4, moisture has a significant influence on T_g of SMP and its interactions with SMP chains were studied. By filling with carbon nano-powders the electrically conductive SMP composites were produced and characterized in Chapter 5. They can be directly heated for recovery by passing an electrical current, so that a wider range of applications can be realized. However, the effects of moisture on the electrically conductive SMP composites are still not known. A good understanding of this issue is significant for engineering applications. Therefore, this chapter aims to address this issue by studying the samples prepared in Chapter 5.

6.1 Absorption of moisture in room temperature water

In order to study the absorption of moisture in the electrically conductive SMP composites, the hot pressed SMP composite sheets with a thickness about 1.0 mm were immersed in 22°C room temperature water. After different immersion hours, these sheets were cut into small pieces for TGA testing in order to determine the moisture fraction in them. In the TGA tests, samples around 20 mg were heated from 30°C to 330°C by a TGA 2950 (TA Instruments) at a heating rate of 20°C/min.

Figure 6.1 presents one set of TGA results for sample CB13 after different immersion hours. Evidently, there is a major weight loss in the range between 100°C and 240°C before decomposition occurs. This weight-loss is directly attributed to the evaporation of moisture absorbed in the SMP composite. For simplicity, same as that in Chapter 4 we take the percentage of weight-loss at 240°C as the total weight percentage of moisture being absorbed. It is obvious that the moisture content in SMP composite increases with the increase of immersion time.

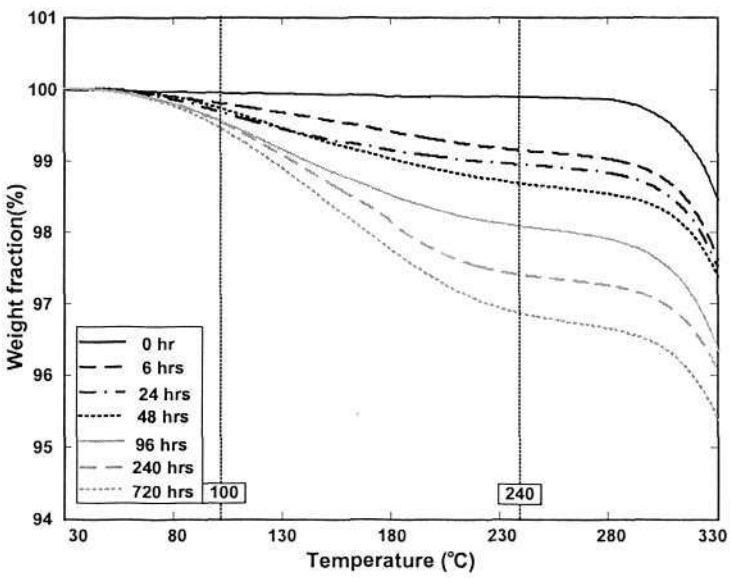

Figure 6.1 TGA results of CB13 after different immersion hours in water.

Figure 6.2 further summarizes the moisture fraction in weight % vs. immersion time of samples with different volume fractions of carbon powders. It shows that the moisture content in the material increases at the beginning and gradually becomes almost constant after 240 hours. Thus, the sample after 720 immersion hours may be considered as saturated. The result also reveals that SMP composites filled with a

higher content of carbon powder tends to have less moisture content in the saturate state. The maximum moisture absorption (in weight %) in the pure polyurethane SMP is at about 3.5%. Furthermore, the loading of carbon powders slows down the speed of moisture absorption. This is more obvious at the beginning of immersion.

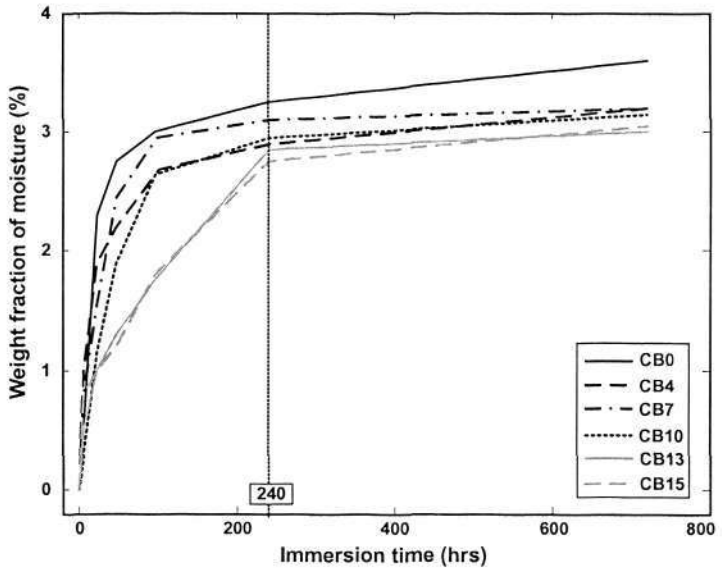

Figure 6.2 Moisture fraction in weight % vs. immersion time.

6.2 Electrical resistivity after immersion

Figure 6.3 plots the electrical resistivity of carbon filled SMPs as a function of immersion time in room temperature water. It reveals that the electrical resistivity of CB7 and CB10 decreases at the beginning of immersion and then quickly reaches a stable state. However, there is almost no change in the electrical resistivity in CB13 and CB15. As the immersion time is directly related to the moisture ratio in SMPs, this improvement of electrical conductivity in CB7 and CB10 can be attributed to the increase of moisture content.

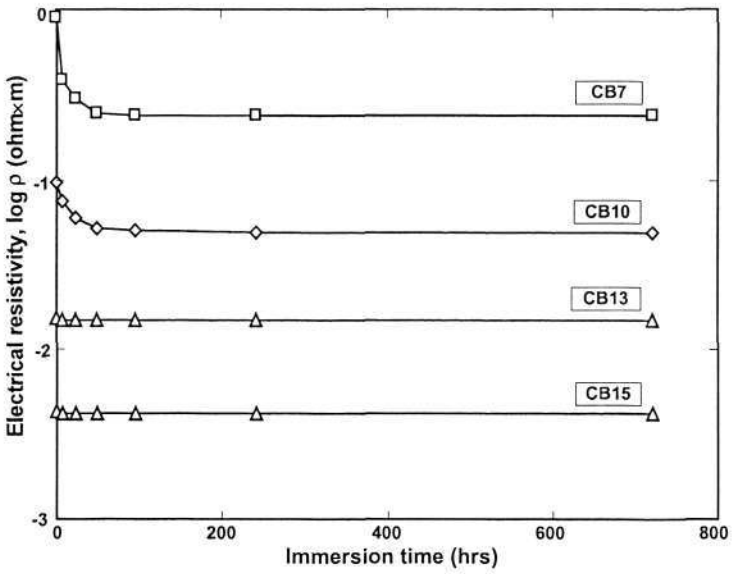

Figure 6.3 Electrical resistivity as a function of immersion time.

It is believed that the conductive fillers may distribute in an insulator in three ways: non-contact, close proximity, and physical contact between the conductive fillers or agglomerates (Bhattacharya 1986). The electrons can jump over the gap between the conductive fillers in the case of close proximity. The jumping causes the tunneling conductivity in conductive polymer composites (Sheng et al 1978, Azulay et al 2003). In CB7 and CB10 the tunneling conductivity may be more dominant than that in CB13 and CB15 because of lower loading of carbon powders. It might be reasonable to assume that moisture improves the mobility of electrons so that more tunneling happens in CB7 and CB10. Subsequently, the decrease in electrical resistivity of them is more remarkable than that in CB 13 and CB15, which have a higher loading of carbon powders. Note that in this study, the electrical resistivity was obtained by measuring the surface resistance of SMP samples, where the material absorbs moisture

much faster. So that the surface can quickly reach the saturated state. Thus, the variation in electrical resistivity is more marked at the beginning of immersion.

6.3 Glass transition temperature after immersion

A DSC 2920 (TA Instruments) was used for testing samples that had been immersed in water for different hours to examine the change in T_g. The samples weigh around 10 mg and the constant heating/cooling rate is 20°C/min in testing. T_g is taken at the median point in the glass transition range during heating.

A set of typical DSC results (CB13) is presented in Figure 6.4. It reveals that T_g decreases remarkably with the increase of immersion time. Furthermore, the temperature range for glass transition widens. Relationships between T_g of the SMP composites with different carbon powder contents and immersion time are summarized in Figure 6.5. It shows that T_g of all samples fall with the increase of immersion time following a similar trend. The decrease is significant at the beginning and then becomes mild for an immersion time over 240 hours, which is consistent with the increase of moisture shown in Figure 6.2. With more moisture absorbed into SMP or it composites, T_g decreases further. This phenomenon persists until the sample is saturated. Figure 6.5 also demonstrates that the added carbon powders have the tendency to lower T_g. This is more obvious if the water content is high. For instance, T_g of pure polyurethane SMP (CB0) at the saturation point (720 hours) is about 10°C higher than all other samples.

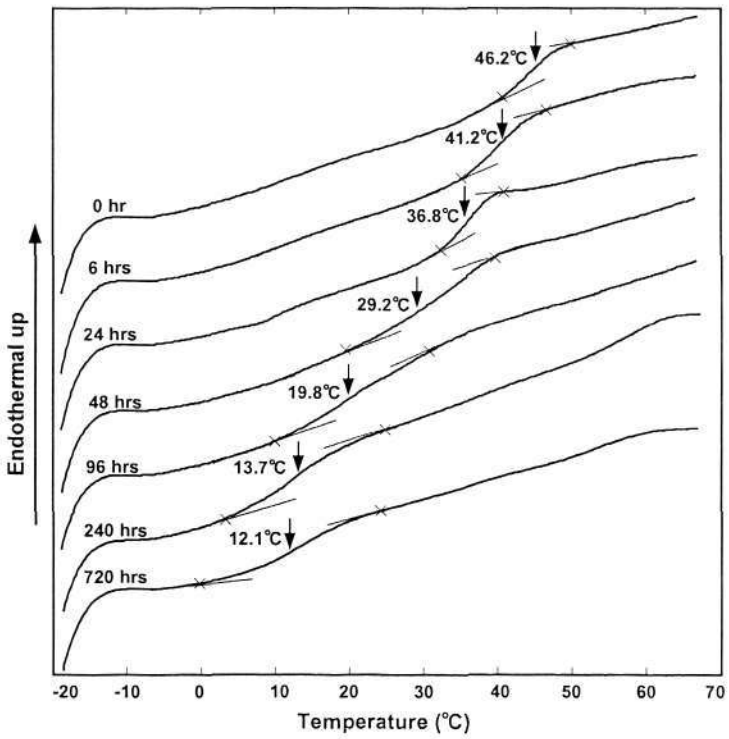

Figure 6.4 DSC results of CB13 after different immersion hours in water.

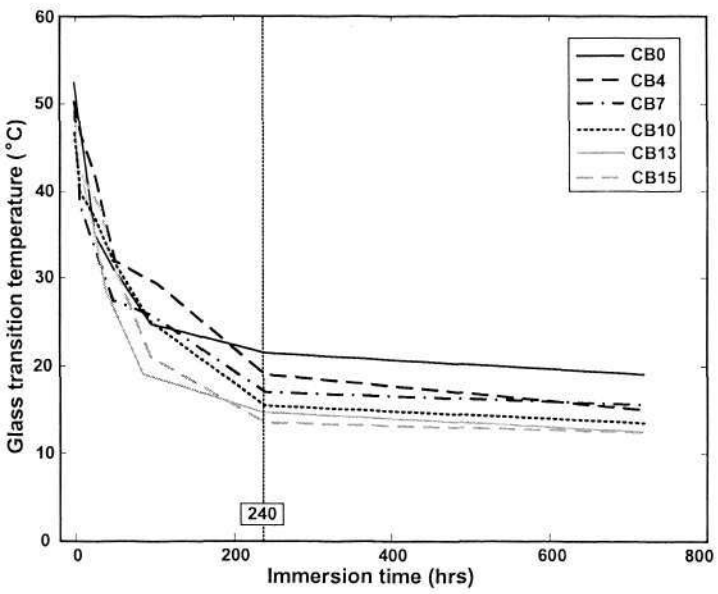

Figure 6.5 T_g vs. immersion time.

6.4 Evolution of glass transition temperature upon thermal cycling

The results from the previous sections show that the moisture uptake can significantly decrease T_g of electrically conductive SMP composites. In order to know whether T_g can be restored to its original value by dehydration, cyclic DSC tests were carried out on the SMP composites after immersion in water following the same testing procedure as described in Section 4.3.

Figure 6.6 plots one typical set of results, which presents the evolution of T_g upon thermal cycling of CB13. Clearly, after six different thermal cycles the specimens all regain their original T_g. In general, the regaining process is more significant in the temperature range from 140°C to 180°C. Figure 6.7 summarizes the evolution of T_g upon thermal cycling in all saturated SMP composites. Again it shows that the most significant recovery in T_g occurs in the temperature range from 140°C to 180°C. Further heating to beyond the melting point (~200°C) can bring T_g almost fully back to its original value.

Note that there is a significant part of the moisture being removed at a temperature above 140°C (Figure 6.1). The increase in T_g can be directly attributed to the evaporation of moisture. Since the moisture is removable, the whole process is reversible, and T_g can be reduced if samples are immersed into water again.

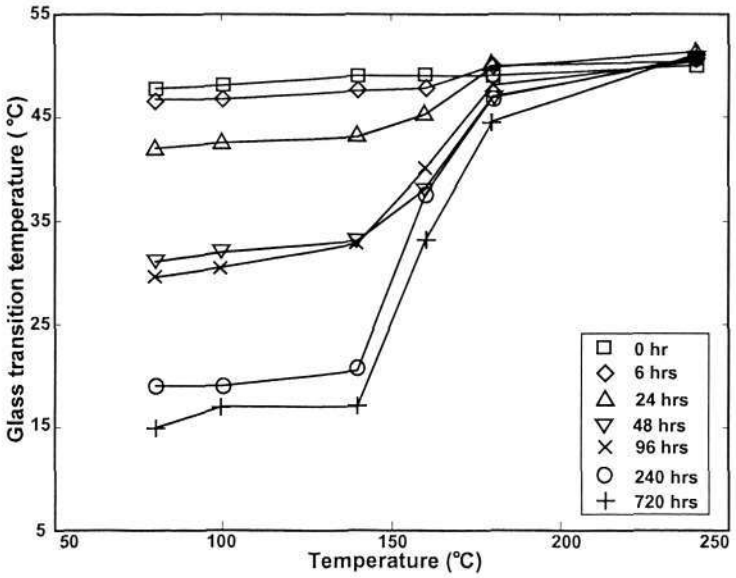

Figure 6.6 Evolution of T_g upon thermal cycling in CB13.

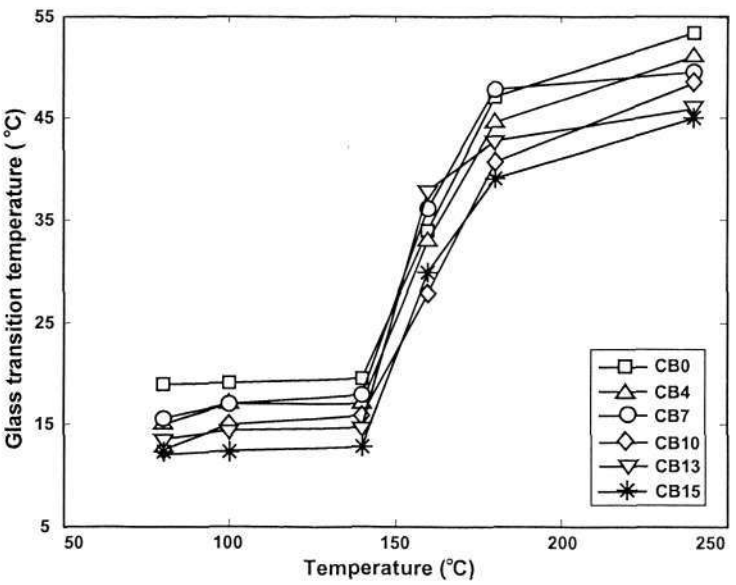

Figure 6.7 Evolution of T_g upon thermal cycling in saturated samples.

6.5 Correlation between moisture absorption, loading of carbon powder and glass transition temperature

Utilizing the data obtained from previous tests, namely the TGA and DSC tests, and following the same approach as that described in Section 4.5, we can figure out the relation between T_g and ratio of moisture to SMP and its composites in weight % for all samples in the immersion and heating processes.

Figure 6.8 shows two typical results. Similar slanted L shape curves between the transition temperature and water content are obtained for all samples upon immersing and later on heating. As indicated, the change in T_g can be obviously divided into two stages. The critical water content (water ratio in weight %) for dividing them is found to be at around 120°C for all cases if the ratios are converted to weight fractions using the water weight fraction at 240°C as the reference. As such, again the total absorbed water can be divided into two parts, namely, the free water and bound water.

Two linear lines were obtained to describe the relationships of T_g vs. ratio of moisture in the immersion and heating processes. These lines have an intersection in the minus zone of moisture content, which corresponds to the real dry state of polyurethane SMP. The ratio of moisture to SMP composite in weight at the positive valued intersection point R_t is listed in Table 6.1 for SMP and its conductive composites.

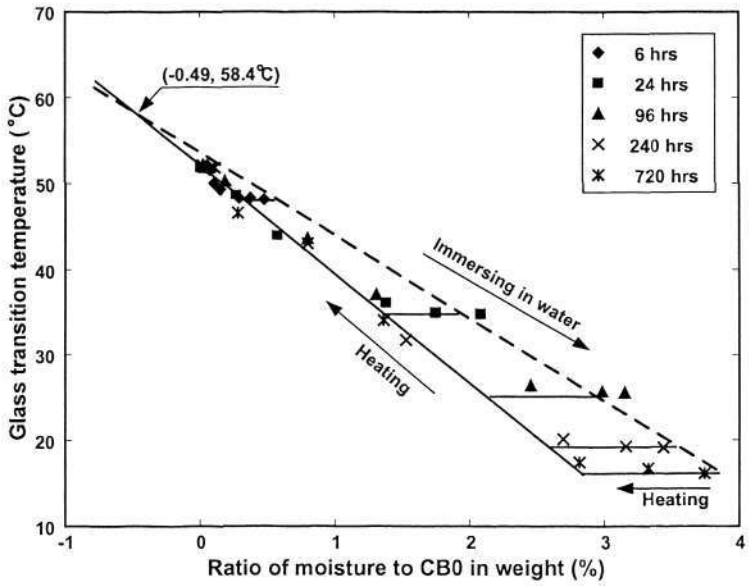

(a)

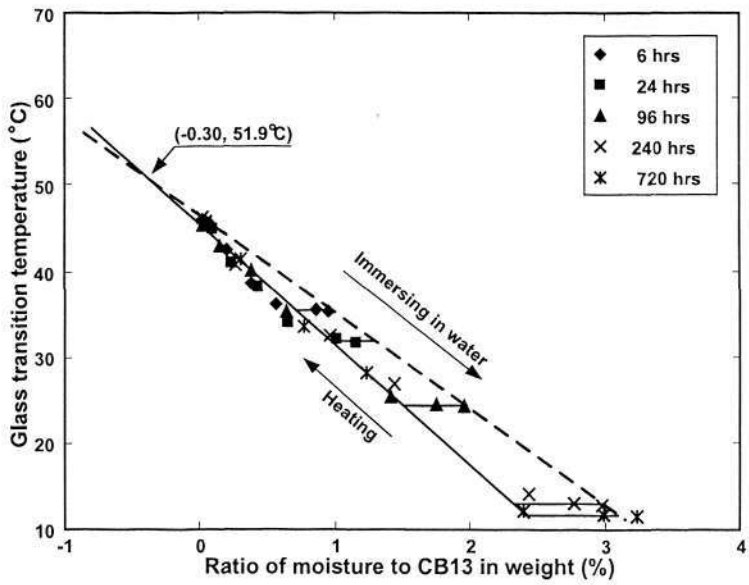

(b)

Figure 6.8 T_g vs. ratio of moisture to SMP composite in weight (a) CB0, (b) CB13.

SMP and its composites	CB0	CB4	CB7	CB10	CB13	CB15
Ratio of moisture evaporated over 240°C (%)	0.49	0.49	0.48	0.38	0.30	0.20

Table 6.1 Ratio of moisture evaporated over 240°C in SMP composites.

After conversion using Equation 4.2 and the values listed in Table 6.1, the linear relationships of the two ratios, namely bound water to SMP and total moisture ratio to SMP, are constructed by data fitting, and plotted in Figure 6.9. Subsequently, T_g of each polyurethane SMP composite at the real dry state and the saturated state are obtained. Figure 6.10 plots T_g of SMP as a function of volume faction of carbon powder. It reveals that T_g of both at the real dry state and the saturated state decreases with the increase of carbon nano-powder. However, in general, the loading of carbon powder has almost no effect on the amplitude of decrease in T_g.

Figure 6.11 plots the moisture ratio in the saturated state against the content of carbon powder. It shows that the loading of carbon powder has negligible effect on the ratio of moisture at the saturated state. Generally, SMP and its electrically conductive composites can absorb about 4.3% moisture in weight when saturated with room temperature water. Figure 6.12 presents the slopes of the lines in Figure 6.9 as functions of volume fraction of carbon powder for immersion and heating processes, respectively. It reveals that all slopes almost linearly increase with the increase of carbon nano-powder. In other words, with the increase of carbon nano-powder content

water has less influence on T_g. Furthermore, the difference between the slopes of immersing in water and heating becomes smaller with the increase of carbon powder.

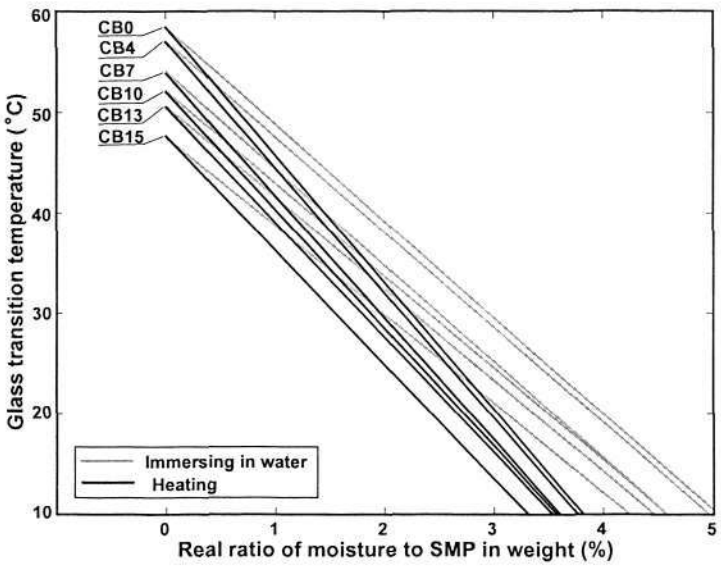

Figure 6.9 T_g vs. real ratio of moisture to SMP in weight.

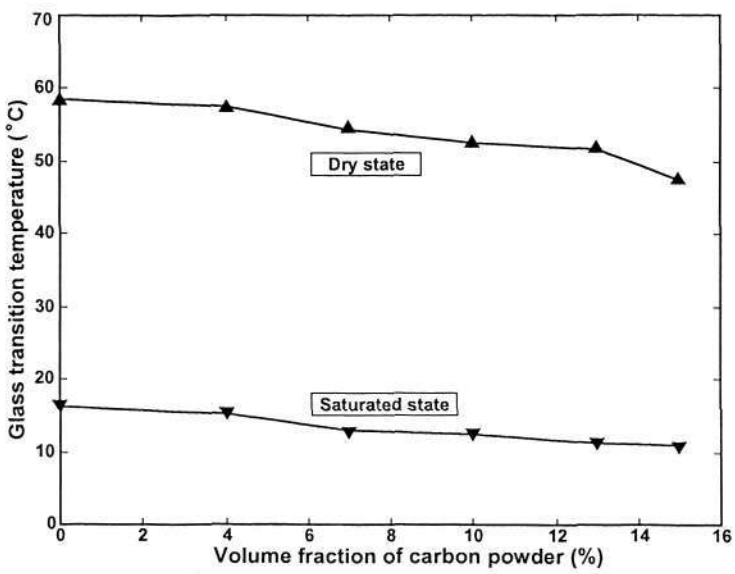

Figure 6.10 T_g vs. volume faction of carbon powder.

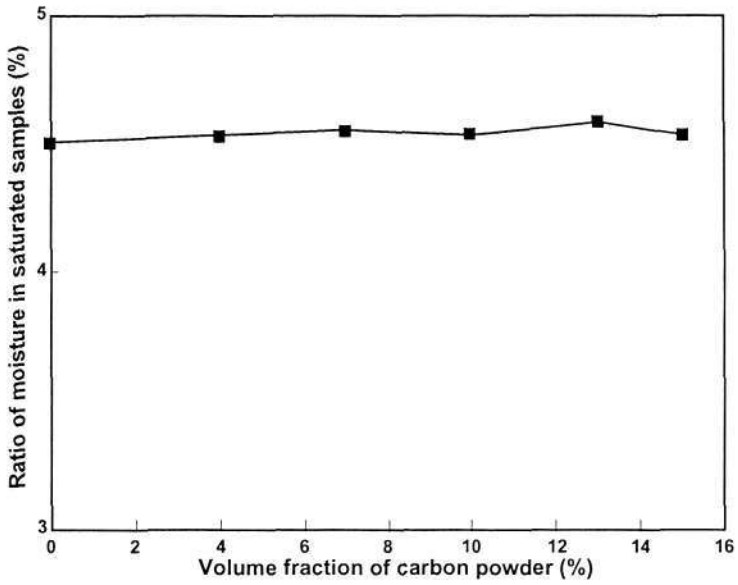

Figure 6.11 Ratio of moisture in saturated samples vs. volume fraction of carbon powder.

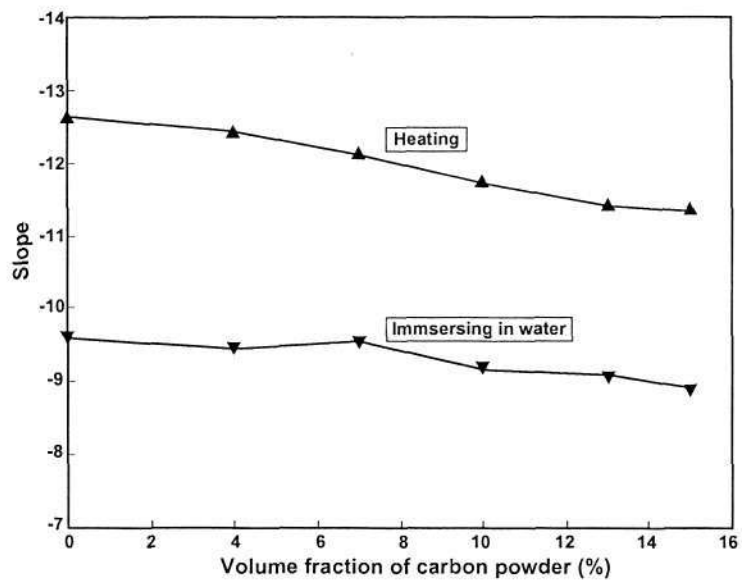

Figure 6.12 Slopes of two theoretical lines vs. volume fraction of carbon powder.

6.6 Effects of moisture on thermomechanical properties

6.6.1 Damping capability

A dynamic mechanical analysis (DMA) test was carried out at a constant frequency of 1Hz on a DMA 2980 (TA Instruments) in film mode. After different immersion hours in room temperature water, the strip samples 15.0 mm long, 3.0 mm wide and 0.5 mm thick were heated at a heating rate of 4°C/min.

A typical result of tangent delta as a function of temperature (CB0) is plotted in Figure 6.13. Note that tangent delta is the ratio of the loss modulus to the storage modulus, which represents the damping capability of a material under shock or vibration. Figure 6.13 shows that, generally, tangent delta reaches a maximum at around T_g in polyurethane SMP. The maximum tangent delta of CB0 without immersing in water is about 1.4, which is much higher than that of a typical high damping rubber. Therefore, CB0 can be used as a superior damping material at around its T_g. Furthermore, this result reveals that the maximum tangent delta of CB0 decreases significantly with the increase in immersion time. The immersion time and the moisture content absorbed by the material are directly related. Therefore, the decrease in damping capability can be directly attributed to the increase of moisture ratio in the material.

Figure 6.14 summarizes the change in maximum tangent delta with the ratio of moisture for SMP and its composites. Note that the ratio of moisture in SMP is determined in the same way as that described in Section 4.1. It shows that, in general, the loading of carbon powder remarkably lowers the damping capability. On the other hand, upon gradually absorbing moisture, the maximum tangent delta of SMP and its

composites decreases to about 0.2. The maximum tangent delta of CB0 almost linearly decreases with the increase of moisture content. However, with the loading of carbon powders, the decrease in the maximum tangent delta becomes less significant. Especially in CB15, there is only a minor change in the maximum tangent delta.

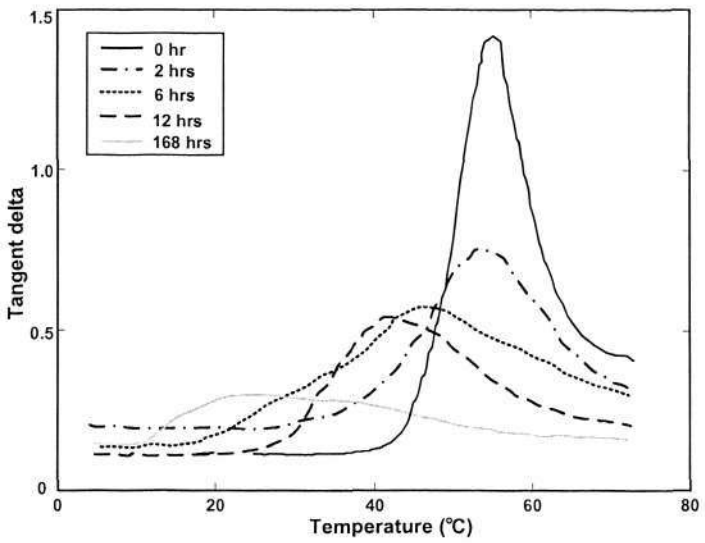

Figure 6.13 Tangent delta as a function of temperature in CB0.

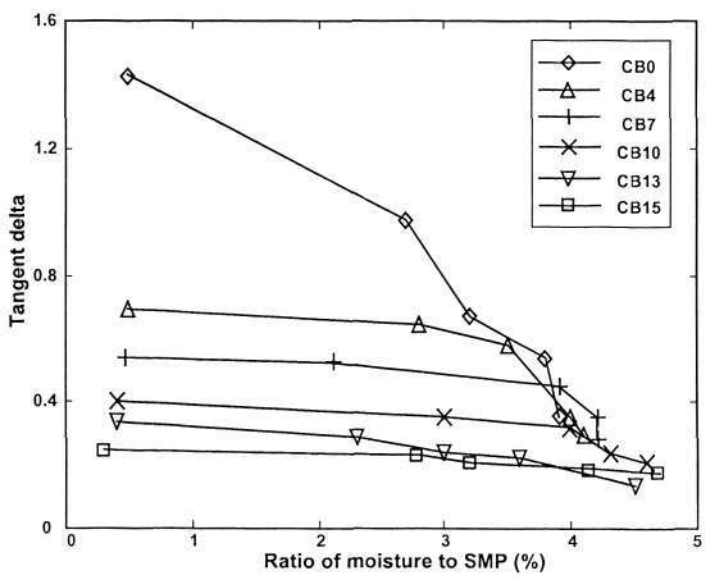

Figure 6.14 Change in the maximum tangent delta with the moisture content.

In order to study whether all materials after immersing in room temperature water can recover their original mechanical properties, two groups of the saturated samples were dried in a vacuum oven for 12 hours. According to previous results, 120°C is the critical point dividing the absorbed water into the two aforementioned parts. Thus, two temperatures, namely, 80°C and 120°C, were chosen for drying the samples in a vacuum oven. It is expected that upon drying at 80°C for 6 hours only free water can be evaporated out, while all free water and some bound water can be removed upon drying at 120°C for 6 hours. The typical results of a saturated sample upon drying are plotted in Figure 6.15. In general, saturated SMP and its composite only partially regained their damping capabilities upon the removal of free water. However, after drying at 120°C for 6 hours their damping capabilities were remarkably regained.

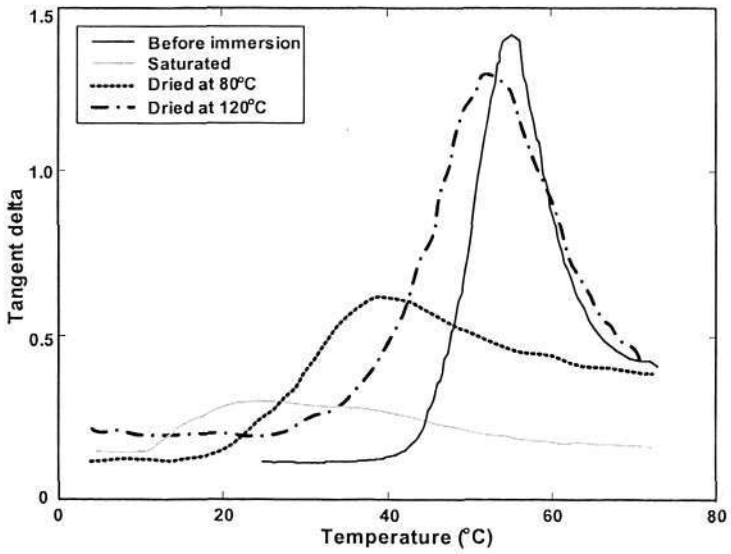

Figure 6.15 Tangent delta as a function of temperature in saturated CB0 upon drying.

6.6.2 Young's modulus

Based on the DMA test results, the Young's modulus of the material is obtained as a function of temperature. Here, one typical result (CB0) is presented in Figure 6.16. The difference in the curves of Young's modulus against temperature with different immersion times is apparent.

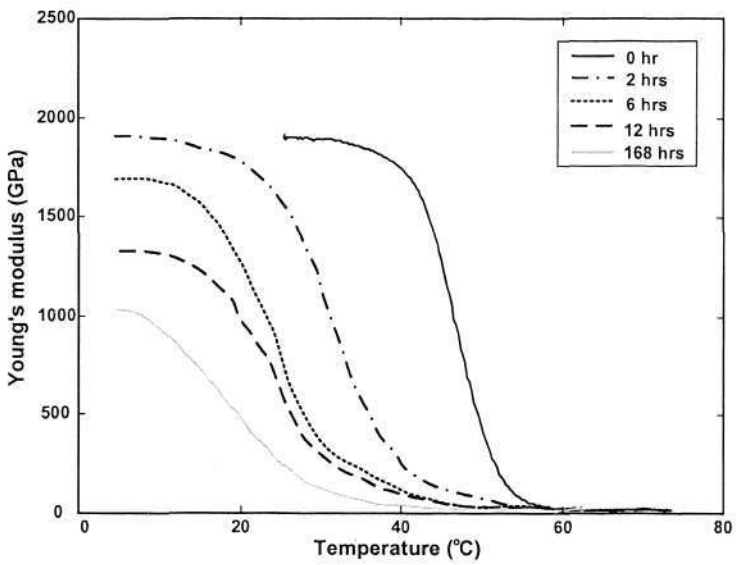

Figure 6.16 Young's modulus as a function of temperature in CB0.

In SMP, the temperature range for glass transition is about 30°C. It can be assumed that SMP is in the glass state at below T_g-15°C, while it is in the rubber state at above T_g+15°C. The influence of temperature on the Young's modulus in SMPs in the glass state or the rubber state is minor. Therefore, it is deemed that the Young's modulus of SMP in the glass state or the rubber state is constant (Tobushi et al 2001). Normally, the Young's modulus of SMP at T_g-15°C is considered as the Young's modulus in the glass state while its Young's modulus at T_g+15°C is considered as the Young's

modulus in the rubber state. For comparison, in this study, the Young's moduli of all samples at T_g -15°C and T_g +15°C are summarized against the moisture content in Figure 6.17. Note that T_g is the temperature corresponding to the peak of tangent delta from the DMA results. It reveals that the Young's modulus of SMP and its composites in the glass state decreases with the increase of moisture content. The decrease of Young's modulus can be attributed to the moisture, which interacts with the polymer chains and plasticizes the polymer. However, there is a negligible change in the Young's modulus in the rubber state.

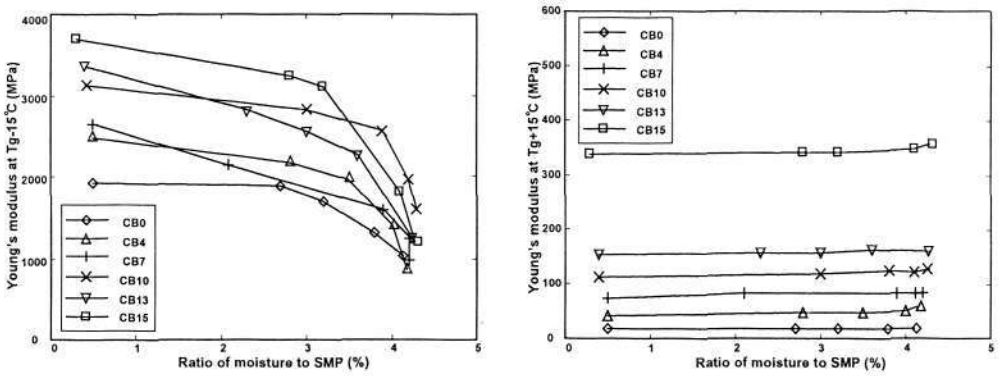

(a) (b)

Figure 6.17 Change in the Young's modulus at different moisture content. (a) At T_g -15°C, (b) at T_g +15°C.

Figure 6.18 presents one typical result of a saturated sample after drying at 80°C and 120°C. It shows that the removal of free water in the sample results in the partial recovery of Young's modulus. Upon drying at 120°C for 6 hours its Young's modulus is remarkably regained.

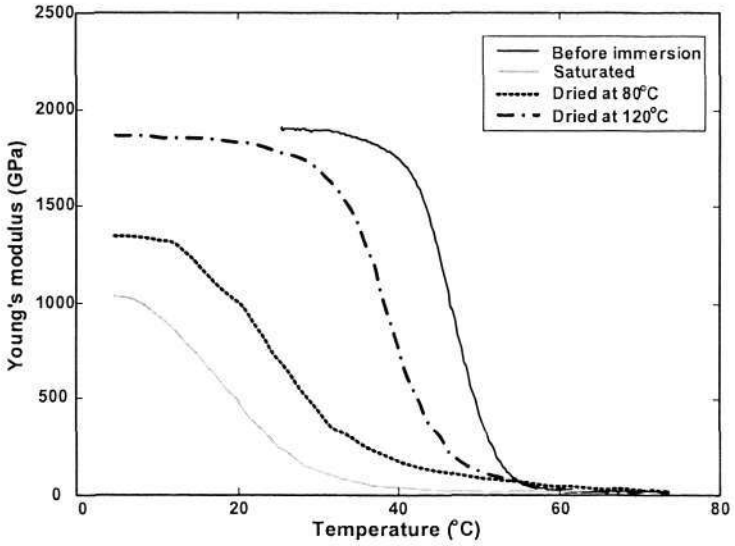

Figure 6.18 Young's modulus as a function of temperature in saturated CB0 upon drying.

6.6.3 Uniaxial tension behavior

Uniaxial tensile tests were carried out on SMP wires with a diameter of 1.0 mm using an Instron 5565 with a 100 N load cell at a constant strain rate of 5×10^{-3}/sec. The gauge length was 40.0 mm. A hot chamber with a tolerance of ±0.5°C was attached to the Instron for temperature control. Two different testing temperatures were chosen, 22°C room temperature and T_g + 25°C at which the polyurethane SMP is in the rubber state. In these experiments, T_g of an individual sample was determined by a DSC test.

Figure 6.19 (a) plots one set of stress-strain curves of SMP wires (CB0) tested at room temperature. It shows two types of distinct behaviors. When the immersion time is shorter than 12 hours, the SMP behaves like a crystalline material, in which a linear

stress-strain relation can be found prior to yielding followed by hardening. When the immersion time exceeds 12 hours, the stress-strain curve is similar to those of rubbers. This curve has no apparent yielding point and shows that a large deformation can be achieved at a low level of stressing. The rubber-like behavior becomes more pronounced over a prolonged immersion period due to the increased mobility of polymer chains. On the other hand, if the uniaxial tensile test is carried out at 25°C above T_g, the SMP becomes more rigid after a longer immersion period as shown in Figure 6.19 (b).

To find the individual roles of free water and bound water on the stress-strain relation additional uniaxial tensile tests were conducted after the following processes. The SMP wires were immersed in water for different hours, and then heated in air up to 80°C and 120°C, respectively, at a constant rate of 10°C/min. Subsequently, the wires were cooled back down to room temperature in 3 minutes. No apparent change in the stress-strain behavior was found in the SMP wires pre-heated to 80°C. The stress-strain curves of SMP wires pre-heated to 120°C are presented as shown in Figure 6.20. Note that according to Figure 6.8, 120°C is the critical point for a full removal of the free water from the SMP. In Figure 6.20 (a), a remarkable change can be found in comparison with the results in Figure 6.19 (a). All samples exhibit a linear stress-strain relation followed by hardening regardless of the immersion duration. The stiffness of the wires obviously increased after the removal of the free water. Apart from this, a very slight increase in T_g is observed after heating to 120°C (Figure 6.8). However, in the tensile test conducted at T_g + 25°C [Figure 6.20 (b)], the removal of free water has no other significant influence apart from that the wires become stiffer after a longer

immersion period of more than 12 hours. At this point, we may conclude that free water only has a very limited effect on the tensile behavior of the SMP, while bound water has a very strong influence.

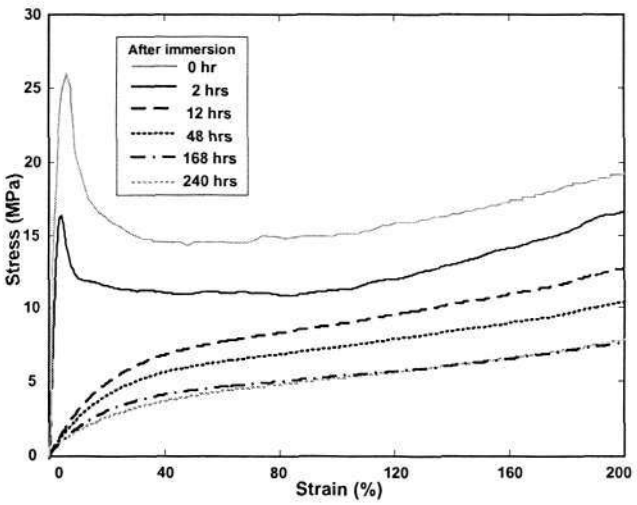

(a)

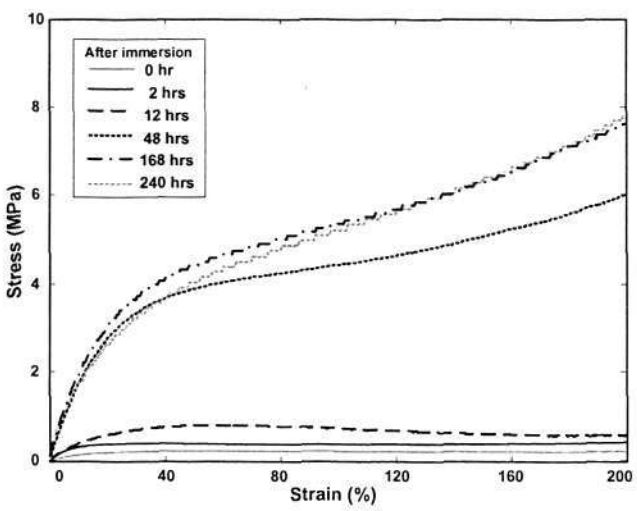

(b)

Figure 6.19 Stress-strain relation after different hour of immersion. (a) At room temperature, (b) at T_g+25°C.

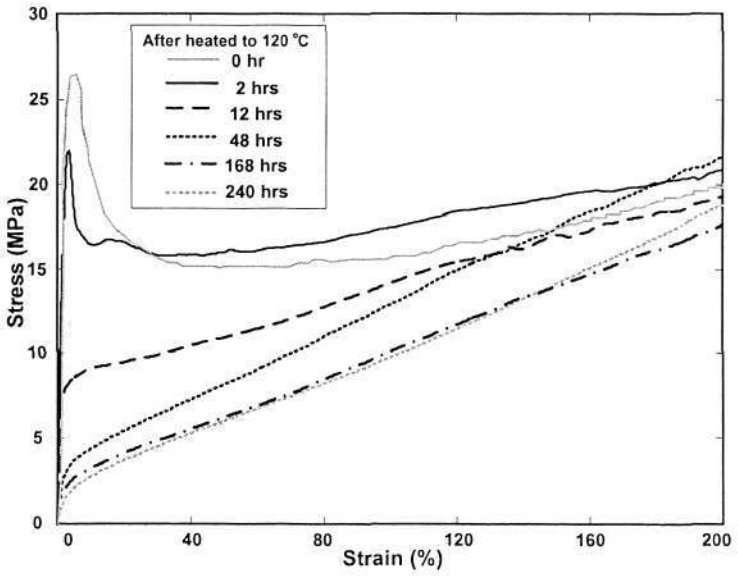

(a)

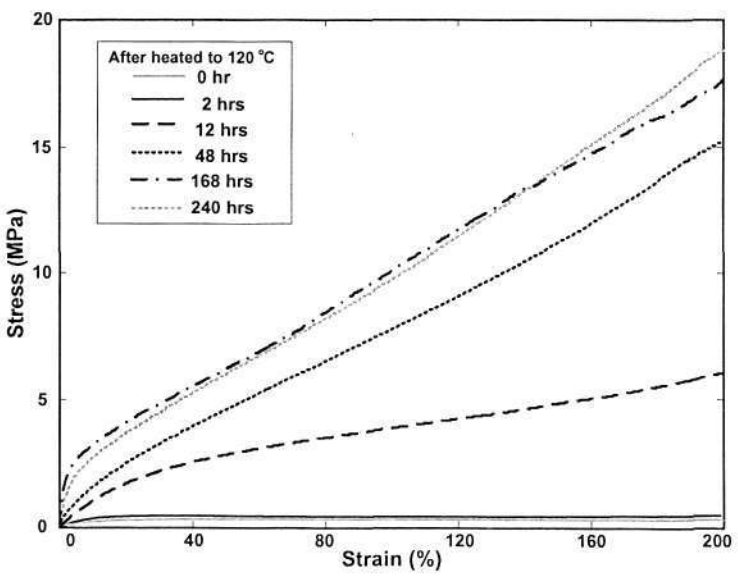

(b)

Figure 6.20 Stress-strain relation after different hour of immersion and heated to 120°C.

(a) At room temperature, (b) at T_g +25°C.

6.6.4 Water actuated shape recovery

In Chapter 4 a new feature of polyurethane SMP, i.e., water actuatable gradient SMP, is proposed. This new feature is also applicable to electrically conductive SMP composites. Figure 6.21 shows the recovery of a CB7 sample actuated by room temperature water.

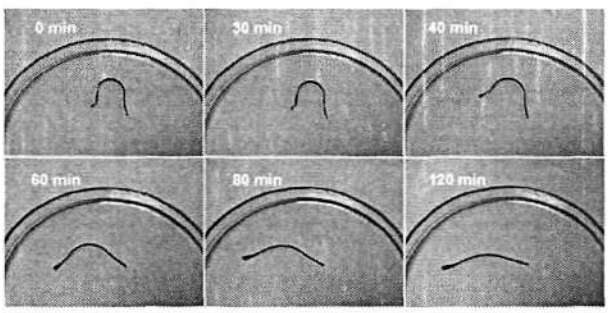

Figure 6.21 Recovery of a CB7 sample actuated by room temperature water.

This section will address the water actuated shape recovery properties of SMP and its composites, which are very important for utilizations of this new feature. Two kinds of tests, water actuated free recovery test and water actuated constrained recovery test, were carried out. Two groups of samples were prepared and pre-strained to 20% following the same procedure as that described in Section 5.7. Subsequently, they were clamped inside an Instron 5569 with a 100 N load cell. A water tank was attached to the Instron machine with the proper sealing and samples were immersed completely in room temperature water for recovery without any heating process as shown in Figure 6.22. One group of samples was unconstrained and could vary their length. The sample was taken out of water and the change in its length was measured after a certain period of time using a microscope. Then the recovered strain was calculated and recorded together with the immersion time. This is the so-called water actuated free recovery test.

The second group of samples was tested under the same conditions except that the length of samples was fixed. The recovery stress was recorded against immersion time using the Instron 5569. This is the so-called water actuated constrained recovery test.

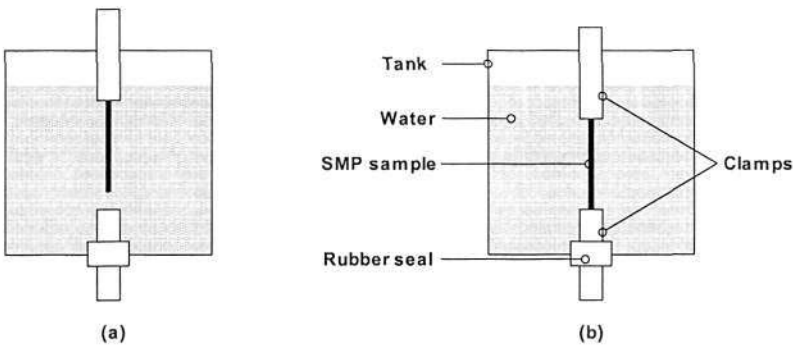

Figure 6.22 Experimental setup of water-actuated recovery tests. (a) Free recovery; (b) constrained recovery.

In Figure 6.23, the recovered strain in the free recovery test is plotted against the immersion time. It shows that after immersion in room temperature water for 60 minutes, all SMPs began to recover. CB0 recovered about 18% strain, which is about 90% of the preloaded maximum strain. However, with the increase of carbon powder content, the recovered strain decreased and the recovery speed became lower.

Figure 6.24 presents the relationship between the recovery stress and immersion time in the constrained recovery test. It shows that, in general, recovery stress begins to increase after 60 minutes of immersion and then gradually reaches a maximum. After that, the recovery stress decreases slowly. About 1.8 MPa stress can be generated in CB0 in the constrained recovery. The loading of carbon powders has a negligible effect on the maximum recovery stress. But the time taken for SMP composite to reach the maximum recovery stress becomes longer with the increase of carbon powder content.

After reaching its maximum, the recovery stress decreases less remarkably with the increase of carbon powder content, which might be attributed to the constraint of carbon powder to the relaxation of polymer.

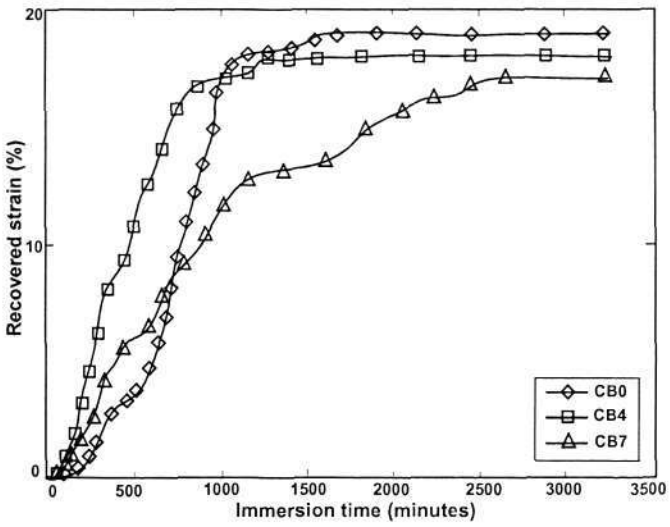

Figure 6.23 Recovered strain vs. immersion time.

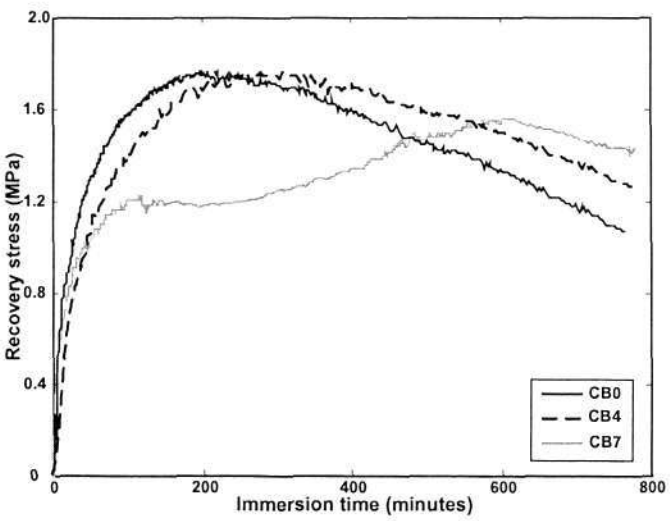

Figure 6.24 Recovery stress vs. immersion time.

6.7 Summary

A series of experiments were carried out to study the effects of moisture on electrically conductive SMP.

Experimental results indicate that the electrical conductivity of conductive SMPs is improved by moisture. This phenomenon is more obvious in SMPs filled with a lower content of carbon powder.

T_g of conductive SMP composites can be reduced effectively by immersing in water. This phenomenon holds valid until the polymer is saturated by water. It is also found that the change in T_g is reversible upon heating or dehydration since the removal and absorption of moisture are physical processes.

The effects of nano-carbon powder and moisture on T_g of conductive SMP composites were separated and qualitatively investigated by a series of TGA and cyclic DSC tests. The relationship of T_g vs. real ratio of moisture to SMP in weight of each SMP composite was obtained. It was found that the added carbon powders have the tendency to reduce T_g. The Bound water in SMP reduces T_g dramatically in a linear fashion, while the influence of free water on T_g is negligible. T_g in the real dry state decreases with the increase of nano-carbon powder in the SMP. With more carbon nano-powder, T_g of SMP becomes less sensitive to water. Overall, T_g is effected by the presence of bound water more than the loading of carbon nano-powder.

The damping capability of conductive SMP composites becomes worse upon immersing in water. The Young's modulus of SMP composites in the glass state decreases with the increase in water content. However, there is almost no change in Young's modulus in the rubber state upon immersing in water. Upon dehydrating the conductive SMP composites remarkably regain the original damping capability and Young's modulus.

Conductive SMP composites can recover a pre-strain by immersing in room temperature water due to the decrease in its T_g. The water actuated recoverable strain decreases with the increase of carbon powder content. However, the carbon powder has negligible influence on the maximum stress generated by water-actuated recovery.

Chapter 7 Conclusions and Future Work

7.1 Conclusions

This dissertation presents a systematic study on a polyurethane SMP, its electrically conductive SMP composites. A particular focus is the influence of moisture on their thermomechanical properties. The following conclusions are obtained.

7.1.1 Effects of moisture on T_g of SMPs

The SMP can absorb about 4.5 wt % of moisture in room temperature water. T_g of the SMP decreases with the increase in immersion time until saturated. The absorbed moisture can be fully removed upon heating and then the polymer can be reused again. Water absorbed in the SMP weakens the hydrogen bonding between N-H and C=O groups and acts as a plasticizer, which causes a significant decrease in T_g.

Water absorbed in the SMP can be split into two parts, namely, free water and bound water. Their respective quantities can be determined by the cyclic DSC test and TGA test. It was found that the free water can be fully removed by evaporation at around 120°C. Free water absorbed in SMP has the negligible effects on T_g (and thus the thermomechanical properties), while bound water significantly reduces T_g in an almost linear manner.

Two new features of the polyurethane SMP are demonstrated. One is the water actuated shape recovery in a programmable way due to the gradient of T_g realized by immersing different parts of the SMP in water for different periods. Another is the formation of porous SMP using moisture as a nontoxic agent.

The difference in water actuated recovery and thermally induced one is revealed.

7.1.2 Electrically conductive SMPs

Nano-carbon powders distribute in the SMP matrix randomly with an agglomerate size of 100~200 nm in diameter. 6% volume fraction of carbon powders is the percolation threshold. At over this threshold, the conductive network is formed in the composite resulting in a sharp transition from being insulating to being electrically conductive.

The thermomechanical properties of the nano-carbon powder filled SMPs are systematically investigated. The major properties are summarized in Appendix C, which can be used as a guideline for any application in the future. The carbon powder-filled SMP composite CB13 shows excellent electrical conductivity as well as good shape memory properties. It can be heated directly and efficiently by passing an electrical current for shape recovery.

The influence of moisture on the nano-carbon powder filled SMPs is investigated. Water- driven shape recovery and gradient T_g, as those in the pure SMP, are demonstrated.

7.2 Future work

In terms of future work, there are several directions to explore.

a. A theoretical model can be built to describe the influences of moisture and carbon powders on the thermomechanical properties of SMPs.

b. Currently water-actuated recovery in polyurethane SMPs is slow. It is necessary to develop SMPs that can react faster to water.

References

[1] Abrahamson ER, Lake MS, Munshi NA, Gall K (2003). Shape memory mechanics of an elastic memory composite resin. Journal of Intelligent Material Systems and Structures, 14 (10), 623-632.

[2] Ahmad MY, Mustafah J, Mansor MS, Mohd Ishak ZA, Mohd Omar AK (1995). Thermal properties of polypropylene/rice husk ash composites. Polymer International, 38 (1), 33-43.

[3] Aklonis JJ, Macknight WJ (1983). Introduction to Polymer Viscoelasticity, New York: John Wiley & Sons.

[4] Alexander M, Dubois P (2000). Polymer-layered silicate nanocomposites: preparation, properties and uses of a new class of materials. Materials Science and Engineering, 28, 1-63.

[5] Aneli, JN, Zaikov GE, Khananashvili LM (1999). Effects of mechanical deformations on the structurization and electric conductivity of electric conducting polymer composites. Journal of Applied Polymer Science, 74 (3), 601-621.

[6] Azulay D, Eylon M, Eshkenazi O, Toker D, Balberg M, Shimori N, Millo O, Balberg I (2003). Electrical-thermal switching in carbon-black-polymer composites as a local effect. Physical Review Letters, 90 (23), 236601/1-4.

[7] Bhattacharyya A, Tobushi H (2000). Analysis of the isothermal mechanical response of a shape memory polymer rheological model. Polymer Engineering and Science, 40 (12), 2498-2510.

[8] Bhattacharya SK (1986). Metal-filled polymers: properties and applications, Marcel Dekker.

[9] Brunette CM, Hsu SL, MacKnight WJ (1982). Hydrogen-bonding properties of hard-segment model compounds in polyurethane block copolymers. Macromolecules, 15 (1), 71-77.

[10] Bryk MT (1991). Degradation of Filled Polymers, Chichester: Ellis Horwood Ltd.

[11] Cadogan DP, Scarborough SE, Lin JK, Sapna III GH (2002). Shape memory composite development for use in gossamer space inflatable structures. Collection of Technical Papers - AIAA/ASME/ASCE/AHS/ASC Structures, Structural Dynamics and Materials Conference, 2, 1294-1304.

[12] Cao YP, Guan Y, Du J, Peng Y, Chan Albert SC, Yip CW (2003). Polymer network-poly(ethylene glycol) complexes with shape memory effect. Chinese Journal of Polymer Science (English Edition), 21 (1), 29-33.

[13] Carmona F, Ravier J (2002). Electrical properties and mesostructure of carbon black-filled polymers. Carbon, 40 (2), 151-156.

[14] Chen TK, Tien YI, Wei KH (2000). Synthesis and characterization of novel segmented polyurethane/clay nanocomposites. Polymer, 41 (4), 1345-1353.

[15] Chiodo JD, Billett EH, Harrison DJ (1999). Active disassembly using shape memory polymers for the mobile phone industry. Proceedings of the 1999 IEEE International Symposium on Electronics and the Environment (Cat. No.99CH36357), 151-156.

[16] Clegg DW, Collyer AA (1986). Mechanical properties of reinforced thermoplastics, Elsevier Applied Science Publishers.

[17] Cho JW, Lee SH (2004). Influence of silica on shape memory effect and mechanical properties of polyurethane-silica hybrids. European Polymer Journal, 40 (7), 1343-1348.

[18] Cotts DB, Reyes Z (1986). Electrically Conductive Polymers for Advanced Applications, Noyes Data Corporation, Park Ridge, New Jersey, US.

[19] Das NC, Chaki TK, Khastgir D (2002). Effect of processing parameters, applied pressure and temperature on the electrical resistivity of rubber-based conductive composites. Carbon, 40 (6), 807-816.

[20] Das NC, Chaki TK, Khastgir D (2002). Effect of axial stretching on electrical resistivity of short carbon fibre and carbon black filled conductive rubber composites. Polymer International, 51 (2), 156-163.

[21] Duerig T, Pelton A, Stöckel D (1999). An overview of nitinol medical applications. Materials Science and Engineering A (Structural Materials: Properties, Microstructure and Processing), A273-275 (15), 149-160.

[22] Eisenberg MA (1980). Introduction to Mechanics of Solids, Addison: Wesley.

[23] El-Tantawy F, Kamada K, Ohnabe H (2002). In situ network structure, electrical and thermal properties of conductive epoxy resin-carbon black composites for electrical heater applications. Materials Letters, 56 (1-2), 112-126.

[24] Flandin L, Chang A, Nazarenko S, Hiltner A, Baer E (2000). Effect of strain on the properties of an ethylene-octene elastomer with conductive carbon fillers. Journal of Applied Polymer Science, 76 (6), 894-905.

[25] Flandin L, Hiltner A, Baer E (2001). Interrelationships between electrical and mechanical properties of a carbon black-filled ethylene-octene elastomer. Polymer, 42 (2), 827-838.

[26] Frenger, Paul (1993). Biomedical uses of shape memory polymers. Journal of Biomedical Sciences Instrumentation, 29, 47-50.

[27] Gall K, Dunn ML, Liu YP, Finch D, Lake M, Munshi NA (2002). Shape memory polymer nanocomposites. Acta Materialia, 50 (20), 5115-5126.

[28] Gall K, Dunn ML, Liu YP, Stefanic G, Balzar D (2004). Internal stress storage in shape memory polymer nanocomposites. Applied Physics Letters, 85 (2), 290-292.

[29] Gall K, Kreiner P, Turner D, Hulse M (2004). Shape-memory polymers for microelectromechanical systems. Journal of Microelectromechanical Systems, 13 (3), 472-483.

[30] Gall K, Mikulas M, Munshi NA, Tupper M (2000). Carbon fiber reinforced shape memory polymer composites. Journal of Intelligent material systems and structures, 11 (11), 877-886.

[31] Gilman JW, Jackson CL, Morgan AB, Jr RH, Manias E, Giannelis EP, Wuthenow M, Hilton D, Phillips SH (2000). Flammability properties of polymer-layered-silicate nanocomposites. Polypropylene and polystyrene nanocomposites. Chemistry of Materials, 12, 1866-1873.

[32] Hatakeyama T, Quinn FX (1994). Thermal analysis: fundamentals and applications to polymer science, Chichester, England; New York: Wiley.

[33] Hayashi S (1990). Technical report on preliminary investigation of shape memory polymers, Nagoya research and development center, Mitsubishi Heavy Industries Inc.

[34] Hayashi S (1993). Properties and applications of polyurethane-series shape memory polymer. International Progress in Urethanes, 6, 90-115.

[35] Hayashi S, Kondo S, Giordano C (1994). Properties and applications of polyurethane-series shape memory polymer. Proceedings of the 52nd Annual Technical Conference ANTEC, Part 2, 1998-1999.

[36] Hayashi S, Kondo S, Kapadia P, Ushioda E (1995). Room-temperature-functional shape-memory polymers. Plastic Engineering, 51 (2), 29-31.

[37] Heintz AM, McKiernan RL, Gido SP, Penelle J, Hsu S, Sasaki S, Takahara A, Kajiyama T (2002). Crystallization behavior of strongly interacting chains. Macromolecules, 35 (8), 3117-3125.

[38] Herrera-Gómez A, Velázquez-Cruz G, Martín-Polo MO (2001). Analysis of the water bound to a polymer matrix by infrared spectroscopy. Journal of Applied Physics, 89 (10), 5431-5437.

[39] Huang W (1998). Shape memory alloys and their application to actuators for deployable structures, PhD Thesis, Cambridge University.

[40] Hu Z, Zhang X, Li Y (1995). Synthesis and application of modulated polymer gels. Science, 269 (5223), 525-7.

[41] Ishigure Y, Iijima S, Ito H, Ota T, Unuma H, Takahashi M, Hikichi Y (1999). Electrical and elastic properties of conductor-polymer composites. Journal of Materials Science, 34 (12), 2979-2985.

[42] Jäger K-M, McQueen DH, Tchmutin IA, Ryvkina NG, Klüppel M (2001). Electron transport and ac electrical properties of carbon black polymer composites. Journal of Physics D: Applied Physics, 34 (17), 2699-2707.

[43] Jeong HM, Ahn BK, Kim BK (2001). Miscibility and shape memory effect of thermoplastic polyurethane blends with phenoxy resin. European Polymer Journal, 37 (11), 2245-2252.

[44] Kim BK, Lee SY, Xu M (1996). Polyurethanes having shape memory effects. Polymer, 37 (26), 5781-5793.

[45] Knite M, Teteris V, Polyakov B, Erts D (2002). Electric and elastic properties of conductive polymeric nanocomposites on macro- and nanoscales. Materials Science and Engineering C, 19 (1-2), 15-19.

[46] Kost J, Narkis M, Foux A (1984). Resistivity behavior of carbon-black-filled silicone rubber in cyclic loading experiments. Journal of Applied Polymer Science, 29 (12), 3937-3946.

[47] Lee AP, Fitch JP (2000). United States Patent 6, 086, 599, 2000.

[48] Lee AP, Northrup MA, Ciarlo DR, Krulevitch PA, Benett WJ (2000). United States Patent 6, 102,933, 2000.

[49] Lee BS, Chun BC, Chung YC, Sul KI, Cho JW (2001). Structure and thermomechanical properties of polyurethane block copolymers with shape memory effect. Macromolecules, 34 (18), 6431-6437.

[50] Lendlein A, Langer R (2002). Biodegradable, elastic shape-memory polymers for potential biomedical applications. Science, 296 (5573), 1673-1676.

[51] Li FK, Chen Y, Zhu W, Zhang X, Xu M (1998). Shape memory effect of polyethylene/nylon 6 graft copolymers. Polymer, 39 (26), 6929-6934.

[52] Li FK, Hou J, Zhu W, Zhang X, Xu M, Luo X, Ma D, Kim BK (1996). Crystallinity and morphology of segmented polyurethanes with different soft-segment length. Journal of Applied Polymer Science, 62 (4), 631-638.

[53] Li FK, Larock RC (2001). New soybean oil-styrene-divinylbenzene thermosetting copolymers. I. Synthesis and characterization. Journal of Applied Polymer Science, 80 (4), 658-670.

[54] Li FK, Perrenoud A, Larock RC (2001). Thermophysical and mechanical properties of novel polymers prepared by the cationic copolymerization of fish oils, styrene and divinylbenzene. Polymer, 42 (26), 10133-10145.

[55] Li FK, Qi L, Yang J, Xu M, Luo X, Ma D (2000). Polyurethane/conducting carbon black composites: structure, electric conductivity, strain recovery behavior, and their relationships. Journal of Applied Polymer Science, 75 (1), 68-77.

[56] Liang C, Rogers CA, Malafeew E (1997). Investigation of shape memory polymers and their hybrid composites. Journal of Intelligent Material Systems and Structures, 8 (4), 380-386.

[57] Lim LT, Britt IJ, Tung MA (1999). Sorption and transport of water vapor in nylon 6, 6 film. Journal of Applied Polymer Science, 71 (2), 197–206.

[58] Liu WG, Zhang JR, Yao KD (2002). DNA/lipid complex organogel with shape-memory behavior Journal of Applied Polymer Science, 86 (1), 259-263.

[59] Luo N, Wang DL, Ying SK (1997). Hydrogen-bonding properties of segmented polyether poly(urethane urea) copolymer. Macromolecules, 30 (15), 4405-4409.

[60] Maitland DJ, Lee AP, Schumann DL, Silva LD (2000). US Patent 6, 102, 917, 2000.

[61] Maitland DJ, Wilson T, Metzger M, Schumann DL (2002). Laser-activated shape memory polymer microactuators for treating stroke. Proceedings of SPIE - The International Society for Optical Engineering, 4626, 394-402.

[62] Metcalfe A, Desfaits A-C, Salazkin I, Yahia LH, Sokolowski WM, Raymond J (2003). Cold hibernated elastic memory foams for endovascular interventions. Biomaterials, 24 (3), 491-497.

[63] Monkman GJ (2000). Advances in shape memory polymer actuation Mechatronics, 10 (4-5), 489-498.

[64] Mooney DJ, Baldwin DF, Suh NP, Vacanti JP, Langer R (1996). Novel approach to fabricate porous sponges of poly(D,L-lactic-co- glycolic acid) without the use of organic solvents. Biomaterials, 17(14), 1417-1422.

[65] Morgan H, Foot PJS (2001). The effects of composition and processing variables on the properties of thermoplastic polyaniline blends and composites. Journal of Materials Science, 36 (22), 5369 – 5677.

[66] Nalwa HS (1997). Handbook of Organic Conductive Molecules and Polymers 2, New York: John Wiely & Sons.

[67] Nelson BA, King WP, Gall K (2005). Shape recovery of nanoscale imprints in a thermoset "shape memory" polymer. Applied Physics Letters, 86 (10), 103108-1-3.

[68] Ota S (1981). Current Status of Irradiated Heat-Shrinkable Tubing in Japan. Radiation Physics and Chemistry, 18 (1-2), 81-87.

[69] Otsuka K, Wayman CM (1998). Shape memory materials, Cambridge University Press.

[70] Pramanik PK, Khastagir D, Saha TN (1993). Effect of extensional strain on the resistivity of electrically conductive nitrile-rubber composites filled with carbon filler. Journal of Materials Science, 28 (13), 3539-3546.

[71] Puffr R, Sebenda J (1967). On structure and properties of polyamides -- 27, 28. Journal of Polymer Science C, 16, 79–93.

[72] Sahimi M (1994). Applications of percolation theory, London: Taylor and Francis.

[73] Sheng P, Sichel EK, Gittleman JI (1978). Fluctuation-induced tunneling conduction in carbon-polyvinylchloride composites. Physical Review Letters, 40 (18), 1197-1200.

[74] Seki T, Tanaka K, Ichimura K (1997). Photomechanical response in monolayered polymer films on Mica at high humidity. Macromolecules, 30 (20), 6401-6403.

[75] Sperling LH (1986). Introduction to physical polymer science, New York: Wiley.

[76] Stauffer D, Aharony A (1994). Introduction to percolation theory, London: Taylor and Francis.

[77] Takahashi T, Hayashi N, Hayashi S (1996). Structure and properties of shape-memory polyurethane block copolymers. Journal of Applied Polymer Science, 60 (7), 1061-1069.

[78] Teo HS, Chen CY, Kuo JF (1997). Fourier transform infrared spectroscopy study on effects of temperature on hydrogen bonding in amine-containing polyurethanes and poly (urethane-urea)s. Macromolecules, 30 (6), 1793-1799.

[79] Thommerel E, Valmalette JC, Musso J, Villain S, Gavarri JR, Spada D (2002). Relations between microstructure, electrical percolation and corrosion in metal - Insulator composites. Materials Science and Engineering A, 328 (1), 67-79.

[80] Thompson RC, Shung AK, Yaszemski MJ, Mikos AG (2000). The Principles of Tissue Engineering, Sam Diego: Academic Press.

[81] Tobushi H, Hara H, Yamada E, Hayashi S (1996). Thermomechanical properties in a thin film of shape memory polymer of polyurethane series. Smart Materials and Structures, 5 (4), 483-491.

[82] Tobushi H, Hashimoto T, Hayashi S, Yamada E (1997). Thermomechanical constitutive modeling in shape memory polymer of polyurethane series. Journal of Intelligent Material Systems and Structures, 8 (8), 711-718.

[83] Tobushi H, Hashimoto T, Ito N, Hayashi S, Yamada E (1998). Shape fixity and shape recovery in a film of shape memory polymer of polyurethane series. Journal of Intelligent Material Systems and Structures, 9 (2), 127-136.

[84] Tobushi H, Hayashi S, Kojima S (1992). Mechanical properties of shape memory polymer of polyurethane series. (Basic characteristics of stress-strain-temperature relationship). JSME International Journal, 35 (3), 296-302.

[85] Tobushi H, Okumura K, Hayashi S, Ito N (2001). Thermomechanical constitutive model of shape memory polymer. Mechanics of Materials, 33 (10), 545-554.

[86] Wache HM, Tartakowska DJ, Hentrich A, Wagner MH (2003). Development of a polymer stent with shape memory effect as a drug delivery system. Journal of Materials Science: Materials in Medicine, 14 (2), 109-112.

[87] Wei ZG, Sandstrom R, Miyazaki S (1998). Shape-memory materials and hybrid composites for smart systems. I. Shape-memory materials. Journal of Materials Science 33 (15), 3743-3762.

[88] Wever DJ, Veldhuizen AG, Vries JD, Busscher HJ, Uges DRA, Horn JR (1998). Electrochemical and surface characterization of a nickel-titanium alloy. Biomaterials, 19 (7-9), 761-769.

[89] Wineman AS, Rajagopal KR (2000). Mechanical response of polymers, Cambridge University Press.

[90] Wu J, Mclachlan DS (1997). Percolation exponents and thresholds obtained from the nearly ideal continuum percolation system graphite-boron nitride. Physical Review B (Condensed Matter), 56 (3), 1236-1248.

[91] Yang JH, Chun BC, Chung YC, Cho JH (2003). Comparison of thermal/mechanical properties and shape memory effect of polyurethane block-copolymers with planar or bent shape of hard segment. Polymer, 44 (11), 3251-3258.

[92] Yang Z (1997). Research of shape memory materials by heating. Polymeric Materials Science and Engineering (Chinese Edition) 13 (4), 19-23.

[93] Yen FS, Lin LL, Hong JL (1999). Hydrogen-bond interactions between urethane-urethane and urethane-ester linkages in a liquid crystalline poly(ester-urethane). Macromolecules, 32 (9), 3068-3079.

[94] Yoon JP, Han CD (2000). Effect of thermal history on the rheological behavior of thermoplastic polyurethanes. Macromolecules, 33 (6), 2171-2183.

[95] Zdrahala RJ, Zdrahala IJ (1999). Biomedical applications of polyurethanes: A review of past promises, present realities, and a vibrant future. Journal of Biomaterials Applications, 14 (1), 67-90.

[96] Zeng J, Saltysiak B, Johnson WS, Schiraldi DA, Kumara S (2004). Processing and properties of poly (methyl methacrylate)/carbon nano fiber composites. Composites Part B: Engineering, 35 (2), 173-178.

[97] Zheng W, Wong SC (2003). Electrical conductivity and dielectric properties of PMMA/expanded graphite composites. Composites Science and Technology, 63 (2), 225-235.

[98] Zhou JS, Yan FY, Tian N, Zhou JF (2005). Effect of temperature on the tribological and dynamic mechanical properties of liquid crystalline polymer. Polymer Testing, 24 (3), 270-4.

[99] Merzlyakov M, Wurm, A, Zorzut M, Schick C (1999). Frequency and temperature amplitude dependence of complex heat capacity in the melting region of polymers. Journal of Macromolecular Science-Physics, 38 (5-6), 1045-54.

Appendix A

Technical Data of Polyurethane SMPs (pellet form)

(From Mitsubishi Heavy Industries)

(a) Ether-base:

Item	Unit	SMP MM2510		SMP MM3510		SMP MM4510		SMP MM5510	
		G/R	R/R	G/R	R/R	G/R	R/R	G/R	R/R
Hardness	H_D D	75	30	78	25	77	25	79	25
100% Modulus	Mpa	/	9	/	8	/	8	/	10
Tensile Strength	MPa	60	35	60	32	71	33	61	33
Elongation	%	/	>600	/	>600	/	>600	/	>600
Bending Modulus	MPa	2200	/	2200	/	2500	/	2000	/
Bending Strength	MPa	80	/	80	/	95	/	90	/
Specific Gravity	/	1.25		1.25		1.25		1.25	
T_g	°C	25		35		45		55	

(b) Ester-based:

Item	Unit	SMP MM2520		SMP MM3520		SMP MM4520		SMP MM5520	
		G/R	R/R	G/R	R/R	G/R	R/R	G/R	R/R
Hardness	H_D D	78	26	77	30	76	30	77	27
100% Modulus	MPa	/	3	/	2.3	/	1.4	/	2.1
Tensile Strength	MPa	45	12	51	10	55	10	48	13
Elongation	%	/	>600	/	>600	/	>600	/	>600
Bending Modulus	MPa	2500	/	2500	/	2200	/	2200	/
Bending Strength	MPa	90	/	85	/	80	/	80	/
Specific Gravity	/	1.25		1.25		1.25		1.25	
T_g	°C	25		35		45		55	

Appendix B

Technical Guide for Injection Molding of Shape Memory Polymer

(From Mitsubishi Heavy Industries)

Injection mold is most popular mass production method. Injection molding provides good finish surface and accurate dimension as well as producing a desired shape. Shape Memory Polymer is a sensitive material to temperature. Especially its viscosity is very sensitive to temperature. SMP shows good fluidability in a mold, so it does not require high pressure for injection. Following are our recommendation. Please refer.

1. Injection molding machine

It is recommended to select an injection machine, which has a capability having short material residence in a barrel not to degrade the material while is in there.

(a) Injection Volume: Injection volume should be 1.5 times larger than that of production volume.

(b) Screw L/D Ratio: (Flight length of screw)/ (outside diameter of screw) =L/D is recommended to be larger than 18.

(c) Compression Ratio; (Depth of feed section) / (Depth of metering section) is recommended to have 2 to 3.5.

2. Mold

As well as thermoplastic Polyurethane, similar care may be necessary.

(a) Sprue

Compared to ordinary plastic like PP or ABS, a shorter Sprue bushing design is recommended. The preferable taper angle of it is 3 to 5 degrees. Because of low softening temperature, the sprue demold risk is exist. So it is recommended to take detachable sprue for a modification.

(b) Runner

If full round runner is taken, it's diameter is recommended to be Φ 5~8mm. Box designed runner is also feasible, in that case a larger draft taper is recommended.

(c) Cold slug well

Use of cold slug well is not always necessary. However in case of cold runner design, cold slug well at the end of runner or sprue is effective to make a product surface smooth.

(d) Gate

The desirable gate location is in thicker portion of a mold for a purpose of maintaining the holding pressure. When the temperature of the melt polymer flow in the mold is low, a viscosity of the material is increased. So in the case of a mold product having a thickness less than 1-mm, it is recommended to increase the number of gates. For your reference, flow length of it is estimated about 70 to 80 mm. A gate sectional area of 1.5 to 2.0 larger compared to ordinary polymer is preferable in order to reduce bubbles voids. Basically any gate type used for popular plastics can be applied.

(e) Cavity

Due to the shape memory character, the deformations created during the ejection process tend to be memorized. When it is required to eject at the temperature above glass transition temperature of the material (T_g), number of ejection pins having more

than 1.5 times for ordinary polymer as well as larger draft angle of the cavity are recommended.

(f) Venting

The depth of a gap for venting shall be 0.01 to 0.03mm. The existence of the insert may alleviate trapped air problem.

(g) Cooling

Large cooling capacity is required, because the ejecting product is cooled down to the temperature lower than the T_g. Especially cooling capacity around the down stream position of sprue having a large diameter is desired to be increased Shrinkage

3. Suggestion for injection mold

(a) Mold shrinkage

Mold shrinkage of the products after injection is estimated about 0.4 to 0.6%. In order to shorten an injection cycle, large shrinkage of several percent may result in, when a product is ejected out before its core is cool down at the temperature lower than the T_g of a material. In summer if the room temperature is above the T_g, due to the release of residual stresses, large heat shrinkage also may occur.

(b) Melt temperature

The desirable melt temperature of SMP for injection mold is 205 to 215 °C. Smaller shrinkage will be obtained with higher melt temperature for a product of thinner than 2 mm. In case of thicker than 5mm, lower melt temperature is better to avoid an appearance of void and babbles. The recommended temperature profiles of injection machine smaller than 10 oz (about 284g) are as follows,

Feed section: 160 to 180°C

1st transition section and metering section: 190 to 210°C

Nozzle: 195 to 205°C

(c) Injection speed

Higher injection speed should be selected for thin product such as 2 mm thick less, that is easy to get higher cooling rate and then the filling material is rapidly cooled. If there is surface defect such as silver streak in the product, slower speed is required. If it is not right remedy for short shot or surface defect, it is recommended to set the barrel temperature lower by 5-10 degree Celsius.

(d) Holding time

1.5 to 2 times longer holding time is recommended compared to ordinary plastic.

e) Screw backpressure

For the purpose of air vent among pellets, about 5Mpa is required. However, the screw backpressure should not exceed 10MPa.

(f) Surface temperature

The surface temperature of the mold is preferably adjusted at 5 to 10°C lower than the T_g temperature of Shape memory polymer. In case of utilizing the material of which T_g is lower than 35°C, the surface temperature of the mold should be lower than 20°C. In this case some care must be taken to avoid dew on the cavity surface.

Appendix C

Properties of nano-carbon powder filled SMPs

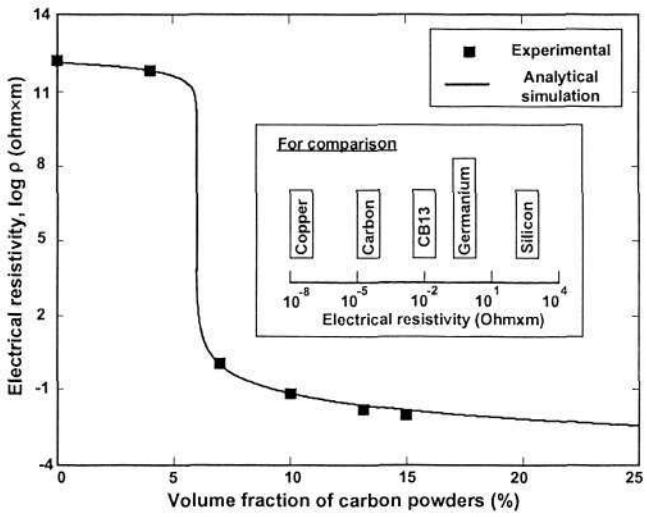

Figure 1 Electrical resistivity vs. volume fraction of carbon powders.

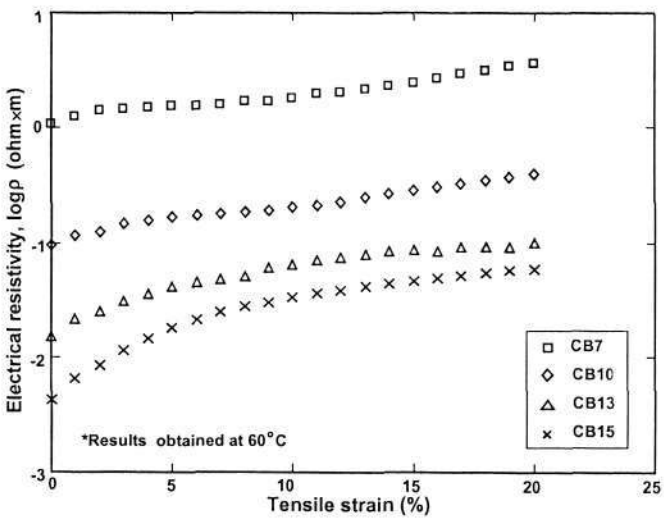

Figure 2 Electrical resistivity vs. tensile strain relationship.

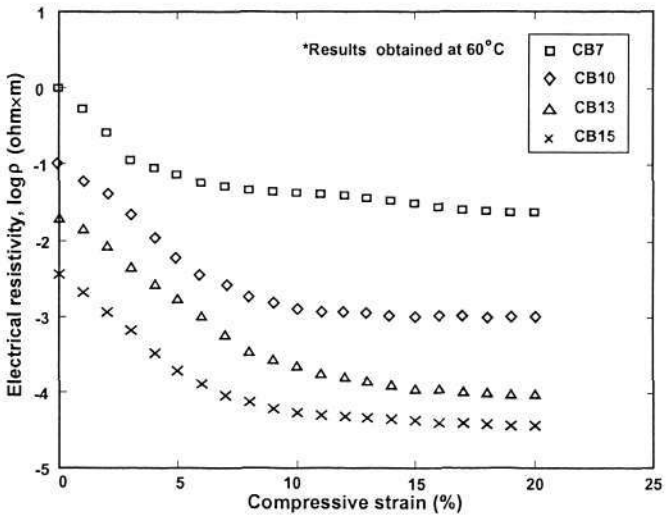

Figure 3 Electrical resistivity vs. compressive strain relationship.

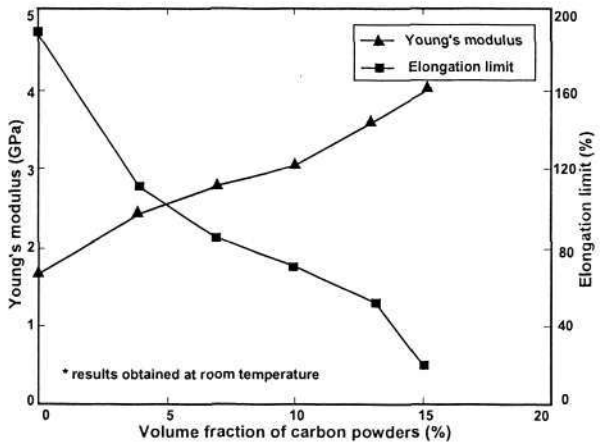

Figure 4 Relationship of Young's modulus and elongation limit vs. volume fraction of carbon powders.

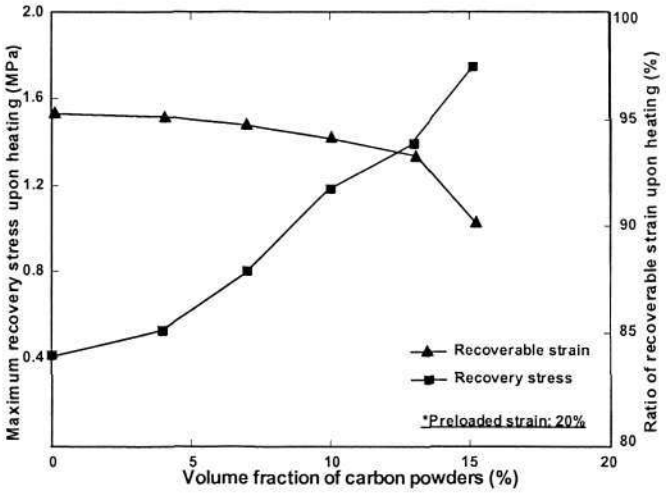

Figure 5 Maximum recovery stress in the constrained recovery test and ratio of recoverable strain in the free recovery test vs. volume fraction of carbon powders.

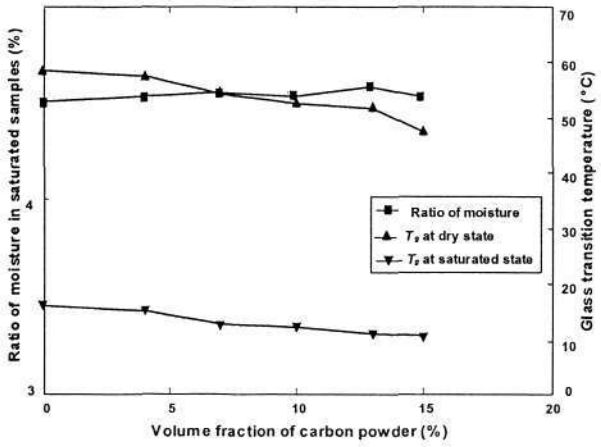

Figure 6 Ratio of moisture at saturated state and glass transition temperature at dry state and at saturated state of SMP vs. volume fraction of carbon powder.

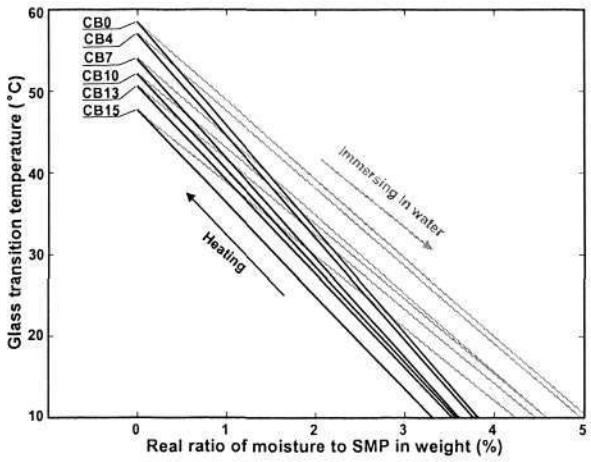

Figure 7 Evolution of glass transition temperature of carbon powder filled SMPs under different processes, i.e. immersing in water and heating.

Appendix D

Testing results repeated with different samples

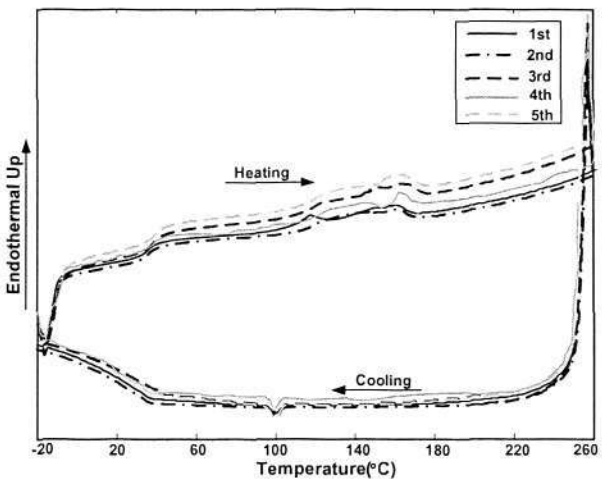

Figure 1 DSC result of SMP MM3520.

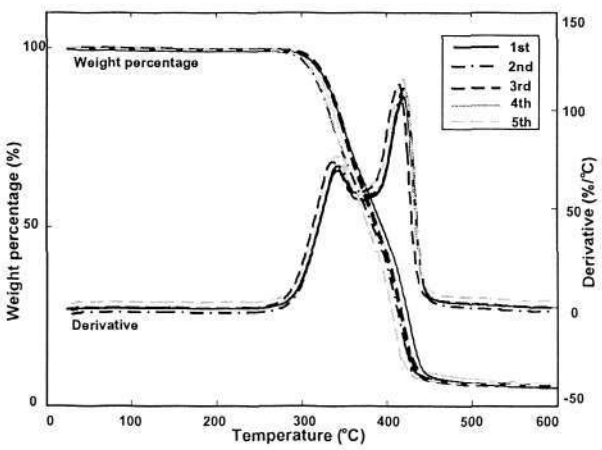

Figure 2 TGA result of SMP MM3520.

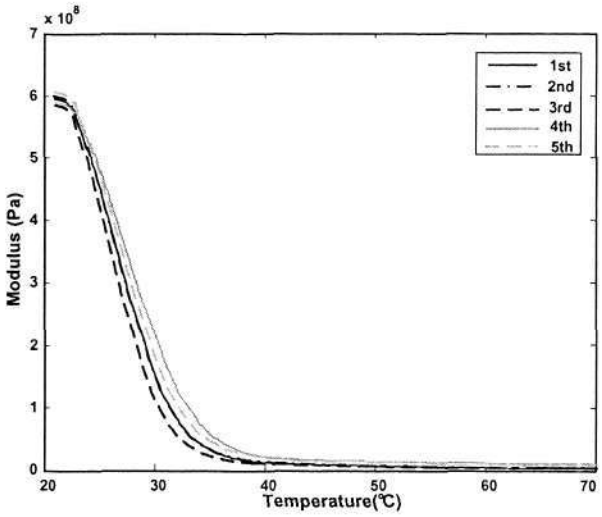

Figure 3 DMA result of SMP MM3520.

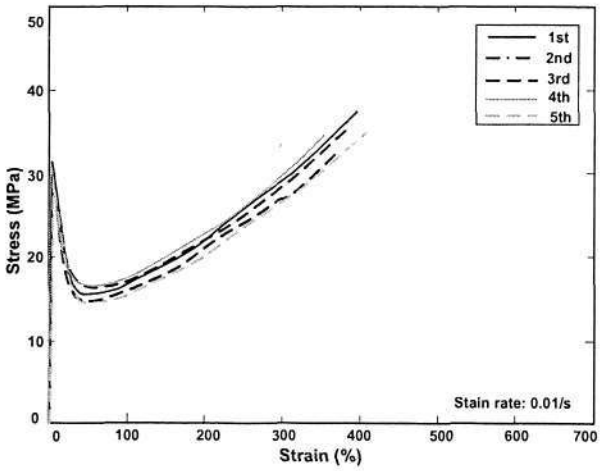

Figure 4 Stress vs. strain relationship of SMP MM3520 at a strain rate of 0.01/s.

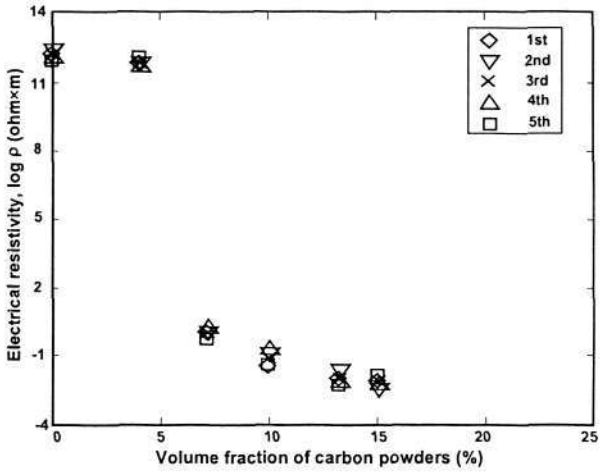

Figure 5 Electrical resistivity vs. volume fraction of carbon powders.

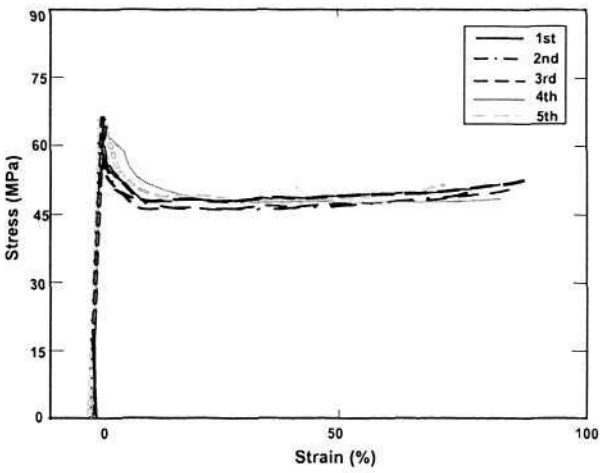

Figure 6 Stress-strain curves of CB7 at room temperature.

List of Publications

1. Yang B, Huang WM, Li C, Lee CM, Li L (2004). On the effects of moisture in a polyurethane shape memory polymer. Smart Materials and Structures, 13 (1), 191-5.

2. Huang WM, Yang B, An L, Li C, Chan YS (2005). Water-driven programmable polyurethane shape memory polymer: demonstration and mechanism. Applied Physics Letters, 86 (11), 114105-1-3.

3. Yang B, Huang WM, Li C, Chor JH (2005). Effects of moisture on the glass transition temperature of polyurethane shape memory polymer filled with nano-carbon powder. European Polymer Journal, 41 (5), 1123-8.

4. Yang B, Huang WM, Li C, Li L, Chor JH (2005). Qualitative separation of the effects of carbon nano-powder and moisture on the glass transition temperature of polyurethane shape memory polymer. Scripta Materialia, 53 (1), 105-7.

5. Yang B, Huang WM, Li C, Li L (2006). Effects of moisture on the thermomechanical properties of a polyurethane shape memory polymer. Polymer, 47 (4), 1348-56.